

UNCLASSIFIED

AD NUMBER
ADB283906
NEW LIMITATION CHANGE
TO Approved for public release, distribution unlimited
FROM Distribution authorized to U.S. Gov't. agencies only; Proprietary Info.; Feb 2000. Other requests shall be referred to U.S. Army Medical Research and Materiel Command, 504 Scott St., Ft. Detrick, MD 21702-5012.
AUTHORITY
USAMRMC ltr, 20 Dec 2002

THIS PAGE IS UNCLASSIFIED

AD _____

Award Number: MIPR 96MM6785

TITLE: The Cytoskeleton and ATP in Sulfur Mustard-Mediated Injury
Endothelial Cells and Keratinocytes

PRINCIPAL INVESTIGATOR: Daniel B. Hinshaw, M.D.

CONTRACTING ORGANIZATION: Ann Arbor Veterans Affairs Medical Center
Ann Arbor, Michigan 48105

REPORT DATE: February 2000

TYPE OF REPORT: Final

PREPARED FOR: U.S. Army Medical Research and Materiel Command
Fort Detrick, Maryland 21702-5012

DISTRIBUTION STATEMENT: Distribution authorized to U.S. Government
agencies only (proprietary information, Feb 00). Other requests
for this document shall be referred to U.S. Army Medical Research
and Materiel Command, 504 Scott Street, Fort Detrick, Maryland
21702-5012.

The views, opinions and/or findings contained in this report are
those of the author(s) and should not be construed as an official
Department of the Army position, policy or decision unless so
designated by other documentation.

1113 005

NOTICE

USING GOVERNMENT DRAWINGS, SPECIFICATIONS, OR OTHER DATA INCLUDED IN THIS DOCUMENT FOR ANY PURPOSE OTHER THAN GOVERNMENT PROCUREMENT DOES NOT IN ANY WAY OBLIGATE THE U.S. GOVERNMENT. THE FACT THAT THE GOVERNMENT FORMULATED OR SUPPLIED THE DRAWINGS, SPECIFICATIONS, OR OTHER DATA DOES NOT LICENSE THE HOLDER OR ANY OTHER PERSON OR CORPORATION; OR CONVEY ANY RIGHTS OR PERMISSION TO MANUFACTURE, USE, OR SELL ANY PATENTED INVENTION THAT MAY RELATE TO THEM.

LIMITED RIGHTS LEGEND

Award Number: MIPR 96MM6785

Organization: Ann Arbor Veterans Affairs Medical Center

Location of Limited Rights Data (Pages):

Those portions of the technical data contained in this report marked as limited rights data shall not, without the written permission of the above contractor, be (a) released or disclosed outside the government, (b) used by the Government for manufacture or, in the case of computer software documentation, for preparing the same or similar computer software, or (c) used by a party other than the Government, except that the Government may release or disclose technical data to persons outside the Government, or permit the use of technical data by such persons, if (i) such release, disclosure, or use is necessary for emergency repair or overhaul or (ii) is a release or disclosure of technical data (other than detailed manufacturing or process data) to, or use of such data by, a foreign government that is in the interest of the Government and is required for evaluational or informational purposes, provided in either case that such release, disclosure or use is made subject to a prohibition that the person to whom the data is released or disclosed may not further use, release or disclose such data, and the contractor or subcontractor or subcontractor asserting the restriction is notified of such release, disclosure or use. This legend, together with the indications of the portions of this data which are subject to such limitations, shall be included on any reproduction hereof which includes any part of the portions subject to such limitations.

THIS TECHNICAL REPORT HAS BEEN REVIEWED AND IS APPROVED FOR PUBLICATION.

REPORT DOCUMENTATION PAGE

Form Approved
OMB No. 074-0188

Public reporting burden for this collection of information is estimated to average 1 hour per response, including the time for reviewing instructions, searching existing data sources, gathering and maintaining the data needed, and completing and reviewing this collection of information. Send comments regarding this burden estimate or any other aspect of this collection of information, including suggestions for reducing this burden to Washington Headquarters Services, Directorate for Information Operations and Reports, 1215 Jefferson Davis Highway, Suite 1204, Arlington, VA 22202-4302, and to the Office of Management and Budget, Paperwork Reduction Project (0704-0188), Washington, DC 20503

1. AGENCY USE ONLY (Leave blank)		2. REPORT DATE February 2000	3. REPORT TYPE AND DATES COVERED Final (1 Oct 96 - 28 Feb 00)	
4. TITLE AND SUBTITLE The Cytoskeleton and ATP in Sulfur Mustard-Mediated Injury to Endothelial Cells and Keratinocytes			5. FUNDING NUMBERS MIPR 96MM6785	
6. AUTHOR(S) Daniel B. Hinshaw, M.D.				
7. PERFORMING ORGANIZATION NAME(S) AND ADDRESS(ES) Ann Arbor Veterans Affairs Medical Center Ann Arbor, Michigan 48105			8. PERFORMING ORGANIZATION REPORT NUMBER	
E-MAIL:				
9. SPONSORING / MONITORING AGENCY NAME(S) AND ADDRESS(ES) U.S. Army Medical Research and Materiel Command Fort Detrick, Maryland 21702-5012			10. SPONSORING / MONITORING AGENCY REPORT NUMBER	
11. SUPPLEMENTARY NOTES				

20021113 005

12a. DISTRIBUTION / AVAILABILITY STATEMENT Distribution authorized to U.S. Government agencies only (proprietary information, Feb 00). Other requests for this document shall be referred to U.S. Army Medical Research and Materiel Command, 504 Scott Street, Fort Detrick, Maryland 21702-5012.	12b. DISTRIBUTION CODE
--	-------------------------------

13. ABSTRACT (Maximum 200 Words)

The major goal of this project has been to test the hypothesis that sulfur mustard (SM)-mediated cell death in keratinocytes and endothelial cells is primarily apoptotic in nature, and that several factors (e.g. cellular levels of adenosine triphosphate (ATP), reactive oxygen species [ROS], the presence of a nucleus) help define this process. Using biochemical and fluorescence microscopic techniques to measure several parameters of cell death, we found that keratinocytes undergo apoptosis in response to SM, but less synchronously than endothelial cells which exhibit a more classical pattern of apoptosis. Caspase-3, a protease which plays a central role in programmed cell death was activated in both cell types by SM, but more slowly in keratinocytes. In models of ATP depletion, endothelial cell and keratinocyte progression into apoptosis was suppressed after SM injury. Experiments with enucleated cytoplasts demonstrated a nuclear-dependence for at least some aspects of SM-mediated cell death. Protective effects of N-acetyl-l-cysteine (NAC) on SM-injured endothelial cells were found to be glutathione (GSH)-dependent but other studies assaying for ROS within SM-injured cells demonstrated no direct role for ROS in SM-mediated toxicity. We have found that cell death induced by SM is irreversible but development of the apoptotic phenotype may be prevented by inhibition of caspase activation, even after SM exposure. Thus, caspase activation appears to be a critical element common to SM-induced endothelial cell and keratinocyte death, and may be an important target for therapeutic intervention.

14. SUBJECT TERMS sulfur mustard, keratinocytes, endothelium, microfilaments, actin, caspases, apoptosis, cell death			15. NUMBER OF PAGES 132
			16. PRICE CODE
17. SECURITY CLASSIFICATION OF REPORT Unclassified	18. SECURITY CLASSIFICATION OF THIS PAGE Unclassified	19. SECURITY CLASSIFICATION OF ABSTRACT Unclassified	20. LIMITATION OF ABSTRACT Limited

FOREWORD

Opinions, interpretations, conclusions and recommendations are those of the author and are not necessarily endorsed by the U.S. Army.

Where copyrighted material is quoted, permission has been obtained to use such material.

Where material from documents designated for limited distribution is quoted, permission has been obtained to use the material.

DM Citations of commercial organizations and trade names in this report do not constitute an official Department of Army endorsement or approval of the products or services of these organizations.

In conducting research using animals, the investigator(s) adhered to the "Guide for the Care and Use of Laboratory Animals," prepared by the Committee on Care and Use of Laboratory Animals of the Institute of Laboratory Resources, National Research Council (NIH Publication No. 86-23, Revised 1985).

For the protection of human subjects, the investigator(s) adhered to policies of applicable Federal Law 45 CFR 46.

In conducting research utilizing recombinant DNA technology, the investigator(s) adhered to current guidelines promulgated by the National Institutes of Health.

In the conduct of research utilizing recombinant DNA, the investigator(s) adhered to the NIH Guidelines for Research Involving Recombinant DNA Molecules.

In the conduct of research involving hazardous organisms, the investigator(s) adhered to the CDC-NIH Guide for Biosafety in Microbiological and Biomedical Laboratories.


PF - Signature 2-24-00
Date

TABLE OF CONTENTS

Final Report Front Cover	
Report Documentation Page	2
Foreword	3
Table of Contents	4
Introduction	5
Body	8
Experimental Methods, Assumptions, and Procedures	8
Results	21
Discussion	38
Key Research Accomplishments	45
Reportable Outcomes	46
Conclusions	47
References	48
Figure Legends	54
Tables	63
Figures	70

INTRODUCTION

The chemical warfare vesicant, sulfur mustard (SM), continues to be an effective weapon of terror more than eighty years after the end of World War I. Largely because of an incomplete understanding of the pathogenesis of SM-induced vesication, no effective therapy currently exists for SM. The primary focus of this project is to test the hypothesis that SM induces programmed cell death or apoptosis in endothelial cells and keratinocytes, two major cellular targets intimately involved in the vesication process. It is further hypothesized that the morphologic and cytoskeletal alterations in SM-injured endothelial cells and keratinocytes are largely apoptotic in character, SM-induced apoptosis is an ATP-dependent process, and reactive oxygen species (ROS) generated within SM-injured cells may act as initiating signals for apoptosis. This final report will present progress we have made in addressing these questions, specifically addressing work proposed in tasks 1-7 of the Statement of Work (SOW) as well as additional work which was a natural outgrowth of Tasks 1-7.

The process of cell death usually follows one of two patterns: necrosis or apoptosis (programmed cell death) (1-4). Necrosis, typically, has been seen as an "accidental" or catastrophic form of cell death, characterized by cellular swelling and loss of plasma membrane integrity. Apoptosis, in contrast, is a highly coordinated form of cellular "suicide", the hallmark of which has been a morphologic pattern of nuclear chromatin condensation and fragmentation associated with cell shrinkage, membrane budding (blebbing), and ultimate fragmentation of the cell and chromatin into many smaller membrane-enclosed apoptotic bodies. The apoptotic bodies retain intact plasma membranes for some time and *in vivo* are phagocytized by neighboring cells or

macrophages (1-4). Apoptosis is thought to occur "silently" with little or no acute inflammation, whereas necrosis usually evokes a prominent acute inflammatory response (1). A wide variety of stimuli can induce the apoptotic process, including physiologic (e.g. normal development, steroid hormones, removal of trophic factors) and pathologic stimuli (e.g. ischemia, oxidants, adverse physical conditions such as hypothermia, chemotherapeutic agents for cancer, and agents which disrupt the cytoskeleton). Many of the pathologic agents which induce apoptosis at low concentrations in a given cell will cause necrosis in the same cell at higher concentrations (1). This appears to also be true for SM (5). Concentrations of SM which alter cellular metabolism (e.g. reduce cellular ATP levels) can induce necrosis in endothelial cells (5). In contrast, a number of laboratories have recently demonstrated the ATP-dependence of apoptosis, underscoring the importance of intact metabolic pathways for successful implementation of the death program of apoptosis (6-10).

Recent advances in understanding the biochemical pathways of apoptosis have led to the identification of two major phases in apoptosis: a potentially reversible initiation phase and a later irreversible execution phase (4). A central component to the apoptotic process is the activity of a family of cysteine proteases known as the caspases (4,11,12). The caspases have been referred to as the "central executioner" of apoptosis (4) because it is thought that they catalyze activity marking the "point of no return" in apoptosis leading to the final events of the execution phase (e.g. nuclear fragmentation and endonucleolytic cleavage of DNA, plasma membrane phospholipid changes, and actin filament depolymerization and actin cleavage).

Although in many cells apoptosis and necrosis appear to be fairly distinct, even mutually exclusive, pathways of cell death, such sharp distinctions do not always exist - even apoptotic cells eventually lose plasma membrane integrity (if they do not undergo phagocytosis) and not all of the individual features of apoptosis (e.g. endonucleolytic cleavage of DNA) may occur in a given cell type or following a particular apoptotic stimulus. In recent work we reported that endothelial cells demonstrate a number of classical features of apoptosis (including nuclear chromatin condensation and fragmentation, endonucleolytic cleavage of DNA, cellular shrinkage, membrane budding, actin filament depolymerization, and apoptotic body formation and release) following exposure to SM (5). In preliminary work presented in our last contract's final report, keratinocytes appeared to undergo necrosis almost exclusively after SM exposure as measured by loss of plasma membrane integrity, and demonstrated little evidence of the apoptotic changes in nuclear chromatin typically seen in SM-injured endothelial cells. Rosenthal, et. al. have reported recently that cleavage of poly (ADP-ribose) polymerase (PARP) by caspase-3, an event central to the apoptotic process, does occur in SM-injured keratinocytes (13). In other models of keratinocyte injury and death, some if not many features of apoptosis (including evidence of nuclear degradation and endonucleolytic cleavage of DNA) have been demonstrated (14-16). These observations coupled with our earlier observations of plasma membrane lysis in keratinocytes following SM exposure suggest that the distinction between apoptosis and necrosis may not be clear-cut. Furthermore, the minimal essential elements that characterize programmed cell death as a distinct entity (particularly with respect to keratinocyte injury by SM) have not

been defined, although Smulson and Rosenthal suggest that caspase activation may indeed be the all sufficient and defining event required for the process (13).

The report which follows details our progress in addressing the work outlined in the SOW and our effort to examine in more detail many of the unique features which characterize keratinocyte and endothelial cell death induced by SM.

BODY

EXPERIMENTAL METHODS, ASSUMPTIONS, AND PROCEDURES.

Cells and culture. Bovine pulmonary artery endothelial cells were purchased from the National Institute of Aging, Aging Cell Culture Repository (Camden, NJ) and maintained in Ham's F12 medium supplemented with 2 mM glutamine (GIBCO), 10% heat-inactivated fetal bovine serum (GIBCO), 10 mM HEPES, 100 U/ml penicillin, and 100 mg/ml streptomycin (GIBCO). Endothelial subculturing was carried out on confluent cultures using 0.05% trypsin and 0.02% EDTA (Sigma) and cells of Passages 3 to 9 were used. Human keratinocytes from redundant skin removed at the time of reduction mammoplasty (courtesy of Dr. Cynthia Marcelo, University of Michigan) were grown in KBM-2 medium (Clonetics) with the addition of growth factors (KGM-2 single quots, Clonetics). Upon reaching 80% confluence, the keratinocytes were passaged by exposure to 0.05% trypsin and 0.02% EDTA. The trypsin was inactivated with 10-15 ml of 0.3 mg/ml soybean trypsin inhibitor (Clonetics). Keratinocytes from the first to third passages were used for experiments. Cells were grown in 75- or 150-cm² flasks (Falcon) in a culture incubator at 37°C under a 5% CO₂ humidified atmosphere.

Injury protocol with SM. Confluent monolayers of endothelial cells or keratinocytes grown in six-well plates (Falcon, Becton Dickinson) were exposed to final concentrations of SM ranging from 0.01 to 0.5 mM in culture media under sterile conditions. Biochemical and morphological parameters of SM injury were monitored at multiple time points up to and even beyond 72 hours after SM addition. Untreated controls were also done under identical conditions and time points.

In the experiments in which cells were pretreated with N-acetyl-cysteine (NAC) to block apoptosis (5,17), the cells were incubated for 20 hours with 50 mM N-acetyl-L-cysteine (Sigma) (5,17). Residual NAC in the media was removed by three washings with media before SM addition.

Cell morphology. Microscopic observations of endothelial cells and keratinocytes were performed during the time course of SM injury with a Nikon optiphot microscope. Wright-Giemsa staining was performed using the Fisher LeukoStat Stain Kit.

Fluorescence microscopy. After varying periods of incubation at 37°C under the different experimental conditions, the adherent cells were fixed with 2% paraformaldehyde for 1 hr at room temperature. The paraformaldehyde was then removed and the cells were washed and permeabilized three times for 5 min with Dulbecco's Cation Free phosphate buffered saline (PBS), pH 7.4, containing 0.2% Triton X-100. Cells were stained with 165 nM rhodamine phalloidin (Molecular Probes)

specific for F-actin in microfilaments (18) for 20 min at room temperature in the dark. Coverslips were sealed to each monolayer and the samples were viewed with the G filter block on a Nikon optiphot fluorescence microscope. Fluorescence micrographs were taken using TMAX 400 film (Kodak).

Assays of Cell Death. Recently many of the biochemical steps in apoptosis have been defined. Cysteine protease (caspase) activity (particularly that of caspase-3) has been identified as critical to induction of the final execution phase of apoptosis which includes destructive irreversible events involving the nucleus, plasma membrane, and cytoskeleton. It is not yet clear how caspase activity is linked to the initiation of events in the execution phase of apoptosis. Since it is possible that the actual pattern of execution phase events may depend on both stimulus and individual cell type, caspase activity may be a more reliable indicator of activation of the apoptotic death program.

Caspase-3 Measurements. Confluent or nearly confluent cultures in 6 well plates were treated with sulfur mustard (SM) at final concentrations of 0, 10, 50, 100, or 250 μM . At harvest, cells were scraped into the medium, which was transferred to microfuge tubes and centrifuged at 1500 rpm in a microfuge. Cell pellets were resuspended in 150 μL insect cell lysis buffer (PharMingen, San Diego, CA), snap frozen in liquid nitrogen and stored at -70°C . At time of assay, lysates were thawed on ice, then centrifuged 10 min at 14,000 rpm in a microcentrifuge at 4°C . Aliquots (100 μL) of the clarified lysates were used for determination of caspase-3 activity.

Caspase-3 activity was measured using a Perkin-Elmer HTS 7000 BioAssay Reader largely as described in product literature for Calbiochem's Caspase-3 colorimetric substrate I, Ac-DEVD-pNA (Calbiochem, La Jolla, CA). However, two important changes were made to the suggested protocol: 1) a fluorogenic substrate, Ac-DEVD-AMC (PharMingen, San Diego, CA) was used, with emission at 450 nm in response to excitation at 380 nm measured, and 2) protein concentrations in the lysates were determined with a Bio-Rad Assay (Bio-Rad, Hercules, CA) to allow expression of the caspase-3 activities in terms of protein. A 7-amino-4-methylcoumarin (Aldrich Chemical Co., Milwaukee, WI) 10 μ M standard was included in each assay.

Determination of apoptotic (chromatin condensation-fragmentation) index and cell viability (plasma membrane integrity) (19). Cells were stained during the time course of SM injury with a dye mixture (10 μ M acridine orange and 10 μ M ethidium bromide; (Sigma), that was prepared in phosphate-buffered saline (PBS)).

Acridine orange (fluorescent DNA-binding) intercalates into DNA, making it appear green, and binds to RNA, staining it red-orange. Ethidium bromide is taken up only by nonviable cells, and its fluorescence overwhelms that of the acridine orange, making the chromatin of lysed cells appear orange.

At the end of each experimental time point, all of the medium was removed and cells were harvested by incubation with 0.05% trypsin and 0.02% EDTA for 1 min and washed with the medium. Then, 250 μ l of cell suspension was mixed with 10 μ l of the dye mix and 200 cells per sample were examined by fluorescence microscopy, according

to the following criteria: (1) viable cells with normal nuclei (fine reticular pattern of green stain in the nucleus and red-orange granules in the cytoplasm); (2) apoptotic cells with apoptotic nuclear changes (green chromatin which is highly condensed or fragmented and uniformly stained by the acridine orange); and (3) nonviable (necrotic) cells with plasma membrane lysis (bright orange chromatin). The study of the viability of cells in the undisturbed monolayers has shown that trypsinization does not promote further cell injury.

Endonuclease activity (5). Cell samples (3×10^6 cells) obtained during the time course of SM injury were lysed in 750 μ l of buffer (100 mM Tris, 5 mM EDTA, 200 mM NaCl, and 0.2% SDS at pH 8.5) to which Proteinase K (100 μ g/ml final concentration) was added. Samples were incubated in a shaking water bath at 37° C for 1 hr. Then, DNA was precipitated by addition of an equal volume of cold isopropanol with gentle mixing. The precipitate was pelleted by centrifugation at 14,000g for 30 min, air dried (after decanting the supernatant) under a fume hood for 20 min, and then resuspended in 50 μ l TE buffer (10 mM Tris, 1 mM EDTA, pH 7.6) containing 40 μ g/ml RNase. Equal volumes of each sample were electrophoresed on a 1% agarose gel stained with ethidium bromide. The gel was photographed under UV light.

Detection of Apoptosis Using Annexin V. At various time points after SM treatment, the cells were harvested by trypsinization and the pattern of cell death was assessed using the flow cytometric Apoptosis Detection Kit (R&D Systems,

Minneapolis, MN). The assay is based on the fact that during the apoptotic process, cells express phosphatidylserine on the outer leaflet of the plasma membrane and will bind Annexin V. The necrotic cells are differentiated from the apoptotic cells because in the former cells the integrity of the plasma membrane has been compromised and will allow uptake of propidium iodide (PI) which binds to DNA. Viable cells are negative for both Annexin V and PI staining. The assay was performed essentially as described by the supplier. The FITC-Annexin V fluorescence was read with the FL1 photomultiplier tube (PMT) and PI fluorescence was detected using the FL3 PMT.

MTT Viability Assay. In some experiments, viability was assessed as the ability of cellular mitochondria to process 3-(4,5-dimethylthiazol-2-yl)-2,5-diphenyl-2H-tetrazolium bromide (MTT) to an insoluble blue formazan product (20). After cellular incubation for varying times following SM addition, MTT (in PBS) was added at a final concentration of 250 $\mu\text{g}/\text{mL}$. After 2 hr, the plates were centrifuged for 5 min at 1500 rpm, the medium was removed and 2 mL DMSO added. After thorough mixing, the absorbance (A) at 560 nm was measured using a Perkin-Elmer HTS-7000 BioAssay Reader. The A560 of the treatment groups was expressed as a percentage of that of the DMSO control.

Western Blot Analysis of Gelsolin Cleavage. At 16, 20 and 24 hr post SM injury, keratinocyte whole cell lysates were prepared. Following SDS-PAGE, the proteins were transferred to a nitrocellulose membrane. The membrane was blocked for 4 hr and then

incubated overnight with a monoclonal anti-gelsolin antibody (Sigma) at 1:1000. After washing, the membrane was incubated for 1 hr with anti-mouse IgG (Jackson Laboratories) at 1:20000. The membrane was then washed and the bands were detected using the ECL-Plus kit (Amersham).

Calcein Assay of Cell Viability. Calcein as an acetoxymethyl (AM) ester is taken up by viable cells and is converted to its fluorescent form by intracellular esterases. The polyanionic calcein is retained within live cells producing intense green fluorescence. Cells resuspended in PBS were labeled with 4 μ M calcein-AM. After a 30 min incubation at 37° C, the fluorescence was detected using the FL1 channel of a FACScan flow cytometer.

Analysis of Mitochondrial Membrane Potential. Early in the apoptotic process, a loss of the mitochondrial membrane potential is observed. Therefore, the mitochondria specific dye, 3,3'-dihexyloxacarbocyanine (DiOC6), is useful for detecting apoptosis. In cells undergoing apoptosis, a loss in DiOC6 fluorescence is observed. Adherent cells were labeled with 4 nM DiOC6 and incubated at 37° C. After 30 min, the cells were harvested by trypsinization and resuspended in PBS to which 4 nM DiOC6 was readded. The fluorescence was read using the FL1 channel of a FACScan flow cytometer.

ATP measurement. Cellular ATP levels were assayed as previously reported by the luciferase-luciferin method of Stanley and Williams (5). The luciferase-

luciferin (Sigma) was reconstituted in a buffer containing 1% bovine serum albumin, 20 mM glycine, and 2 mM EDTA, pH 8.0. Measurements were performed in an LKB Model 1251 automated luminometer (LKB Instruments, Inc., Gaithersburg, MD). ATP data were expressed as nanomoles of ATP per 1×10^6 cells. The whole cell population, including any floating cells, was subjected to the assay.

Measurement of Myosin Light Chain Kinase (MLCK) activity (21).

Immunoprecipitation and blotting of phosphorylated myosin light chain. Confluent or nearly confluent cultures of human keratinocytes in 6 well plates were treated with sulfur mustard (SM) concentrations of 0, 10, 50, 100 or 250 μ M for 16 hr. At harvest, the cells were scraped into the medium, which was transferred to microfuge tubes and centrifuged at 1500 rpm in a microfuge. Cell pellets were resuspended in 100 μ L lysis buffer (25 mM Tris, pH 7.5; 50 mM NaF, 1.5 mM dithiothreitol, 2 mM Na_3VO_4 , 0.5% Triton X-100, 100 μ M phenylmethylsulfonyl fluoride [PMSF], 10 μ g aprotinin, 10 μ g leupeptin), then mixed at 4° C. After 30 min, 25 μ L Protein A-agarose (Sigma, St. Louis, MO) was added to each tube, which was then mixed an additional 30 min at 4° C, followed by centrifugation at 14,000 rpm for 20 min in a microfuge at 4° C. Aliquots (100 μ l) of the cleared lysates were added to 0.9 mL immunoprecipitation buffer (final concentrations: 10 mM Tris, pH 7.5, 150 mM NaCl; 1% Triton X-100; 1.0% NP-40; 1 mM EDTA; 1 mM EGTA; 0.2 mM Na_3VO_4 , 0.4 mM PMSF and 0.4 mM benzamidine) and 20 μ L rabbit anti-myosin IgG (Biomedical Technologies, Inc., Stoughton, MA). After mixing for 2 hr at 4° C, 50 μ L Protein A-agarose was added, followed by another 2

hr mixing. IgG-Protein A-agarose complexes were recovered by 5 min centrifugation at 500 rpm in a microfuge at 4° C. After addition of 60 µL sample buffer, samples were boiled 10 min prior to being frozen and stored at -70° C. A 10 µL aliquot of each sample and a prestained standard (Bio-Rad, Hercules, CA) were electrophoresed in a 4-20% Tris-HCl gradient gel (Bio-Rad, Hercules, CA), then transferred to a nitrocellulose membrane (Bio-Rad, Hercules, CA) with a Trans-Blot SD Transfer Cell (Bio-Rad, Hercules, CA). The membrane was blocked 2 hr in TBST (100 mM Tris, pH 7.5, 0.9% NaCl, 1% Tween-20) containing 2% BSA, then incubated overnight with rabbit anti-phosphoserine IgG (1:2000 in TBST), then for 1 hr with peroxidase-conjugated goat anti-rabbit IgG (Jackson Labs, West Grove, PA). Detection was performed with an ECL+ Kit (Amersham, Arlington Heights, IL) in conjunction with Molecular Dynamics 860-WKSN PhosphorImager and Storm software. Annotation was added in PhotoShop 4.0.

Cytoplasm preparation. Cytoplasm were prepared using a modification of the method of Roos et al. (22). Briefly, endothelial cells were incubated for 5 min. at 37° C in 12.5% Ficoll 70 with 10 µM dihydrocytochalasin B. The cells were then layered on a discontinuous gradient of 16% Ficoll 70 on 25% Ficoll 70 at 33° C. The Ficoll solutions were mixed in phosphate-buffered saline. The gradients contained dihydrocytochalasin B throughout. The gradients were spun at 81,000 G (SW-41 rotor) for 50 min. at 33° C. Cytoplasm were collected from the 12.5 to 16% interface. Control cells were incubated for 60 min. in 12.5% Ficoll 70 and dihydrocytochalasin B. The control cells and

cytoplasts were washed at least four times with calcium-free MGB. The standard buffer (MGB) used for assays was the same with 1.5 mM CaCl₂ present. After filtration through 74 µm nylon mesh (Small Parts, Inc., Miami, FL) to remove aggregates and debris, recoveries were determined by counting leukostat stained cytoplasts. Volumes are estimated from forward light scatter with a Becton Dickinson (Mountain View, CA) flow cytometer (FACScan) with Becton Dickinson standard beads as references. Cytoplast viability was determined by assessing the ability of the cytoplasts to take up and concentrate calcein-AM (23). The purity of cytoplast preparations was confirmed by ethidium bromide (10 µM) staining on fluorescence microscopy demonstrating the absence of a nucleus and also by propidium iodide (PI) staining of cytoplasts on flow cytometry.

Determination of Cytoplast Purity. Cytoplasts and control cells resuspended in PBS containing 0.02% digitonin were labeled with 5 µg/ml propidium iodide (PI). After a 10 min incubation at room temperature, the fluorescence was read using the FL3 channel of a FACScan flow cytometer. Cytoplasts, in general, exhibit an order of magnitude less PI fluorescence than nucleated cells.

ATP depletion during SM injury. After removing the normal growth media, the adherent endothelial cells were washed twice with PBS and then incubated in the presence of glucose-free RPMI 1640 plus 5% bovine serum to which 5.5 mM glucose or no glucose and 4 mM KCN was added. After a 30 min equilibration at 37° C, the cells

were treated with 0, 100, 250, or 500 μM SM. ATP levels were determined at 1, 6 and 24 hr and cellular viability was assessed at 6 and 24 hr.

In initial experiments it was found that the keratinocytes did not tolerate exposure to KCN. A milder form of ATP depletion was accomplished using progressively lower levels of available glucose combined with increasing concentrations of the non-metabolizable glucose analogue, 2-deoxyglucose, as a competitive inhibitor of glycolysis in the keratinocytes.

Glyceraldehyde 3-phosphate dehydrogenase (GAPDH) assay (24). The activity of GAPDH in the cells was measured with a one-step assay in the forward direction as follows: Glyceraldehyde 3-phosphate + HAsO_4^{-2} + NAD^+ $\xrightarrow{\text{GAPDH}}$ 3-phosphoglycerate + $\text{NADH} + \text{H}^+ + \text{HAsO}_4^{-2}$. The arsenate substitutes for phosphate and drives the reaction to the right through an unstable arsenophosphoglycerate intermediate. At 1, 3 and 6 hr after treatment with 0, 100, 250 or 500 μM SM, the cells were harvested and resuspended at 1×10^7 cells/ml in 30 μl sonicating buffer (0.1 M Tris-HCl and 0.5 mM EGTA) and sonicated for 30 sec. To 195 μl of sonicating buffer containing 0.2 mM NAD, 6 mM glyceraldehyde-3-phosphate, and 300 mM Na_2HAsO_4 , 5 μl of sonicate was added. The initial rate of formation of NADH was monitored at 340 nm in a Perkin Elmer HTS 7000 Bio Assay Reader. For the blank, glyceraldehyde-3-phosphate was not added. The extinction coefficient for NADH is $6220 \text{ mol/L}^{-1}\text{cm}^{-1}$.

Glutathione Measurements. Total glutathione (GSH) and oxidized GSH (GSSG) were measured using standard methods (25,26). Briefly, 0.5×10^6 cells were centrifuged for 30 s in a microcentrifuge, the supernatant removed and the pellet deproteinized with 55 μ l 2.5% sulfosalicylic acid in 0.2% Triton x-100. Total GSH was determined in 24-well plates using 25- μ l samples for total GSH after addition of 250 μ l 0.3 mM 5,5'-dithiobis 2-nitrobenzoic acid (DTNB), 250 μ l 0.4 mM NADPH containing 0.12 U glutathione reductase and 250 μ l phosphate/imidazole buffer, pH 7.2. The difference in optical density at 412 nm was read on a Perkin-Elmer HTS 7000 BioAssay Reader.

Assay of Membrane Lipid Peroxidation (17). 1×10^6 cells in multiwell plates were gently washed with PBS and then to each well 1 ml PBS containing 5.5 mM glucose was added and the cells were labelled with 10 μ M cis-parinaric acid (Molecular Probes) in ethanol. After 1 hr at 37° C, the cells were washed twice with fresh PBS and then treated with 0 or 500 μ M alpha-tocopherol (Sigma) in ethanol for 30 min at 37° C. The cells were then injured with 0, 250 or 500 μ M SM or 50 μ M tert-butylhydroperoxide (positive control). After 3 hr, the cells were harvested, washed, and resuspended in PBS. The fluorescence was read using the SLM 8000C spectrofluorometer with excitation at 324 nm and emission at 413 nm.

Dihydrorhodamine 123 Assay of Intracellular Oxidant Production(27).
Adherent cells were loaded with 30 μ M dihydrorhodamine 123 (Molecular Probes,

Eugene, OR) and then treated with 0, 250 or 500 μ M SM. At 1, 2 and 3 hr post treatment, the cells were harvested by trypsinization and resuspended in MGB at 10^7 cells/ml. To 1 ml of MGB, 100 μ l of cell suspension was added. Fluorescence was detected with the FL1 photomultiplier tube (PMT) (488 nm excitation wavelength) on the FACScan flow cytometer (Becton-Dickinson).

Electrophoretic Mobility Shift Assays of NF κ B Activity. Confluent endothelial cells were treated with or without 50 mM NAC for at least 16 h. Cells were then treated with or without 250 μ M SM or 500 μ M SM for 2 or 5 h. Cells were harvested by scraping and the cells and media were pelleted. The pellet was processed for nuclear protein as described (28). The nuclear extracts were normalized for protein content (Bio-Rad, Hercules, CA) and analyzed for binding to a radiolabeled consensus nuclear factor κ B sequence (NF κ B; 5'GGGGACTTTCCGCTGGGGACTTTCCAGGGGGACTTTCC 3') as described (29). Specific binding was determined utilizing a 100-fold excess unlabeled NF κ B sequence.

Statistics. Data have been expressed as mean \pm standard deviation (S.D.) and were analyzed by two-tailed Student's *t*-test. Differences were considered significant where $p \leq 0.05$.

RESULTS

Cell death in endothelial cells and keratinocytes induced by SM (Task 1 of SOW). We have demonstrated that endothelial cells exposed to SM concentrations $\leq 250 \mu\text{M}$ undergo the characteristic morphologic and biochemical changes typical of apoptosis including: nuclear condensation and fragmentation, endonucleolytic cleavage of DNA, cellular shrinkage, membrane budding (blebbing), actin depolymerization, and apoptotic body formation and release (5). A unique feature affecting the outer cortical band of actin filaments in endothelial cells undergoing apoptosis was the apparent constriction of this band to a much smaller ring-like structure overlying the nucleus of the shrunken apoptotic cells (5). Concentrations of SM $\geq 500 \mu\text{M}$ produced a mixed pattern of apoptosis and necrosis in the endothelial cells. The appearance of necrosis at these higher concentrations of SM correlated well with reduction of cellular ATP levels (5). In contrast, preliminary work with keratinocytes presented in the final report from our previous contract period, suggested that keratinocytes primarily undergo necrosis in response to SM. This was largely based on assays of plasma membrane integrity and nuclear morphologic features typical for apoptosis. Recent observations by Rosenthal, et. al. (13) suggest that caspase activation can occur in keratinocytes following SM exposure, thus it is possible that apoptosis and necrosis may represent a continuum with various hybrid patterns of cell death potentially occurring between the extremes, rather than two separate distinct patterns of cell death. To examine this possibility we injured the cells with 0, 10, 50, 100, and 250 μM SM over a longer time course (16, 24, 48, and 72 hours) than in our earlier work to assess keratinocytes for the presence of the classical

morphological and nuclear/DNA criteria for apoptosis which we had seen in endothelial cells over a shorter time course. We also measured two additional non-nuclear parameters of apoptosis: 1) activation of caspase-3, the “central executioner” of apoptosis (4) and 2) Annexin V binding to exposed phosphatidylserine residues translocated to the outer leaflet of the plasma membrane, an execution phase event facilitating phagocytic recognition of apoptotic cells and bodies.

Figure 1 depicts the appearance of keratinocytes 72 hours after exposure to 0-100 μ M SM. Cellular shrinkage, chromatin condensation, nuclear fragmentation, and apoptotic body formation typical for apoptosis were seen (Fig. 1). Keratinocytes assayed (19) under these conditions demonstrated some evidence of the nuclear morphologic changes of apoptosis (Table 1), more than that seen earlier with higher SM concentrations, but still considerably less than that seen in SM-injured endothelial cells (5). There was still much evidence present for plasma membrane lysis (Table 1), even with low concentrations of SM (e.g. 50 μ M). DNA isolated from the keratinocytes during the long time course following exposure to lower doses of SM demonstrated a variable pattern of degradation. DNA ladders, indicative of endonucleolytic cleavage, could be detected under conditions of more synchronous injury (i.e. higher SM concentrations) (Fig. 2A), but smearing indicative of nonspecific DNA degradation typical for necrosis was also present (data not shown). Caspase-3-dependent cleavage of gelsolin is another feature of the execution phase of apoptosis. Using western blotting for the 41kDa cleavage product of gelsolin, gelsolin cleavage was seen under the same conditions as in Fig. 2A (Fig. 2B). This provided additional evidence confirming that

the execution phase of apoptosis is activated in keratinocytes by SM. Adherent keratinocytes stained with rhodamine phalloidin to visualize actin filaments demonstrated progressive loss of normal actin filament organization in dying cells over the 72-hour time course of SM injury with concentrations of SM as low as 50 μ M (Fig. 3). The disruption and loss of actin filaments developed very slowly at the low concentrations of SM and was rarely present in cells exposed to 10 μ M SM (Fig. 3), a concentration which was typically associated with minimal cell death over the same time course (e.g. Table 1). When Annexin V binding to phosphatidylserine residues was measured in SM-injured keratinocytes by flow cytometry, ~16% of cells demonstrated binding 24 hours after exposure to 250 μ M SM (Table 2). These increases in Annexin V binding occurred in keratinocytes with intact plasma membranes as confirmed with propidium iodide (Fig. 4), and thus were developing prior to the plasma membrane lysis seen in keratinocytes after SM exposure.

Measurement of caspase-3 activity in keratinocytes demonstrated some interesting findings (Fig. 5A). Caspase-3 activity was increased in SM-injured keratinocytes, and became evident before increased Annexin V binding was detected. There was a dose response of caspase-3 activity with progressive increases in activity particularly evident in response to 100 and 250 μ M SM 16 hours after SM addition (Fig. 5A). Endothelial cell caspase-3 activity was also increased over the same time course, particularly at 16 and 24 hours after SM exposure (Fig. 5A). To test the hypothesis that differences in the pattern of caspase activation over the time course of SM injury may account for the less synchronous pattern of cell death seen in keratinocytes versus

endothelial cells, caspase-3 activity was measured over the earlier (0-24 hr) time course after exposure to 100 and 250 μ M SM (Fig. 5B). Endothelial cells consistently demonstrated an earlier pattern of caspase-3 activation starting between 4-8 hr after SM exposure whereas keratinocytes began to demonstrate increased caspase-3 activity usually beginning 8 hr after SM exposure.

Actin-myosin contraction induced in SM-injured cells (Task 2 - SOW).

Using an immunoprecipitation strategy in which a precipitating antibody to the heavy chain of myosin precipitates both the heavy and light chains of myosin together from cellular extracts, we have attempted to examine the phosphorylation state of the light chain of myosin separated on polyacrylamide gels (PAGE) with antiphosphoserine immunoblotting as a measure of myosin light chain kinase (MLCK) activity. MLCK activity is required for actin-myosin contraction to occur and thus could be used as a biochemical confirmation of the apparent actin filament contraction seen in SM-injured endothelial cells stained with rhodamine phalloidin (5). In our preliminary work with this assay we had identified a band on PAGE of the appropriate molecular weight (\sim 20 kDa) (Fig. 6A). Unfortunately, later repetition of the experiment, in which a control for precipitating antibody alone was included, revealed a pattern identical to that seen with cellular extracts (Fig. 6B). Thus, we have been unable to isolate the myosin light chain using this technique.

Inhibition of cytoskeletal function and SM-mediated cell death (Task 3 -

SOW). In this task, we have examined the ability of a variety of agents which act on the microfilament system to alter or prevent the progression of apoptosis (particularly the cytoskeletal changes of apoptosis). To determine if we should further pursue the measurement of MLCK activity attempted in Task 2, we used the MLCK inhibitors ML9 and ML7 to block actin-myosin contraction which may occur early in the process of apoptosis. Dihydrocytochalasin B (H₂CB), an agent which binds to and caps the rapid growing end of actin filaments, thereby inducing actin depolymerization was used along with phalloidin which stabilizes actin filaments to determine if either of these agents might substantially alter the pattern of death induced by SM.

To address these questions, we evaluated the effect of these agents on several measures of cell viability including: the MTT assay, mitochondrial membrane potential, cleavage and intracellular concentration of the cell permeant fluorescent vital stain calcein-AM as calcein. Fluorescence micrographs were also taken of SM-injured cells treated with the agents and stained with rhodamine phalloidin to characterize morphologic and cytoskeletal effects of the different agents in relation to SM injury. Many different techniques were performed (often only once) to screen for any protective effects of ML7, ML9, phalloidin, or H₂CB in SM injury since after our initial pilot experiments with ML9 it became evident that agents which alter microfilament architecture or function have considerable toxicity alone. The rationale to pursue these experiments was based on many microscopic observations of SM-injured endothelial cells and keratinocytes undergoing rounding and apparent reduction in size (e.g. Fig. 3). This phenomenon is also demonstrable on flow cytometric analysis of forward light

scatter (size) characteristics of injured cells, in which the entire population of cells following injury demonstrates substantial reductions in size of individual cells (Fig. 7). We hypothesized that agents which might interfere with the SM-induced cellular rounding/decrease in size by inhibiting actin-myosin contraction (i.e. ML7, ML9) or by stabilizing microfilaments (e.g. phalloidin) might delay or mitigate SM toxicity, whereas an agent which could accelerate cytoskeletal (microfilament) disruption (i.e. H₂CB) might exacerbate/accelerate SM injury. Unfortunately, some of the agents (e.g. ML7, ML9) demonstrated some toxicity of their own, thus limiting their usefulness in these experiments and creating the need to screen several measures of cell death/toxicity.

Figure 8 summarizes viability data (MTT assay) for endothelial cells 40 hr after injury with 100 μ M SM which were also treated with ML7, ML9, H₂CB, or phalloidin at various concentrations. The MLCK inhibitors ML7 and ML9 both exhibited considerable toxicity of their own and no enhancement of viability of SM-injured endothelial cells. While phalloidin demonstrated less toxicity than H₂CB and the other agents, it also did not enhance the viability of SM-injured endothelial cells (Fig. 8). Similar results were also seen in an experiment with keratinocytes (data not shown).

Figure 9 demonstrates cellular morphology after SM injury with or without treatment with ML7, ML9, phalloidin, or H₂CB. None of the agents prevented the changes in microfilament architecture or cellular rounding and volume loss induced by SM (Fig. 9). H₂CB alone, as might be expected, induced considerable loss of actin filament staining with rhodamine phalloidin and cellular volume loss/rounding (Fig. 9).

This effect was additive to that of SM on the cells (Fig. 9). Similar results were also seen with SM-injured keratinocytes (data not shown).

Finally, we compared the effects of the inhibitors on SM injury in two very different assays of cellular toxicity - cellular cleavage and retention of calcein-AM as calcein (a measure of plasma membrane integrity) and DiOC₆ fluorescence (a measure of mitochondrial membrane potential). Measures of plasma membrane integrity (e.g. trypan blue uptake, calcein staining) only assess the final stage of cell death for either apoptosis or necrosis. Recently, loss of mitochondrial membrane potential has been described as a relatively early indicator of a cell's commitment to die (30). It may ultimately be an indicator of cellular commitment to death regardless of the pattern of death (necrosis vs. apoptosis). Figure 10 depicts dose response experiments in which endothelial cells and keratinocytes were exposed to different concentrations of each inhibitor one hour prior to addition of 100 μ M SM and then monitored at 16 and 40 hr after SM exposure for calcein fluorescence by flow cytometry. Boxed (gated) populations were defined by the vehicle (dimethylsulfoxide, DMSO) control (upper left dot plot of each panel). Interestingly, in these screening experiments, the lowest concentrations of each inhibitor were associated with increased percentages of cells in the gated region exhibiting increased calcein fluorescence compared to SM alone 40 hr after SM exposure. However, when mitochondrial membrane potential was measured with DiOC₆ by flow cytometry of the endothelial cells 40 hr after exposure to SM with similar pretreatments with the more effective concentrations of the inhibitors in the

calcein assay, there was no prevention of the loss of the mitochondrial membrane potential seen following SM injury (Fig. 11).

In summary, the work accomplished in Task 3 demonstrated the limited ability of the inhibitors to alter the outcome of SM injury. The experience with the inhibitors of MLCK activity and the technical difficulties encountered in Task 2 suggest that further pursuit of MLCK as an important target in developing treatment strategies for SM injury may not be worthwhile (particularly after consideration of other work presented below).

Cytoplasm Studies (Task 4-SOW). To determine if the presence of a nucleus is necessary for SM-mediated apoptosis to proceed, endothelial cytoplasts were prepared as described in the Methods section. This same methodology has been used by others to produce neutrophil cytoplasts which demonstrated normal physiologic responsiveness to stimulatory ligands (22). For typical experiments, the endothelial cytoplasts were allowed to adhere to tissue culture plates overnight prior to exposure to SM. The viability (plasma membrane integrity) of the cytoplasts prior to SM exposure was confirmed with the calcein assay (Fig. 12) and by the ability of cytoplasts to adhere and spread on tissue culture surfaces (Fig. 13). The purity of the standard cytoplasm preparation was confirmed by flow cytometry of cytoplasts permeabilized with digitonin and stained with propidium iodide (PI), a DNA stain, and compared to a control population of endothelial cells. The purity of cytoplasm preparations as determined by this methodology was ~ 90% (i.e. ~ 10% contaminating nucleated endothelial cells

present). Typically, cytoplasts demonstrated a log order decrease in PI fluorescence (the residual fluorescence primarily reflecting mitochondrial DNA) (Fig. 14).

When adherent endothelial cytoplasts (~ 20 hr after preparation) were exposed to SM, rounding, microfilament disruption, and loss of adherence occurred which was similar to that seen after SM injury to nucleated endothelial cells (Fig. 13). Paradoxically, the marked increase in caspase-3 activity induced by SM in nucleated endothelial cells was not observed in cytoplasts (Fig. 15). Interestingly, baseline levels of caspase-3 activity normalized to protein content were higher ($p \leq 0.05$) in untreated cytoplasts compared to the essentially unmeasurable levels of caspase-3 activity in nucleated control endothelial cells (Fig. 15). This lack of caspase-3 responsiveness to SM in cytoplasts was not a result of an inability to respond to other toxic stimuli, e.g. chelerythrine chloride, an agent which is a rapid activator of caspase-3 in human neutrophils (31) (Fig. 15). This suggests that DNA alkylation by SM in intact endothelial cells may be an important factor in the SM-mediated induction of caspase activation as well as other aspects of the apoptotic phenotype. Other toxic effects of SM on cytoplasts, particularly related to the cytoskeleton and adherence apparently may be decoupled from the caspase system. Interestingly, Annexin V staining (measured by flow cytometry) which increases in apoptosis as a result of exposure of phosphatidylserine residues in the plasma membrane was also increased as a result of cytoplast preparation and did not increase further in response to SM injury (fig. 16).

To clarify the nature of the baseline increase in caspase-3 activity in endothelial cytoplasts, caspase-3 activity was measured over a time course starting

immediately after cytoplasm preparation and extending for several hours (Fig. 17). These measurements suggest that the process of cytoplasm preparation, specifically enucleation, activates the caspase system and that this activation may be transient and reversible. Control endothelial cells were exposed to all the same conditions (e.g. H₂CB treatment, layering on the ficoll gradients described in the Methods) except for centrifugation. Keratinocytes, in our hands, did not tolerate the enucleation process (i.e. keratinocyte cytoplasm would not adhere after preparation), thus we restricted our work with this model to endothelial cells.

ATP-dependence of SM-induced cell death (Task 5 - SOW). Recently, it has been reported that apoptosis is a process which requires ATP (6-10). Using a combination of glucose depletion and mitochondrial inhibition with 4 mM KCN (32), we examined the hypothesis that cell death induced by SM is an ATP-dependent process. Endothelial cell ATP levels measured at 1, 6 and 24 hours after exposure to 0, 100, 250 and 500 μ M SM were correlated with viability measurements at 6 and 24 hr using the assay of apoptotic nuclear features. Depletion of ATP levels (Fig. 18) to stable levels at 24 hrs which were ~50% of control was associated with modest but significant protection of endothelial cells exposed to 100 μ M SM (Table 3). The effect of ATP depletion was primarily to decrease the number of cells demonstrating apoptotic nuclear features. At higher concentrations of SM (e.g. 500 μ M), the effect of ATP depletion was primarily a delay in the progression into apoptosis seen at 6 hr and a later potentiating of the necrosis-inducing effects of SM at 24 hr (Table 3). This data suggests that apoptosis

induced by SM in endothelial cells requires ATP and that ATP depletion can shift SM-induced cell death to a more necrotic pattern as has been seen in other models of cell death. When apoptosis is inhibited, SM-mediated cell death appears to progress more slowly. Work presented in the final report from the last contract demonstrated that although glutamine can partially restore ATP levels in endothelial cells injured by oxidants and thus help to shift a predominantly necrotic pattern of cell death to an apoptotic one (10), its utility in SM injury to endothelium is limited.

Keratinocytes did not tolerate exposure to KCN (data not shown). An alternative method of inducing ATP depletion was developed by limiting the glucose present in the culture media while at the same time replacing it with the non-metabolizable substrate level inhibitor of glycolysis, 2-deoxyglucose (Fig. 19). When keratinocyte viability at 24 hours after exposure to 0, 250, or 500 μ M SM was assessed using the fluorescence microscopic assay for apoptotic nuclear features (Table 4), the most striking finding was a decrease ($p = 0.05$) in the percentage of SM-injured cells exhibiting apoptotic nuclear features when ATP levels were markedly depleted. This observation is again consistent with the ATP-dependence of apoptosis.

SM injury, ATP loss, and the activity of glyceraldehyde 3-phosphate dehydrogenase (GAPDH) in endothelial cells and keratinocytes (Task 6 - SOW). The glycolytic enzyme, GAPDH, has been demonstrated to be a target of inhibition by reactive oxygen species (ROS) (24,33). Inhibition of GAPDH by ROS partially accounts for the suppression of ATP synthesis in oxidant-injured cells (24,33). We

tested the hypothesis that GAPDH might also be inhibited by SM and contribute to the ATP loss seen with higher dose SM injury in keratinocytes and endothelial cells. Figure 20 depicts the activity of GAPDH (measured spectrophotometrically) in endothelial cells and keratinocytes following exposure to 0, 250, and 500 μM SM. SM (500 μM) inhibited ~15% of the activity of GAPDH in endothelial cells as early as 3 hr after SM addition, but did not alter GAPDH activity in keratinocytes.

Reactive oxygen species (ROS) and SM injury (Task 7 - SOW). ROS have been implicated as important signalling intermediates in cell death (17). We tested the hypothesis that ROS may play a role in SM-mediated cell death. Three different assays have been used to examine the possibility that ROS may be generated during cellular injury with SM. Measurement of total and oxidized glutathione (GSH and GSSG, respectively) has been used in models of oxidant stress as a fairly sensitive marker for the presence of ROS in tissues and cells (34). Reduction in the levels of measurable GSH (which under normal circumstances is predominantly in the reduced form) is a less specific indicator of oxidant stress than demonstration of formation of GSSG which is a highly specific marker for oxidant stress. GSSG and total GSH levels were measured in endothelial cells and keratinocytes after exposure to a high dose SM injury (500 μM). GSSG was expressed as a % of total GSH equivalents where 1GSSG = 2GSH equivalents (Fig. 21). There was wide variation in the low levels of GSSG measured (reflected in the variances in Fig. 21). The small % of GSH equivalents consumed in the formation of GSSG (~5-10% of total GSH equivalents at 6 hr) could

not account for the > 30% loss of GSH seen 6 hr after exposure to 500 μ M SM in both cell types (Fig. 22). This provides strong circumstantial evidence for a direct interaction between SM and GSH. The effect of the GSH-altering agents, buthionine sulfoximine (BSO) and N-acetyl-cysteine (NAC) (inhibitors and stimulators of GSH synthesis, respectively), on SM-mediated injury to endothelial cells and keratinocytes was examined. Figure 22 depicts the effects of pretreatment with these GSH-altering agents on total GSH levels in endothelial cells and keratinocytes 1 and 6 hr after exposure to 500 μ M SM. SM injury without any other treatment resulted in a significant ($p \leq 0.05$) reduction in the level of total GSH in endothelial cells at 6 hours (Fig. 22A).

Pretreatment with 50 mM NAC resulted in a > 50% increase ($p \leq 0.05$) in the level of total GSH in uninjured endothelial cells and was also associated with preservation of GSH during SM injury (Fig. 22A). Pretreatment with 200 μ M BSO caused a > 50% reduction ($p \leq 0.05$) in the level of total GSH in uninjured endothelial cells and completely blocked the enhancement of endothelial GSH levels associated with NAC pretreatment (Fig. 22A).

Consistent with the beneficial effect of NAC pretreatment on endothelial GSH levels, endothelial viability was enhanced at 6 hr after injury with 500 μ M SM when GSH levels were augmented with NAC ($69.3 \pm 1.7\%$ viable vs. 50.4 ± 4.0 , control) (Table 5). This enhanced viability was primarily reflected in a reduction in the number of apoptotic cells (Table 5). GSH depletion with BSO treatment exacerbated SM injury ($35.7 \pm 8.4\%$ viable vs. $50.4 \pm 4.0\%$, control) and resulted in an increased number of necrotic cells (Table 5). The combination of BSO with NAC eliminated any

of the beneficial effect seen with NAC alone ($51.7 \pm 4.7\%$ viable vs. $50.4 \pm 4.0\%$, control) (Table 5).

We also examined the possibility that exogenous GSH might have some protective effect on endothelial cells during SM injury. Indeed, when GSH was added an hour prior to SM exposure, there was substantial protection of the cells (Table 6). The primary effect of the GSH was to reduce the number of cells demonstrating apoptotic nuclear features. The effect of GSH appeared to be dose-related, although its benefit was limited to some extent by an associated toxicity at higher concentrations (Table 6).

The effect of the GSH-altering agents BSO and NAC on SM-mediated injury to keratinocytes was also examined. Figure 22B demonstrates the effects of pretreatment with these GSH-altering agents on total GSH levels in keratinocytes at 1 and 6 hours after exposure to 0 or 500 μM SM. Although NAC pretreatment enhanced total GSH levels early in the course of SM injury (at 1 hr), this effect was lost by 6 hr even in the control (Fig. 22B). As with endothelial cells, BSO antagonized the effect of NAC on total GSH levels in keratinocytes, but did not further potentiate the effect of SM on GSH levels. Most interestingly, real reductions in total GSH associated with SM exposure were not evident after 1 hr, but did become apparent by 6 hr (40-50% decrease) ($p \leq 0.05$) (Fig. 22B), suggesting that the metabolism of SM involving GSH is a fairly slow process. Surprisingly, pretreatment with NAC did not provide much protection for SM-injured keratinocytes (Table 7).

Since it is possible that generation of ROS within cells may be compartmentalized, we have examined other ways to assess ROS generation within cells after SM exposure. Parinaric acid, a fluorescent lipid which intercalates within the lipid bilayer of cellular membranes, loses fluorescence upon oxidation and thus can serve as an indicator of either background or supranormal levels of lipid peroxidation occurring within cellular membranes (17). Figure 23 demonstrates our experience with this assay during SM injury in endothelial cells. There was a background level of lipid peroxidation present in the control cells which was clearly increased in the positive control (t-butylhydroperoxide) and which was substantially reduced when vitamin E (α -tocopherol) was present (Fig. 23B). Although a trend towards increased parinaric acid oxidation (decreased fluorescence) appeared to occur with SM exposure, this did not achieve statistical significance (Fig. 23).

Another approach to measuring ROS generation during SM injury we have taken is measurement of oxidation of dihydrorhodamine 123 (H_2Rh123). In cells in which ROS are being generated, H_2Rh123 is oxidized to the highly fluorescent Rh123 which is trapped in cells due to its charged state (27). This measure of cytosolic oxidative (ROS) activity thus complements the parinaric acid assay by giving specific information about cytosolic ROS generation and may also be a more sensitive indicator than GSSG levels. Figure 24 demonstrates our experience with this assay in SM-injured endothelial cells and keratinocytes. Although there was a clear increase in Rh-123 fluorescence in the positive control (100 $\mu M H_2O_2$), no definite increases in Rh-123

fluorescence were seen after significant SM injury in either keratinocytes or endothelial cells (Fig. 24).

Unfortunately, our collaborator for the measurement of hydroxylated DNA bases (hydroxyl radical) moved out of state and we have been unable to pursue this approach further. Although our data does not support the hypothesis that SM induces a "large" (potentially toxic) burst of ROS generation within injured cells, the possibility remains that low level ROS activity (as part of cellular signal transduction events) may be initiated by SM injury. Current understanding of the process governing activation of the nuclear transcription factor, NF κ B, has demonstrated the involvement of low level ROS (e.g. 30-50 μ M H₂O₂) (35). In work in press (36), it was found that SM can activate NF κ B in endothelial cells (Fig. 25). This observation is consistent with the hypothesis that SM may secondarily induce low level ROS generation as a part of signaling cascades initiated by its toxic effect on cells.

Inhibition of SM-induced Apoptosis and Cellular Survival. In additional work beyond the scope of the Tasks outlined in the SOW, we tested the hypothesis that apoptosis induced by SM can be inhibited by blocking activation of the caspase system. Furthermore, we also hypothesized that preventing the development of the apoptotic phenotype would alter the timing of cell death in SM-injured cells, but not necessarily prevent it completely.

Adherent endothelial cells were pretreated with 100 μ M zVAD-FMK (a generalized inhibitor of caspases) for 1 hr prior to exposure to 0 or 100 μ M SM. The

MTT viability assay was then performed 2, 3, and 7 days after exposure to SM. Figure 26 demonstrates only slight improvement in cellular viability as measured with the MTT assay after generalized inhibition of caspases on days 2 and 3 and no difference after a week. Overall cellular morphology including spreading and cell-cell contact was better preserved initially after SM injury in cells treated with generalized caspase inhibition (Figure 27). A difference in appearance of surviving cells persisted at 7 days, however the SM-injured cells treated with a generalized caspase inhibitor demonstrated morphologic features (e.g. distorted cellular processes) that appeared to be more pathologic than the general appearance of cells surviving SM injury without any intervention (Fig. 27).

To clarify these observations, adherent endothelial cells exposed to 0 or 100 μ M SM with/without pretreatment with zVAD-FMK were harvested for assay of mitochondrial membrane potential (DiOC₆ fluorescence) and plasma membrane integrity (propidium iodide uptake) by flow cytometry at 16, 40, and 64 hr after SM exposure (Figure 28). By 40 hr there was substantial loss of mitochondrial membrane potential in cells exposed to SM alone, as well as loss of plasma membrane integrity (Fig. 28). Generalized inhibition of caspases largely prevented the loss of mitochondrial membrane potential and plasma membrane integrity seen in SM-injured cells at 40 hr. The protection persisted to a large extent at 64 hr as well (Figure 28).

Since there is a lag of several hours between SM exposure and activation of caspases (Figure 5B), we hypothesized that there might be a "window" of time after SM exposure during which caspase inhibition might be initiated to block development of the

apoptotic phenotype. Using the combined flow cytometric analysis of mitochondrial membrane potential and plasma membrane integrity, endothelial cells 20 hr after exposure to SM to which 100 μ M zVAD-FMK was added at various times pre or post SM injury were assayed (Figure 29). Substantial preservation of mitochondrial membrane potential and plasma membrane integrity was seen in cells exposed to both 100 and 250 μ M SM compared to control when the caspase inhibitor was added 1 hr after SM exposure (Fig. 29). In additional experiments (data not shown), caspase inhibition initiated as late as 6 hr after SM addition also limited the toxicity seen at 20 hr. Since caspase inhibition appears to delay or modulate some of the early toxicity of SM, these observations might have important implications for the treatment and prevention of SM-induced vesication.

DISCUSSION

In our work specifically addressing Task 1 of the SOW, we have found that keratinocytes do not as readily demonstrate many of the classical features of apoptosis as do endothelial cells. This has led to initial observations suggesting that necrosis may be the predominant form of keratinocyte death induced by SM. This impression was based on measurements of plasma membrane integrity in cells injured primarily with higher concentrations of SM (>250 μ M) and observed over relatively short time courses (0-6 hrs). With the recent explosion of interest in cell death, rapid additions to the basic understanding of the biochemical pathways regulating the process have occurred (4). This has necessitated the use of additional techniques to help more

completely address the hypotheses to be tested in this Task. The combination of assaying for phosphatidylserine translocation (Annexin V assay) and caspase-3 activation with a focus on longer time courses for measurement of the other cell death parameters have yielded a more complete and hopefully more accurate picture of keratinocyte death following SM exposure. The sometimes variable and ambiguous results with assays of nuclear changes associated with apoptosis probably reflect a relative lack of synchrony in the process of programmed cell death in keratinocytes compared to that seen with endothelial cells (5). Activation of caspase-3, the "central executioner" of apoptosis, as well as phosphatidylserine translocation, actin filament breakdown, and membrane budding, coupled with evidence of endonucleolytic cleavage of DNA on agarose gels and cleavage of gelsolin (Fig. 2) suggest that many of the classical execution phase events of apoptosis are induced by SM in keratinocytes. Data presented in Fig. 5B demonstrate a slower onset of caspase activation in keratinocytes than in endothelial cells. This observation may help account for the less synchronous demonstration of the apoptotic phenotype in keratinocytes. We request that the use of these additional techniques, which have been so helpful, be accepted as a revision to our SOW for completion of Task 1.

The concept that actin-myosin contraction may be an important element in apoptosis has been demonstrated by others in a model of cell death involving PC 12 cells (21). We have been unable to isolate the light chain of myosin (MLC) in Task 2 of the SOW to ultimately determine whether actin-myosin contraction, measured as MLC phosphorylation, occurs during SM injury. The technique has been difficult, and perhaps too dependent on a precipitating antibody of questionable utility. Our screening

experiments in Task 3 were designed to determine as much as possible with the use of inhibitors, a role for MLCK in SM injury which might be amenable to therapeutic interventions.

In Task 3 of the SOW, several screening techniques were used to determine if agents which affect actin filament organization and function would be potentially useful for altering the progression of apoptosis in SM-injured cells. The data which has been presented in Figures 7-11 of the Results section is largely negative. The MLCK inhibitors (ML7, ML9) exert toxic effects of their own and H₂CB does potentiate the morphologic effects of SM. Although the agents at low concentrations appeared to have modest protective effects during SM injury on the crudest parameter of cell death (plasma membrane integrity in the calcein assay), the MTT assay and measurement of mitochondrial membrane potential as well as cellular and cytoskeletal morphology demonstrated no protective effect with these inhibitors. Thus, even though limited effects can be obtained in late assays of viability using these agents in SM injury, the net effect is the same - no real change in the process or outcome of the injury. It is possible, however, (as will be discussed further below) that if the development of the characteristic apoptotic phenotype induced by SM can be delayed or significantly altered, pathophysiologic effects (e.g. capillary leak, keratinocyte separation from the basal lamina during vesication) which may be a result of apoptosis might be mitigated even though individual cells affected by SM may still ultimately be nonviable.

Studies with endothelial cytoplasts in Task 4 of the SOW yielded provocative and interesting findings. Although some of the SM-induced changes in endothelial cell and cytoskeletal morphology could be replicated in the cytoplasts,

caspace-3 activity and phosphatidylserine translocation induced by preparation of the cytoplasts was not enhanced or altered by SM injury. These studies have a number of implications for understanding SM injury. It is possible that caspace activation per se may not always be 'the point of no return' or sufficient to ensure that cell death will occur (37). The lack of the dramatic increase in caspace-3 activity (normalized to protein content) in cytoplasts which was seen in nucleated endothelial cells suggests that SM-mediated alkylation of nuclear DNA may be an important stimulus for caspace-3 in nucleated endothelial cells. That a different non-DNA damaging activator of caspaces, chelerythrine (Fig. 15) can induce essentially equal activation of endothelial cells and cytoplasts independent of the presence of a nucleus supports this possibility. SM-mediated changes in the cytoskeleton and morphology of cytoplasts suggest that either some elements of the apoptotic phenotype may be regulated independently of the caspace system or the changes detected are not truly apoptotic (i.e. cellular/cytoplast rounding may occur as a result of apoptotic or non-apoptotic mechanisms). Finally, it is possible that the baseline activation of caspace-3 associated with cytoplast preparation while not further responsive to SM may yet play a permissive role in supporting SM-mediated apoptotic morphological effects in cytoplasts. Thus, the experiments of Task 4 are supportive of the concept that DNA damage induced by SM may be a critical element necessary to the complete induction of the death program in cells exposed to SM. The cytoplast model may be quite useful in the toxicological assessment of agents which are thought to exert their toxicity via DNA damage.

In Task 5 of the SOW we have been able to reproducibly demonstrate in a model of moderate ATP depletion in endothelial cells the ATP-dependence of SM-

induced apoptosis (Fig. 18, Table 3) Furthermore, these studies have also underscored the role of metabolic effects (i.e. ATP loss) in regulating the interconversion between apoptosis and necrosis and has also confirmed and extended earlier work with other models demonstrating the ATP dependence of apoptosis (6-10). To effectively deplete keratinocyte ATP after killing the cells, a milder strategy based on glycolytic inhibition was used (Fig. 19). The same pattern of apoptotic dependence on ATP was seen in SM-injured keratinocytes (Table 4), as was seen with endothelial cells. The results of experiments addressing this task suggest that inhibition of apoptosis induced by SM results in a slower pattern of cell death.

Studies of GAPDH activity in endothelial cells and keratinocytes after exposure to SM (addressing Task 6 of the SOW) demonstrate that GAPDH is inhibited slightly during SM injury in endothelial cells (Fig. 20). The inhibition of GAPDH at the higher concentrations of SM (>250 μ M) may at least in part account for the ATP loss seen in cells after injury at these concentrations of SM. Since we have found very little evidence of ROS generation during SM injury (Task 7), GAPDH is probably inhibited directly by SM alkylation. However, direct inhibition of GAPDH by SM is a minor contributor to ATP loss during SM injury. Poly-(ADP-ribose) polymerase (PARP) activation and NAD loss after SM injury (38) are probably more critical to this process.

In our work addressing Task 7 we have found no clear-cut evidence of ROS generation during SM injury in endothelial cells and keratinocytes. Minimal levels of GSSG were generated in response to high dose SM exposure. Total GSH and viability measurements with and without the use of GSH-altering conditions (Fig. 22 and

Table 5) confirmed and extended other observations (39-41) demonstrating loss of GSH after SM exposure as well as the GSH-dependence of protective effects associated with NAC pretreatment. As has been seen by others (42) exogenous GSH addition also provided considerable protection during SM injury (e.g. Table 6). These results, in light of very low ROS activity measured as GSSG, are consistent with GSH acting in SM injury as a direct scavenger of SM.

Hockenbery, et. al. (17) have demonstrated in a physiologic (hormone-withdrawal) model of apoptosis the presence of ROS using parinaric acid oxidation within membranes and oxidation of dichlorofluorescein (a cytosolic marker of oxidation analogous to dihydrorhodamine 123) as ROS indicators. Where parinaric acid oxidation (lipid peroxidation) was inhibited either by overexpression of the proto-oncogene *bcl₂* or pretreatment with NAC, apoptosis was inhibited (17). We have adopted a similar strategy to determine if SM-injured cells generate ROS and then to examine the role of any ROS generated in SM-induced cell death.

The parinaric acid and dihydrorhodamine 123 assays have not provided supportive evidence for ROS generation during SM injury. Demonstration of NFκB activation following SM exposure, an event which is thought to involve ROS (35), suggests that SM may induce low level ROS generation as a byproduct of its activation of signal transduction processes within injured cells. Thus, our work in Task 7 does not support the hypothesis that the cellular toxicity seen in SM injury is mediated by a large burst of ROS induced by SM.

As a logical extension of the work addressing the seven tasks of the SOW, we have performed additional experiments to test the hypotheses that cellular commitment to death after SM exposure is irreversible but the pattern (and potentially the rate) of cell death can be modified by inhibition of the caspase system. In the experiments presented in Figs. 26-29 of the Results section, it was confirmed that generalized caspase inhibition did not alter the ultimate number of surviving cells (Fig. 26) seven days after SM exposure but it did prevent at least some of the elements of the apoptotic phenotype from developing, preserving, for example, a more intact cellular morphology in the short term (Fig. 27). In the first two to three days after SM exposure, pre and even post treatment with the generalized inhibitor of caspases, zVAD-FMK, was associated with substantial preservation of mitochondrial membrane potential and plasma membrane integrity. Preservation of cellular viability and morphology to a greater extent during this period of time could be relevant to preventing SM-induced vesication since vesication typically develops over a similar time course *in vivo*. Since the default mode of SM-induced cell death for both endothelial cells and keratinocytes is apoptotic, blocking the development of the apoptotic phenotype may well suppress or mitigate the process of SM-induced vesication.

We request that the additional work presented in this final report be accepted as a part of our SOW. We hope that our success in these areas will in part compensate for our inability to accomplish some of the other goals in the SOW (e.g. MLCK measurement in Task 2).

KEY RESEARCH ACCOMPLISHMENTS

- Confirmation and extension of others' work demonstrating that sulfur mustard activates many of the elements of programmed cell death or apoptosis in human keratinocytes, including activation of the caspase system.
- Demonstration that a variety of agents which act to alter microfilament organization or function are not particularly useful for the purpose of blocking the development of the apoptotic phenotype after sulfur mustard exposure.
- Development of a cytoplast (enucleated cell) model for evaluation of the role of the nucleus in sulfur mustard-mediated cell death in endothelial cells. Demonstration with this model that caspase activation and phosphatidylserine translocation induced by sulfur mustard appeared to require the presence of a nucleus.
- Apoptosis induced by sulfur mustard requires energy.
- Reaction oxygen species are not generated in large amounts in sulfur mustard injured cells and do not play a primary role in mediating sulfur mustard-induced cytotoxicity.
- Demonstration that sulfur mustard activates the nuclear transcription factor, NFκB.
- Demonstration with long-term culture (7 days) that cellular commitment to death after sulfur mustard exposure is largely irreversible.
- Demonstration that generalized caspase inhibition administered pre or post sulfur mustard exposure can suppress development of the apoptotic phenotype induced by sulfur mustard. Non-apoptotic cell death induced by sulfur mustard appears to develop more slowly over the first few days after SM exposure.

REPORTABLE OUTCOMES

Manuscripts Published During Funding Period Supported by the Department of Defense.

- 1) Lelli, Jr., J. L., Becks, L.L., Dabrowska, M.I., Hinshaw, D.B. ATP Converts Necrosis to Apoptosis in Oxidant-Injured Endothelial Cells. *Free Rad. Biol. Med.* 25:694-702, 1998.
- 2) Hinshaw, D.B., Lodhi, I.J., Hurley, L.L., Atkins, K.B., and Dabrowska, M.I. Activation of Poly [ADP-Ribose] Polymerase in Endothelial Cells and Keratinocytes: Role in an In Vitro Model of Sulfur Mustard-Mediated Vesication. *Toxicol. Appl. Pharmacol.* 156:17-29, 1999.
- 3) Sweeney, J.F., Nguyen, P.K., Atkins, K.B., and Hinshaw, D.B. Chelerythrine Chloride Induces Rapid PMN Apoptosis through Activation of Caspase-3. *Shock*. In Press, 2000.
- 4) Atkins, K.B., Lodhi, I.J., Hurley, L.L., and Hinshaw, D.B. N-acetyl-L-cysteine (NAC) and endothelial cell injury by sulfur mustard (SM). *J. Appl. Toxicol.* In Press, 2000.
- 5) Three additional manuscripts are in preparation addressing unpublished data presented in the final report.

Abstracts and Presentations.

- 1) Medical Defense Bioscience Review, Department of Defense, Hunt Valley, MD, "N-acetyl-L-cysteine (NAC) and endothelial cell injury by sulfur mustard (SM)." June, 1998.

Patents and Licenses Applied for and/or Issued. None.

Degrees Obtained that are Supported by this Award. None.

Development of Cell Lines, Tissue or Serum Repositories. None.

Informatics Such as Databases and Animal Models, etc. None.

Funding Applied for Based on Work Supported by this Award.

U.S. Department of Defense Log #99329002 (2000-2003) "Regulation of Polymorphonuclear Leukocyte Survival and Function by Proinflammatory Agents that are Released as a Consequence of Sulfur Mustard-Mediated Injury (\$490,338) Co-Investigator (P.I. John Sweeney, M.D.)

Employment or Research Opportunities Applied for and/or Received on

Experiences/Training Supported by this Award.

Principal Investigator promoted to Full Professor of Surgery, University of Michigan during the period of the award.

List of Personnel Receiving Pay from this Research Effort.

Lauren Becks

Kevin Atkins

Irfan Lodhi

Russell Clift

CONCLUSIONS

The work presented in this final report has helped to clarify the nature of cell death induced in endothelial cells and keratinocytes by SM. Although the "classic" features of apoptosis are demonstrated in a fairly rapid and synchronous manner in

endothelial cells (5), keratinocyte death after SM exposure follows a somewhat less synchronous pattern of apoptosis. We have confirmed and extended the work of others (13) that SM activates caspases in keratinocytes. The time course of caspase-3 activation by SM in keratinocytes was slower than that in endothelial cells which may help to account for the less synchronous pattern of apoptosis in keratinocytes. The ATP dependence of SM-induced apoptosis was confirmed. Cell death induced by SM when apoptosis is inhibited appears to develop more slowly. Work with enucleated cytoplasts suggests that DNA alkylation by SM may be an important element required for full caspase activation in SM-induced apoptosis. ROS are not important direct mediators of SM toxicity. Thus, our work suggests that the alkylating effects of SM induce apoptosis in endothelial cells and keratinocytes. Cellular commitment to death after SM injury is irreversible. However, the pattern and timing of death-related events can be altered by inhibition of caspase activation (even when inhibition is initiated a few hours after SM exposure). Interruption of the full development of the apoptotic phenotype after SM exposure by blockade of caspase activation may represent a potentially useful therapeutic strategy for managing cutaneous exposure to SM.

REFERENCES

1. Schwartzman, R.A. and Cidlowski, J.A. Apoptosis: the biochemistry and molecular biology of programmed cell death. *Endocrine Rev.* 14:133-151, 1993.
2. Schwartz, L.M. and Osborne, B.A. Programmed cell death, apoptosis and killer genes. *Immunol. Today* 14:582-590, 1993.

3. Gerschenson, L.E. and Rotello, R.J. Apoptosis: a different type of cell death. *FASEB J.* 6:2450-2455, 1992.
4. Hetts, S.W. To die or not to die: An overview of apoptosis and its role in disease. *JAMA* 279:300-307, 1998.
5. Dabrowska, M.I., Becks, L.L., Lelli, Jr., J.L., Levee, M.G., and Hinshaw, D.B. Sulfur mustard induces apoptosis and necrosis in endothelial cells. *Toxicol. Appl. Pharmacol.* 141:568-583, 1996.
6. Leist, M., Single, B., Castoldi, A.F., Kuhnle, S., Nicotera, P. Intracellular adenosine triphosphate (ATP) concentration: A switch in the decision between apoptosis and necrosis. *J. Exp. Med.* 185:1481-1486, 1997.
7. Eguchi, Y., Shimizu, S., and Tsujimoto, Y. Intracellular ATP levels determine cell death fate by apoptosis or necrosis. *Cancer Res.* 57:1835-1840, 1997.
8. Stefanelli, C., Bonavita, F., Stanie, I., Farruggia, G., Falcieri, E., Robuffo, I., Pignatti, C., Muscari, C., Rossoni, C., Guarnieri, C., Caldarella, C.M. ATP depletion inhibits glucocorticoid-induced thymocyte Apoptosis. *Biochem. J.* 322:909-917, 1997.
9. Kass, G.E.N., Eriksson, J.E., Weis, M., Orrenius, S., and Chow, S.C. Chromatin condensation during apoptosis requires ATP. *Biochem. J.* 318:749-752, 1996.
10. Lelli, Jr., J.L., Becks, L.L., Dabrowska, M.I., and Hinshaw, D.B. ATP converts necrosis to apoptosis in oxidant-injured endothelial cells. *Free Rad. Biol. Med.* 25(6):694-702, 1998.
11. Nagata, S. Apoptosis by death factor. *Cell* 88:355-365, 1997.

12. Alnemri, E.S., Livingston, D.J., Nicholson, D.W., Salvesen, G., Thornberry, N.A., Wong, W.W., and Yuan, J. Human ICE/CED-3 protease nomenclature. *Cell* 87(2):171, 1996.
13. Rosenthal, D.S., Simbulan-Rosenthal, C.M., Iyer, S., Spoonde, A., Smith, W., Ray, R., and Smulson, M.E. Sulfur mustard induces markers of terminal differentiation and apoptosis in keratinocytes via a Ca^{+2} -calmodulin and caspase-dependent pathway. *J. Invest. Dermatol.* 111:64-71, 1998.
14. Mitra, R.S., Wrone-Smith, T., Simonian, P., Foreman, K.E., Nunez, G., and Nickoloff, B.J. Apoptosis in keratinocytes is not dependent on induction of differentiation. *Lab. Invest.* 76:99-107, 1997.
15. Korb, L.C. and Ahearn, J.M. Clq binds directly and specifically to surface blebs of apoptotic human keratinocytes: Complement deficiency and systemic lupus erythematosus revisited. *J. Immunol.* 158:4525-4528, 1997.
16. Leverkus, M., Yaar, M., and Gilchrist, B.A. Fas/Fas ligand interaction contributes to UV-induced apoptosis in human keratinocytes. *Exp. Cell Res.* 232:255-262, 1997.
17. Hockenbery, D.M., Altvai, Z.N., Yin, X-M, Milliman, C.L., and Korsmeyer, S.J. Bcl-2 functions in an antioxidant pathway to prevent apoptosis. *Cell* 75:241-251, 1993.
18. Wulf, E., Deboren, A., Bantz, F.A., Faulstich, H., and Wieland, T.H. Fluorescent phallotoxin, a tool for the visualization of cellular actin. *Proc. Natl. Acad. Sci. USA* 76:4498-4502, 1979.
19. Duke, R.C. and Cohen, J.J. Morphological and biochemical assays of apoptosis. *Current Protocols in Immunology Suppl.* 3.17:1-16, 1992.

20. Mosmann, T. Rapid colorimetric assay for cellular growth and survival: Application to proliferation and cytotoxicity assays. *J. Immunol. Meth.* 65:55-63, 1983.
21. Mills, J.C., Stone, N.L., Erhardt, J., and Pittman, R.N. Apoptotic membrane blebbing is regulated by myosin light chain phosphorylation. *J. Cell Biol.* 140:627-636, 1998.
22. Roos, D., Voetman, A.A., and Meerhof, L. J. Functional activity of enucleated human polymorphonuclear leukocytes. *J. Cell Biol.* 97:368-377, 1983.
23. Hinshaw, D.B., Miller, M.T., Omann, G.M., Beals, T.F., and Hyslop, P.A. A cellular model of oxidant-mediated neuronal injury. *Brain Res.* 615:13-26, 1993.
24. Hinshaw, D.B., Burger, J.M., Delius, R.E., and Hyslop, P.A. Mechanism of protection of oxidant-injured endothelial cells by glutamine. *Surgery* 108:298-304, 1990.
25. Brehe, J.E., and Burch, H.B. Enzymatic assay for glutathione. *Anal. Biochem.* 74:189, 1976.
26. Griffith, O.W. Determination of glutathione and glutathione disulfide using glutathione reductase and 2-vinyl-pyridine. *Anal. Biochem.* 106:207, 1980.
27. Royall, J.A. and Ischiropoulos, H. Evaluation of 2',7'-Dichlorofluorescein and Dihydrorhodamine 123 as Fluorescent Probes for Intracellular H₂O₂ in Cultured Endothelial Cells. *Arch. Biochem. Biophys.* 302:348-355, 1993.
28. Schreiber, E., Matthias, P., Muller, M.M., and Schaffner, W. Rapid detection of octamer binding proteins with 'mini-extracts', prepared from a small number of cells. *Nucleic Acids Res.* 17(15):6419.

29. Dignam, J.D., Lebovitz, R.M., and Roeder, R.G. Accurate transcription initiation by RNA polymerase II in a soluble extract from isolated mammalian nuclei. *Nucleic Acid Res.* 11:1(5):1475-1489, 1983.
30. Bedner, E., Li, X., Gorczyca, W., Melamed, M.R., and Darzynkiewicz, Z. Analysis of apoptosis by laser scanning cytometry. *Cytometry* 35(3):181-195, 1999.
31. Sweeney, J.F., Nguyen, P.K., Atkins, K.B., and Hinshaw, D.B. Chelerythrine Chloride Induces Rapid PMN Apoptosis through Activation of Caspase-3. *Shock*. In press, 2000.
32. Hinshaw, D.B., Burger, J.M., Miller, M.T., Adams, J.A., Beals, T.F., and Omann, G.M. ATP depletion induces an increase in the assembly of a labile pool of polymerized actin in endothelial cells. *Am. J. Physiol.* 264 (Cell Physiol. 33):C1171-C1179, 1993.
33. Hyslop, P.A., Hinshaw, D.B., Halsey, W.A., Jr., Schraufstatter, I.U., Sauerheber, R.D., Spragg, R.G., Jackson, J.H., Cochrane, C.B. Mechanisms of oxidant-mediated cell injury: The glycolytic and mitochondrial pathways of ADP phosphorylation are major intracellular targets inactivated by hydrogen peroxide. *J. Biol. Chem.* 263:1665, 1988.
34. Schraufstatter, I.U., Hinshaw, D.B., Hyslop, P.A., Spragg, R.G., and Cochrane, C.G. Glutathione cycle activity and pyridine nucleotide levels in oxidant-induced injury of cells. *J. Clin. Invest.* 76:1131-1139, 1985.
35. Meyer, M., Schreck, R., and Baeuerle, P.A. H₂O₂ and antioxidants have opposite effects on activation of NF-kappa B and AP-1 in intact cells: AP-1 as secondary antioxidant-responsive factor. *EMBO J* 12(5):2005-2015, 1993.

36. Atkins, K.B., Lodhi, I.J., Hurley, L.L., and Hinshaw, D.B. N-acetyl-L-cysteine (NAC) and endothelial cell injury by sulfur mustard (SM). *J. Appl. Toxicol.* In Press, 2000.
37. Zeuner, A., Eramo, A., Peschle, C., and DeMaria, R. Caspase activation without death. *Cell Death and Differentiation* 6:1075-1080, 1999.
38. Hinshaw, D.B., Lodhi, I.J., Hurley, L.L., Atkins, K.B., and Dabrowska, M.I. Activation of Poly [ADP-Ribose] Polymerase in Endothelial Cells and Keratinocytes: Role in an In Vitro Model of Sulfur Mustard-Mediated Vesication. *Toxicol. Appl. Pharmacol.* 156:17-29, 1999.
39. Langford, A.M., Hobbs, M.J., Upshall, D.G., Blain, P.G., Williams, F.M. The effect of sulphur mustard on glutathione levels in rat lung slices and the influence of treatment with arylthiols and cysteine esters. *Human & Exp. Toxicol.* 15(8):619-624, 1996.
40. Ray, R., Legere, R.H., Majerus, B.J., Petrali, J.P. Sulfur mustard-induced increase in intracellular free calcium level and arachidonic acid release from cell membrane. *Toxicol. & Applied Pharm.* 131(1):44-52, 1995.
41. Gross, C.L., Innace, J.K., Hovatter, R.C., Meier, H.L., and Smith, W.J. Biochemical manipulation of intracellular glutathione levels influences cytotoxicity to isolated human lymphocytes by sulfur mustard. *Cell Biol. & Toxicol.* 9:259-267, 1993.
42. Smith, C.N., Lindsay, C.D., Upshall, D.G. Presence of methenamine/glutathione mixtures reduces the cytotoxic effect of sulphur mustard on cultured SVK-14 human keratinocytes in vitro. *Human & Exp. Toxicol.* 16(5):247-253, 1997.

FIGURE LEGENDS

Figure 1. Micrographs of SM-treated keratinocytes. Keratinocytes grown in six-well plates were treated with 0, 10, 50, and 100 μ M SM and stained with Wright-Giemsa after 72 hours. A) 0 μ M SM; B) 10 μ M SM; C) 50 μ M SM; D) 100 μ M SM. Note the appearance of apoptotic bodies at 50 μ M (C) and 100 μ M (D) SM. 400X original magnification.

Figure 2. Execution phase events in SM-injured keratinocytes. A) Agarose gel analysis of DNA extracted from keratinocytes after SM injury. DNA from control and SM-injured keratinocytes was isolated at various time points and run on a 1.6% agarose gel, as described in the Methods Section. Lane 1, control (vehicle alone). Lanes 2, 4, and 6, cells 16, 20, and 24 hr after exposure to 100 μ M SM, respectively. Lanes 3, 5, and 7 cells 16, 20, and 24 hr after exposure to 250 μ M SM, respectively. Note the presence of "DNA ladders" in lanes 3 and 5, evidence of endonucleolytic cleavage of DNA after injury with 250 μ M SM.

B) Gelsolin cleavage induced by SM in keratinocytes. Whole cell lysates from control and SM-injured cells were harvested at various times and immunoblotted with an anti-gelsolin monoclonal antibody that recognizes the full length (80 kDa) and the 41 kDa cleavage product. Lanes are as in A.

Figure 3. Fluorescence micrographs of microfilaments in SM-injured keratinocytes. Keratinocytes grown in six-well plates were treated with 0, 10 or 50 μ M SM and were stained with rhodamine phalloidin at the times indicated. A) 0 μ M SM, 72h; B) 50 μ M SM, 24h; C) 50 μ M SM, 48h; D) 50 μ M SM, 72h; E) 10 μ M SM, 72h. Note the progressive disruption of cytoskeletal organization with 50 μ M SM (B-D) and the appearance of many apoptotic cells at 72 hr. 400X original magnification.

Figure 4. The effect of SM on keratinocyte viability was assessed flow cytometrically using annexin V binding (a measure of apoptosis) and propidium iodide (PI) staining (an indicator of necrosis) as described in the methods. Dot plots (A-E) are for cells at 24 hr after treatment with 0, 10, 50, 100 and 250 μ M SM, respectively. Cells in the lower left quadrants are viable cells (annexin and PI negative). Cells in the lower

right quadrants are apoptotic (annexin positive). Cells in the upper quadrants are necrotic cells (PI positive). The dot plots are from a representative experiment repeated three times. Note the increase in the number of apoptotic cells in the lower right quadrants of panels C and D. In panel E, note the shift in the population to the upper quadrants, an indication of a loss of membrane integrity.

Figure 5. Caspase-3 activities in sulfur mustard-treated human keratinocytes and bovine endothelial cells.

A) Cells were treated with 0, 10, 50, 100 and 250 μ M sulfur mustard and harvested at indicated intervals after treatment. Caspase-3 activities were determined as described in Experimental Methods and Procedures. Graphs indicate mean \pm SD for N = 3 separate determinations. Note the considerable variation from day to day in the absolute increase in caspase activity after SM exposure (particularly in the keratinocytes). B) Shorter time course of caspase activation in keratinocytes and endothelial cells. Cells were exposed to 0, 100, or 250 μ M SM and then caspase activity was measured at the indicated times. Data are from representative experiments performed in triplicate on three separate occasions. The other experiments are presented as insets above each figure.

Figure 6. Western blot analysis of myosin light chain phosphorylation in response to sulfur mustard treatment. Human keratinocytes were harvested 16 hr after treatment with 0, 10, 50, 100, or 250 μ M sulfur mustard. Myosin complexes were immunoprecipitated with a myosin heavy chain-specific antibody, electrophoresed and transferred to a membrane as described in Experimental Methods and Procedures. Probing with an anti-phosphoserine antibody detected a band of ~20 kDa, which was thought to be the myosin light chain (indicated by arrow) (Fig. 6A). Unfortunately, on further repetition with the precipitating antibody alone as a control (Fig. 6B, lane CF [cell free]), it was determined that the ~20 kDa band identified earlier in Fig. 6A was the light chain of the precipitating antibody.

Figure 7. Forward light scatter analysis of cell size changes associated with SM injury. Endothelial cells and keratinocytes 16 and 40 hr after exposure to 0, 100, or 250 μ M SM were analyzed by flow cytometry for their forward light scatter characteristics (a correlate of cell size). Note the reductions in mean forward

light scatter (size) particularly at 40 hr after SM exposure for both cell types and the apparent dose-dependence. Compare this representative experiment with the visual confirmation of cell shrinkage/rounding in Figs. 1 and 3.

Figure 8. Effects of 1 hour pretreatment with various doses of ML7, ML9, phalloidin and dihydrocytochalasin B on viability 40 hours after injury with 100 μ M sulfur mustard. Endothelial cells were pretreated with the indicated doses of ML7, ML9, phalloidin, H₂CB or DMSO (vehicle control) for one hour prior to the addition of 100 μ M sulfur mustard. 40 hours after SM exposure, MTT was added to a final concentration of 125 μ g/ml. After 1 hr incubation at 37° C, the medium was aspirated and the plates were stored at -70° C. To assay, the precipitated dye was solubilized in 1 ml DMSO and the absorbance was measured at 560 nm. Values are expressed as the percent of the A560 measured in the DMSO pretreated, uninjured samples and represent the average + S.D. of three independent experiments.

Figure 9. Fluorescence micrographs of adherent endothelial cells stained with rhodamine phalloidin - effect of cytoskeletal inhibitors on cellular and microfilament morphology during SM injury. The cells which had been pretreated for 1 hr with the designated concentrations of the different inhibitors were incubated for 16 hrs after exposure to 0 or 100 μ M SM and then fixed and stained with rhodamine phalloidin to visualize the microfilament architecture. A) control, uninjured cells, B) SM alone, C) 1 μ M ML7 alone, D) 1 μ M ML7 plus SM, E) 10 μ M ML9 alone, F) 10 μ M ML9 plus SM, G) 10 μ g/ml phalloidin alone, H) 10 μ g/ml phalloidin plus SM, I) 10 μ M H₂CB alone, J) 10 μ M H₂CB plus SM, 400x magnification.

Figure 10. Flow cytometric analysis of endothelial and keratinocyte plasma membrane integrity (calcein assay) 16 and 40 hr after SM injury - effect of cytoskeletal inhibitors. Cells pretreated with the different concentrations of each inhibitor as indicated were assayed by flow cytometry for uptake, cleavage of calcein AM, and retention of calcein as an indication of plasma membrane integrity 16 and 40 hr after exposure to 100 μ M SM. A) effect of ML7 (0-30 μ M), B) effect of ML9 (0-30 μ M), c) effect of phalloidin

(0-10 $\mu\text{g/ml}$), and D) effect of H_2CB (0-10 μM). Note the loss of cells from the gated (boxed) control region to a lower fluorescence (less viable) and decreased forward light scatter (smaller size) in cells injured with SM alone. The lower concentrations of each agent appeared to inhibit the loss of plasma membrane integrity and decrease in cell size (particularly at 40 hr).

Figure 11. Mitochondrial membrane potential in endothelial cells 40 hr after exposure to 100 μM SM - effect of cytoskeletal inhibitors. Changes in mitochondrial membrane potential ($\Delta\psi\text{m}$) were measured by flow cytometry of cells stained with DiOC_6 (please see Methods). SM injury dramatically reduced the DiOC_6 fluorescence of $\sim 50\%$ of the cells (upper right histogram). None of the inhibitors blocked the loss of DiOC_6 fluorescence induced by SM. Indeed, ML7, ML9 and H_2CB alone induced some loss of DiOC_6 fluorescence. Representative experiment repeated three times. Higher concentrations of the inhibitors did not alter the outcome (data not shown).

Figure 12. Viability of endothelial cytoplasts. The viability of endothelial cytoplasts which had been prepared and allowed to adhere overnight was assessed by their ability to cleave calcein AM and retain calcein fluorescence within their cytosol. The calcein fluorescence (viability) of control nucleated endothelial cells and enucleated endothelial cytoplasts loaded with 4 μM calcein AM was confirmed by flow cytometry before and after membrane lysis was induced by the addition of 1% Triton X100 (final concentration). Representative experiment repeated more than once.

Figure 13. Fluorescence micrographs of endothelial cells and cytoplasts after SM exposure. Adherent cells/cytoplasts were fixed and stained with rhodamine phalloidin to visualize microfilaments. A) control, uninjured endothelial cells, B) control, uninjured cytoplasts, C) endothelial cells 2 hr after exposure to 250 μM SM, D) cytoplasts 2 hr after exposure to 250 μM SM, E) endothelial cells 2 hr after exposure to 500 μM SM, F) cytoplasts 2 hr after exposure to 500 μM SM. 400x original magnification for all. Note the presence of long actin filaments in cytoplasts (B) and rounding after SM, especially in F.

Figure 14. Flow cytometric confirmation of cytoplast purity. Endothelial cells and cytoplasts were permeabilized with .02% digitonin and exposed to 5 $\mu\text{g}/\text{ml}$ propidium iodide (PI). The two PI stained populations (cells/cytoplasts) were then compared by flow cytometry. Figure is from a representative experiment repeated five times.

Figure 15. Caspase-3 activity in endothelial cells and cytoplasts. Cytoplasts which had been allowed to adhere and grow overnight in culture after preparation were exposed to SM (500 μM) or chelerythrine (25 μM) (a potent activator of caspases in neutrophils) for 6 hr and were compared to intact endothelial cells. Caspase activity was normalized to protein content. Each bar represents the mean \pm S.D. of N = 3-6 separate determinations. *, ($p < 0.05$) vs control cells; #, ($p < 0.05$) vs control cytoplasts. Note the significant ($p < 0.05$) baseline increase in caspase activity in untreated cytoplasts compared to untreated control endothelial cells. Also, note the large increase in caspase activity of endothelial cells in response to 500 μM SM and the minimal (N.S.) increase in caspase activity seen in the SM-injured cytoplasts. There was a better response (increase in caspase activity) in cytoplasts to chelerythrine, which was comparable to the response of nucleated endothelial cells.

Figure 16. Annexin V analysis of endothelial cells and cytoplasts. The Annexin V (a measure of apoptosis) and PI (a measure of plasma membrane integrity) staining techniques as described in the Methods were used to assess apoptotic changes in endothelial cells and cytoplasts 6 hr after exposure to 500 μM SM. A) dot plot of control endothelial cells, B) dot plot of endothelial cells 6 hr after exposure to 500 μM SM, C) dot plot of control cytoplasts, D) dot plot of cytoplasts after exposure to 500 μM SM. Representative experiment repeated 3 times. Upper panel - nonviable cells; lower left panel - viable non-apoptotic cells/cytoplasts; lower right panel - apoptotic cells/cytoplasts (i.e. exposed phosphatidylserine residues with increased Annexin V staining). Note the large number of cytoplasts with exposed phosphatidylserine residues in the control C compared with essentially the same dot plot for SM-injured cytoplasts in D.

Figure 17. Time course of caspase activation in cytoplasts after preparation. Caspase-3 activity normalized to protein content was measured as described in the Methods starting two hours after the end of cytoplast preparation and was compared at 12 hr to control endothelial cells in this single experiment.

Figure 18. The effect of SM on ATP levels in endothelial cells. Cells incubated in the absence (A) or presence (B) of ATP depletion conditions described in the Methods were treated with 0-500 μ M SM and harvested at 1, 6 and 24 hr. The ATP levels were determined as previously described.

Figure 19. The effect of glycolytic inhibition and SM on keratinocyte ATP levels. Decreasing levels of available glucose were combined with increasing levels of the glycolytic inhibitor, 2-deoxyglucose to produce variable reductions in ATP levels in keratinocytes during exposure to 0-500 μ M SM. Steady state ATP levels were measured at 24 hr after SM exposure for comparison with viability determinations in Table 4. Solid bar = 5.5 mM glucose; open bar = 2.75 mM glucose and 2.75 mM 2-deoxyglucose; gray bar = 1.375 mM glucose and 4.125 mM 2-deoxyglucose; hatched bar = 5.5 mM 2-deoxyglucose. Each bar represents the mean + S.D. of N=3 separate determinations. Complete substitution of 2-deoxyglucose for glucose in the cellular media resulted in a steady state reduction in endothelial cell ATP levels of ~10% of control levels and created the possibility to examine the role of ATP in keratinocyte death patterns after SM exposure.

Figure 20. The effect of SM on glyceraldehyde-3-phosphate dehydrogenase (GAPDH) activity was determined in endothelial cells (A) and keratinocytes (B) as described in the methods. The activity is expressed as the rate of NAD reduction measured at 340 nm. n=3

Figure 21. Formation of oxidized glutathione (GSSG) in endothelial cells and keratinocytes after SM exposure. GSSG levels (expressed as a percentage of total GSH equivalents) were measured at 1 and 6 hr after exposure to 0 or 500 μ M SM as described in the Methods. Each data point represents the mean \pm S.D. of N=3 separate determinations.

Figure 22. Effects of buthionine sulfoximine (BSO) and N-acetyl-cysteine (NAC) on GSH levels in SM-treated endothelial cells (A) and keratinocytes (B). After an overnight treatment with BSO and NAC, controls and cells treated with 500 μ M SM were harvested at 1 and 6 hrs post injury and the total GSH levels were determined as described in the methods. n=3-6

Figure 23. Effect of SM on lipid peroxidation in endothelial cells. Parinaric acid labeled cells were treated with SM or tert-butylhydroperoxide (t-BuOOH) in the absence (A) or presence (B) of 500 μ M alpha-tocopherol. Fluorescence was read at 1 and 3 hr using a spectrofluorometer. Data are expressed as a percent of the control at 1 hr (minus alpha-tocopherol). n=3

Figure 24. Measurement of oxidant production in SM-treated endothelial cells and keratinocytes using dihydrorhodamine-123 (H2Rh-123). Control and SM-treated cells labeled with 30 μ M h2Rh-123 were harvested at 1 and 3 hr and the fluorescence was read using a FACScan flow cytometer. Data are presented as histograms of Rh-123 fluorescence within endothelial cells (A) and keratinocytes (B) 1 and 3 hr after exposure to i) 0 SM, ii) 250 μ M SM, iii) 500 μ M SM, and in A, iv) 100 μ M H₂O₂, a positive control. Numbers in the upper right of each histogram are the mean channel number for fluorescence of that sample. Representative experiment repeated 3-6 times.

Figure 25. Electrophoretic mobility shift analysis of nuclear extracts of endothelial cells exposed to sulfur mustard. Confluent endothelial cells were pretreated with or without 50 mM NAC for at least 16h. Cells were then treated with 0, 250 μ M or 500 μ M SM for 2 or 5h without media change. Nuclear extracts were prepared and 5 μ g of protein was incubated with a ³²P-labeled consensus NF κ B oligonucleotide (30,000 cpm) for 20 min. at room temp. The binding reactions were then resolved by polyacrylamide gel electrophoresis and exposed to x-ray film at -70°C. Note the increase in NF κ B activity induced by 500 μ M SM as early as 2 hr. At 5 hr, 250 μ M SM also induced a smaller increase in NF κ B activity. NAC alone

also induced NF κ B activity. The variable effects of NAC may reflect its ability to act both as an oxidant and as a stimulus for GSH synthesis (36).

Figure 26. Effect of caspase inhibition on SM-induced loss of viability. Endothelial cells were treated with 100 μ M zVAD-FMK for 1 hr prior to exposure to 100 μ M sulfur mustard. At indicated intervals following SM exposure, 250 μ g/ml MTT was added and the cells were incubated for 1 hr at 37 $^{\circ}$ C before the medium was removed and the cells stored at -70 $^{\circ}$ C. At the time of assay, the precipitated dye was solubilized in DMSO and the absorbance was read at 560 nm. Values represent the mean + S.D. for multiple experiments. (n= 2 for 2 and 3 day values, n=3 for 7 day values).

Figure 27. The effect of caspase inhibition on endothelial cell morphology after SM exposure. Phase contrast photomicrographs were taken of adherent endothelial cells 16 hr and 7 days after exposure to 100 μ M SM with/without pretreatment with 100 μ M zVAD-FMK. A) control, uninjured cells at 16 hr, B) cells 16 hr after exposure to 100 μ M SM, C) cells 16 hr after exposure to 100 μ M SM pretreated with zVAD-FMK, D) control, uninjured cells at 7 days, E) surviving cells 7 days after exposure to 100 μ M SM, and F) surviving cells pretreated with zVAD-FMK 7 days after exposure to 100 μ M SM. Note the presence of giant cells in E and the attenuation and distortion of cellular processes in F. 200x original magnification for all.

Figure 28. The effect of generalized caspase inhibition with zVAD-FMK on endothelial mitochondrial membrane potential and plasma membrane integrity. Endothelial cells at 16, 40, and 64 hr after exposure to 100 μ M SM with or without pretreatment with 100 μ M zVAD-FMK were assayed by flow cytometry for mitochondrial membrane potential and propidium iodide (PI) uptake. A) R₁ = population of cells (control) with high mitochondrial membrane potential (increased DiOC₆ fluorescence). R₂ = population of cells with low mitochondrial membrane potential (decreased DiOC₆ fluorescence). R₃ = PI positive cells (i.e. cells with loss of plasma membrane integrity). Representative experiment repeated 3 times. Note the loss of cells from R₁ into R₂ and R₃ from 40 hr after exposure to 100 μ M SM, which is largely attenuated

by pretreatment with zVAD-FMK. B) Graphical depiction of mean \pm S.D. of % of cells in R₁ for 3 different experiments over 64 hr time course demonstrating marked preservation of mitochondrial membrane potential and plasma membrane integrity in SM-injured cells pretreated with zVAD-FMK.

Figure 29. The effect of generalized caspase inhibition pre and post exposure to SM on endothelial cell viability. Endothelial cells 20 hr after exposure to either 100 or 250 μ M SM, which had received treatment with 100 μ M zVAD-FMK at either 1 hr or 5 min before SM addition or 30 min and 1 hr after SM addition were assayed as described in the legend for Fig. 28 for mitochondrial membrane potential and plasma membrane integrity. Substantial protection (preservation of the population in R₁) was seen for both concentrations of SM at all times of addition of the zVAD-FMK. Representative experiment repeated 3 times.

TABLE 1 Effect of Sulfur Mustard on Keratinocyte viability.**16 hr**

<u>μM SM</u>	<u>%Viable</u>	<u>%Apoptotic</u>	<u>%Necrotic</u>
0	91.4± 3.7	0.4± 0.5	8.6± 3.8
10	85.1±10.5	3.3± 3.7	13.1± 8.3
50	68.4±17.0	10.6±11.1	14.6± 9.7
100	71.2±15.7	12.1± 8.2	16.8±14.0
250	58.1±14.8	16.4±10.8	25.6±11.3

24 hr

<u>μM SM</u>	<u>%Viable</u>	<u>%Apoptotic</u>	<u>%Necrotic</u>
0	86.8± 5.0	2.3± 1.7	10.9± 5.0
10	71.4± 8.9	14.0±11.2	14.7± 6.3
50	70.9±12.2	18.1±15.4	13.9± 5.1
100	63.7± 7.1	12.8± 4.8	23.5±10.2
250	41.1±15.6	19.9± 5.0	39.0±12.1

48 hr

<u>μM SM</u>	<u>%Viable</u>	<u>%Apoptotic</u>	<u>%Necrotic</u>
0	83.4± 7.9	3.7± 3.7	14.6± 7.3
10	71.5±15.1	2.7± 2.1	25.8±13.8
50	60.7±21.7	2.4± 2.5	36.7±22.8
100	41.8±13.5	5.6± 3.2	52.5±16.1
250	12.0± 4.2	5.6± 2.9	82.4± 6.1

72 hr

<u>μM SM</u>	<u>%Viable</u>	<u>%Apoptotic</u>	<u>%Necrotic</u>
0	78.1±13.4	3.3± 2.9	18.5±15.4
10	64.3±26.9	5.7± 8.7	29.9±27.6
50	60.3±27.8	3.3± 3.2	36.6±28.8
100	35.3±24.1	5.3± 4.6	61.0±26.2

Cells grown in six-well plates were treated with sulfur mustard at the concentrations and for the times indicated. Cells were trypsinized and stained with a mixture of acridine orange and ethidium bromide as described in the Methods. At least 100 cells were counted and the number for each category (i.e. Viable (V), Apoptotic (A) or Necrotic (N)) represents the mean percentage of total cells counted demonstrating that pattern. (n=5).

TABLE 2 Viability Determination in SM-Treated Keratinocytes using Annexin V and Propidium Iodide.

24 hr

<u>μM SM</u>	<u>%Viable</u>	<u>%Apoptotic</u>	<u>%Necrotic</u>
0	85.9±9.2	3.6±1.4	7.9±5.5
10	81.1±5.8	6.2±5.9	6.8±3.4
50	69.7±8.6	11.4±8.8	11.7±7.2
100	69.1±9.8	13.9±3.6	12.3±4.4
250	52.1±23.4	16.7±5.8	22.8±6.2

48 hr

<u>μM SM</u>	<u>%Viable</u>	<u>%Apoptotic</u>	<u>%Necrotic</u>
0	84.1±3.7	4.6±1.9	11.2±3.8
10	71.0±6.6	7.5±4.2	21.5±5.2
50	64.9±10.3	8.6±1.5	26.5±11.8
100	46.2±10.7	18.0±8.3	35.8±5.9
250	14.9±9.3	29.9±17.2	54.9±8.2

72 hr

<u>μM SM</u>	<u>%Viable</u>	<u>%Apoptotic</u>	<u>%Necrotic</u>
0	80.6±10.4	4.2±3.0	14.4±8.5
10	73.9±13.9	5.8±4.9	17.4±11.6
50	67.2±11.1	7.4±2.4	22.7±12.8
100	32.4±18.6	26.8±18.1	38.7±6.1

Control and SM-Treated keratinocytes were harvested at 24, 48 and 72 hr and stained with FITC-conjugated annexin V and propidium iodide. The fluorescence was read on a FACScan flow cytometer. N=3.

Table 3A. Effect of ATP Depletion on Sulfur Mustard Injury in Endothelial Cells (6H)

<u>ATP Depletion</u>		<u>μM SM</u>			
		<u>0</u>	<u>100</u>	<u>250</u>	<u>500</u>
%V	Y	91.5±5.06	86.5±4.44	83.25±3.59	67.5±10.02
%V	N	91.5±2.38	86.75±4.5	82.25±2.75	53.25±15.04
%A	Y	1.5±0.58	2.5±1.0	5.75±.96	13.25±6.45
%A	N	1.75±0.5	5.0±2.94	8.5±2.89	27.0±8.29
%N	Y	7.0±4.97	11.0±3.65	11.0±2.83	19.5±5.75
%N	N	6.75±2.22	8.25±3.30	9.25±1.71	19.8±8.5

Table 3B. Effect of ATP Depletion on Sulfur Mustard Injury in Endothelial Cells (24H)

<u>ATP Depletion</u>		<u>μM SM</u>			
		<u>0</u>	<u>100</u>	<u>250</u>	<u>500</u>
%V	Y	89.66±2.52	66.33±10.41	19.0±10.15	4.0±1.41
%V	N	88.67±2.89	56.33±7.64	17.67±10.02	11.5±12.02
%A	Y	1.67±1.15	20.33±11.24	52.0±11.14	12.5±7.78
%A	N	3.0±0.0	38.0±12.49	60.67±22.5	31.5±17.68
%N	Y	8.67±2.89	12.33±1.53	27.67±8.14	83.5±6.36
%N	N	6.67±2.89	10.33±2.52	20.67±14.15	57.0±29.70

Endothelial cells were incubated in the presence or absence of ATP depletion conditions as described in the Methods and then injured with 0-500 μM SM. Cellular viability was determined at 6 hr (A) and 24 hr (B) using the acridine orange and ethidium bromide staining method described in the text.

Table 4. Effect of ATP Depletion on Sulfur Mustard Injury in Keratinocytes

mM Glucose	mM 2-Deoxyglucose	%	$\mu\text{M SM}$		
			0	250	500
5.5	0	V	94 \pm 1.0	78 \pm 3.5	50 \pm 18.5
5.5	0	A	0.7 \pm 1.2	6 \pm 2.6	8 \pm 4.6
5.5	0	N	5.7 \pm 1.5	15.3 \pm 4.7	42 \pm 18.2
2.75	2.75	V	88 \pm 7.8	65 \pm 9.2	51 \pm 5.8
2.75	2.75	A	2 \pm 2.6	8.3 \pm 5.5	11 \pm 8.5
2.75	2.75	N	10 \pm 7.8	26.7 \pm 11.2	38.3 \pm 9.8
1.375	4.125	V	87 \pm 6.7	70 \pm 4.9	59 \pm 7.6
1.375	4.125	A	1.6 \pm 2.1	5.3 \pm 3.2	8.7 \pm 7.5
1.375	4.125	N	11 \pm 6.9	23.3 \pm 9.1	32.7 \pm 9
0	5.5	V	79 \pm 8.0	68 \pm 14.6	64 \pm 17.0
0	5.5	A	2 \pm 2.6	4 \pm 3.6	2 \pm 2.0
0	5.5	N	19 \pm 11.1	28 \pm 17.8	33.7 \pm 19

Keratinocytes cultured in normal growth media were washed twice with PBS and the media was replaced with glucose-free RPMI 1640 to which keratinocyte growth factors (SingleQuot from Clonetics) and the indicated concentrations of glucose and/or 2-deoxyglucose were added. The cells were allowed to equilibrate at 37 °C for 30 min and then treated with control, 250 or 500 $\mu\text{M SM}$. At 24 hr, the viability was assessed using the acridine orange/ethidium bromide assay described in the Methods. A significant decrease ($p=0.05$) in percentage of cells exhibiting apoptotic nuclear features was observed in 500 $\mu\text{M SM}$ treated cells in which the ATP was markedly depleted (8 \pm 4.6% apoptotic under non-ATP depletion conditions vs. 2 \pm 2.0 under ATP depletion conditions, i.e 0 mM glucose, 5.5 mM 2-deoxyglucose). The data is presented as the mean \pm SD of 3-4 separate determinations.

Table 5. Effects of BSO and NAC on sulfur mustard-treated endothelial cells.

	Control			500 μ M SM		
	%V	%A	%N	%V	%A	%N
Untreated	90.3 \pm 3.1	3.6 \pm 2.1	6.1 \pm 2.8	50.4 \pm 4.0	33.1 \pm 5.0	16.3 \pm 4.5
0.2 mM BSO	91.0 \pm 3.0	2.7 \pm 0.6	6.3 \pm 3.1	35.7 \pm 8.4	32.7 \pm 10.3	31.7 \pm 17.8
50 mM NAC	93.3 \pm 3.6	2.5 \pm 1.0	4.3 \pm 2.6	69.3 \pm 1.7	21.2 \pm 4.3	9.5 \pm 4.4
BSO + NAC	92.7 \pm 4.0	2.0 \pm 1.0	5.3 \pm 3.2	51.7 \pm 4.7	37.0 \pm 5.7	11.3 \pm 1.2

Endothelial cells were pretreated overnight with 0.2 mM and 50 mM NAC as described in the Methods and then treated with 0 or 500 μ M SM. Six hours later, the viability was determined using the acridine orange and ethidium bromide assay described in the Methods.

Table 6. Effect of exogenous GSH on sulfur mustard-induced injury in endothelial cells.

mM GSH	Control			500 μ M SM		
	%V	%A	%N	%V	%A	%N
0	90.3 \pm 3.1	3.6 \pm 2.1	6.1 \pm 2.8	50.4 \pm 4.0	33.1 \pm 5.0	16.3 \pm 4.5
2.5	88.0 \pm 0.0	5.0 \pm 2.6	7.0 \pm 2.6	72.7 \pm 5.9	15.7 \pm 5.5	1.7 \pm 4.2
5.0	88.0 \pm 5.5	4.8 \pm 2.5	9.8 \pm 5.6	75.4 \pm 5.6	11.3 \pm 1.3	11.3 \pm 4.2
10	83.0 \pm 4.0	4.0 \pm 1.7	13.3 \pm 3.0	66.7 \pm 6.4	10.7 \pm 3.2	23.0 \pm 3.6

Cells treated with 0-10 mM GSH were treated with 0 or 500 μ M SM. After six hours, the viability was determined using the acridine orange and ethidium bromide assay described in the Methods.

Table 7. Effects of BSO and NAC on sulfur mustard-treated keratinocytes.

	Control			500 μ M SM		
	%V	%A	%N	%V	%A	%N
Untreated	84.6 \pm 0.73	5.8 \pm 0.74	9.6 \pm 0.93	80.9 \pm 2.01	6.9 \pm 0.35	12.2 \pm 1.77
0.2 mM BSO	86.0 \pm 2.26	4.8 \pm 1.48	9.2 \pm 1.28	70.0 \pm 1.71	6.7 \pm 2.40	23.3 \pm 2.10
50 mM NAC	87.4 \pm 2.44	4.1 \pm 2.69	8.5 \pm 0.92	79.0 \pm 3.22	7.2 \pm 1.10	13.8 \pm 2.40
BSO + NAC	89.9 \pm 2.23	4.5 \pm 1.43	5.6 \pm 0.43	80.7 \pm 3.84	6.4 \pm 2.03	12.9 \pm 3.00

Keratinocytes were pretreated overnight with 0.2 mM BSO and 50 mM NAC as described in the Methods and then treated with 0 or 500 μ M SM. Six hours later, the viability was determined using the the annexin V/propidium iodide assay. N=3.

Please see attached glossies.

Fig.1A-D

FIGURE 1A



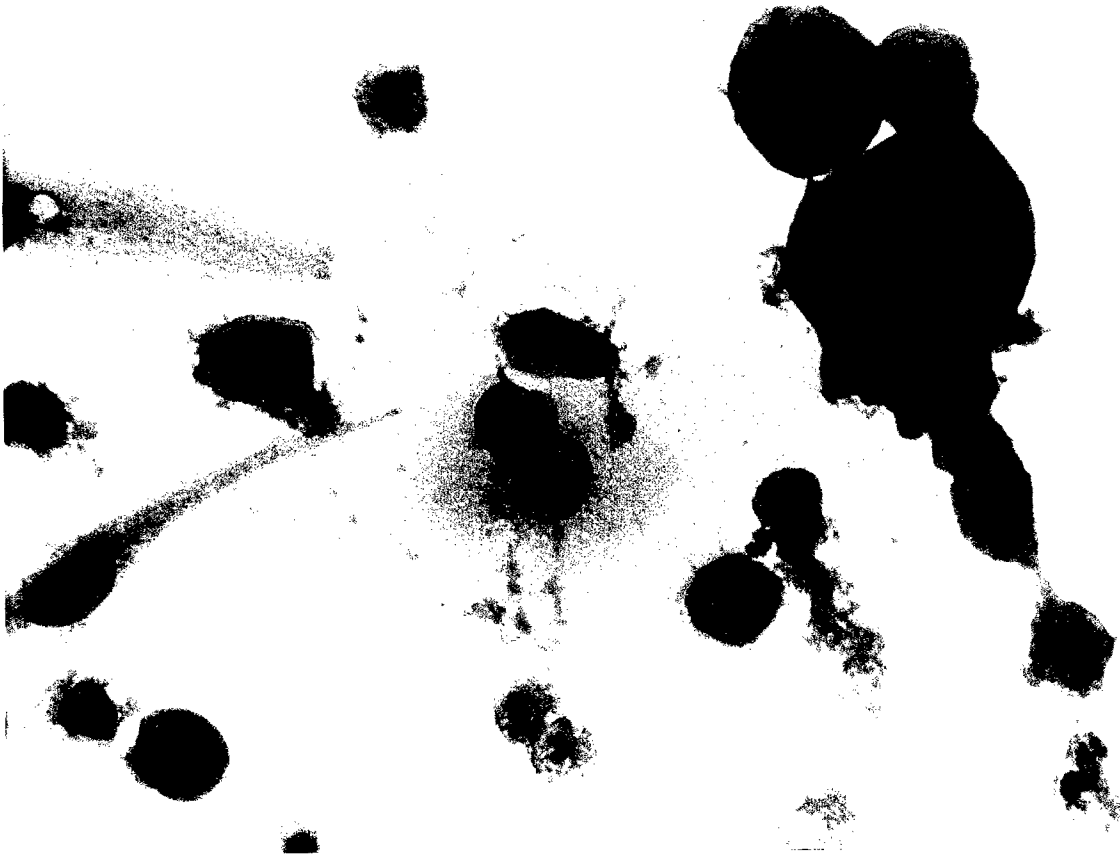
FIGURE 1B



FIGURE 1C



FIGURE 1D



1 2 3 4 5 6 7

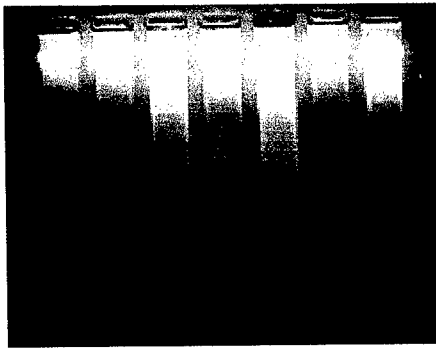


Figure 2A

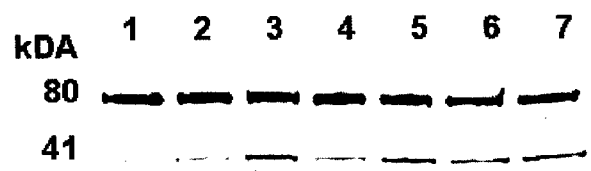


Figure 2B

Please see attached glossies.

Fig.3A-E

FIGURE 3A



FIGURE 3B



FIGURE 3C

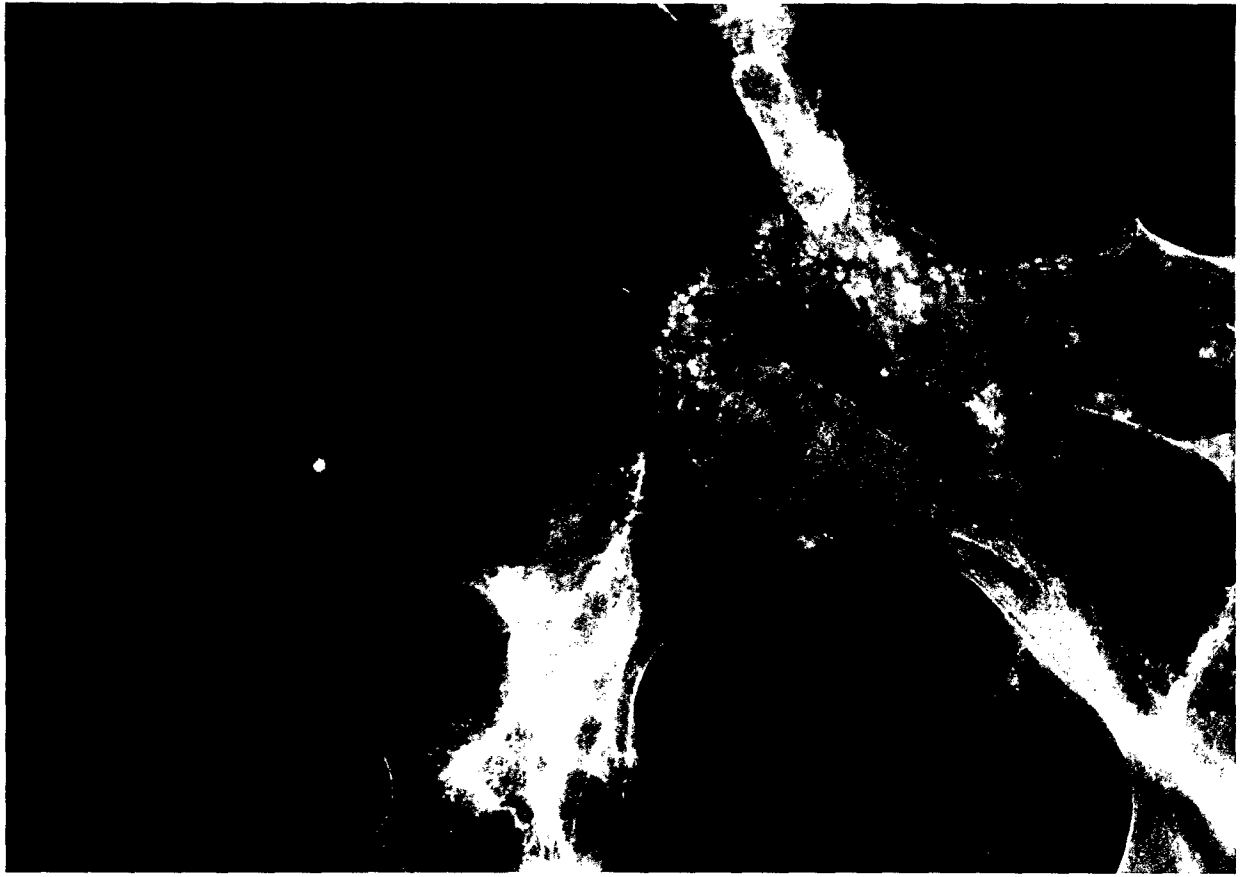


FIGURE 3D



FIGURE 3E



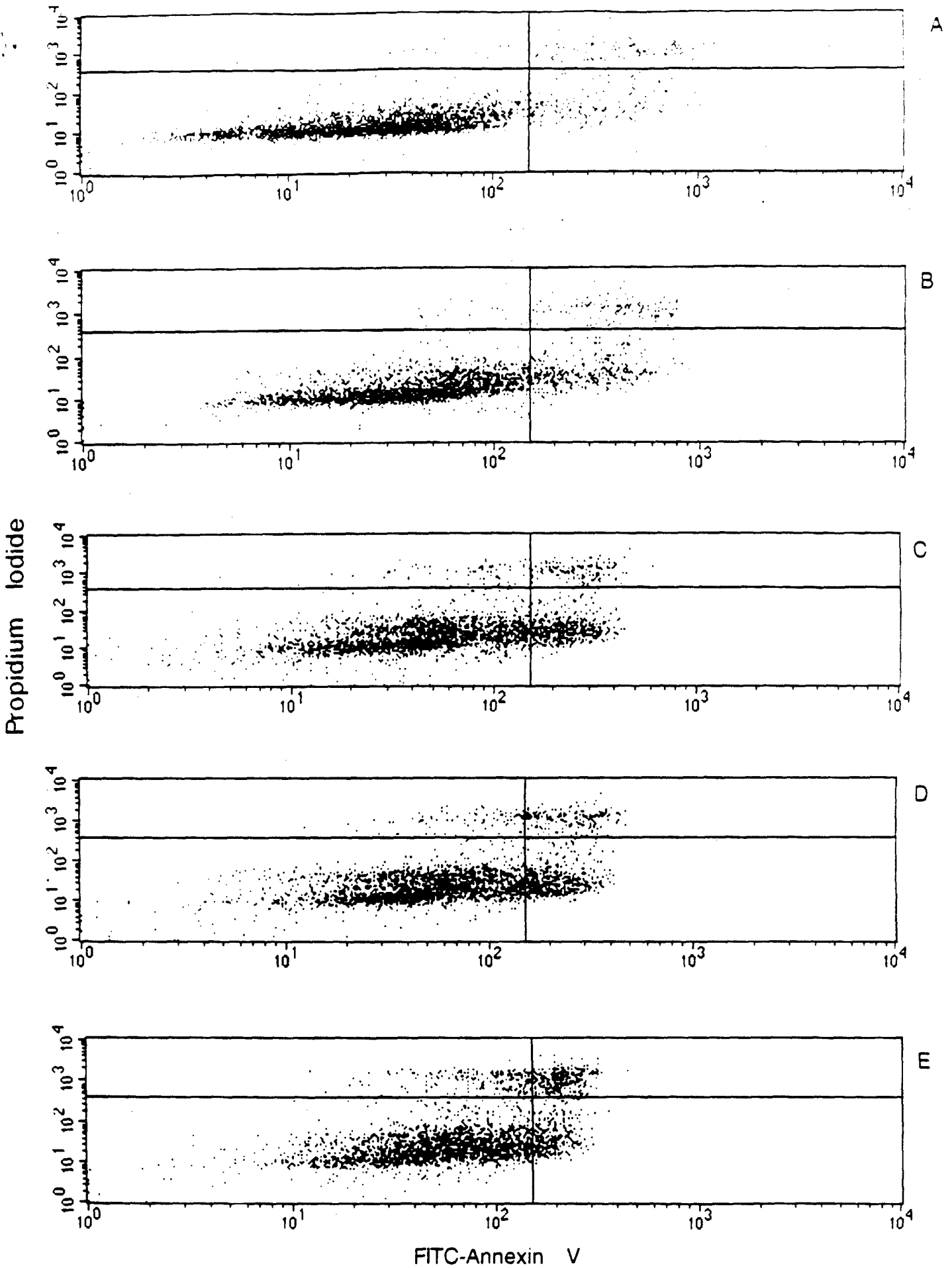


Fig. 4

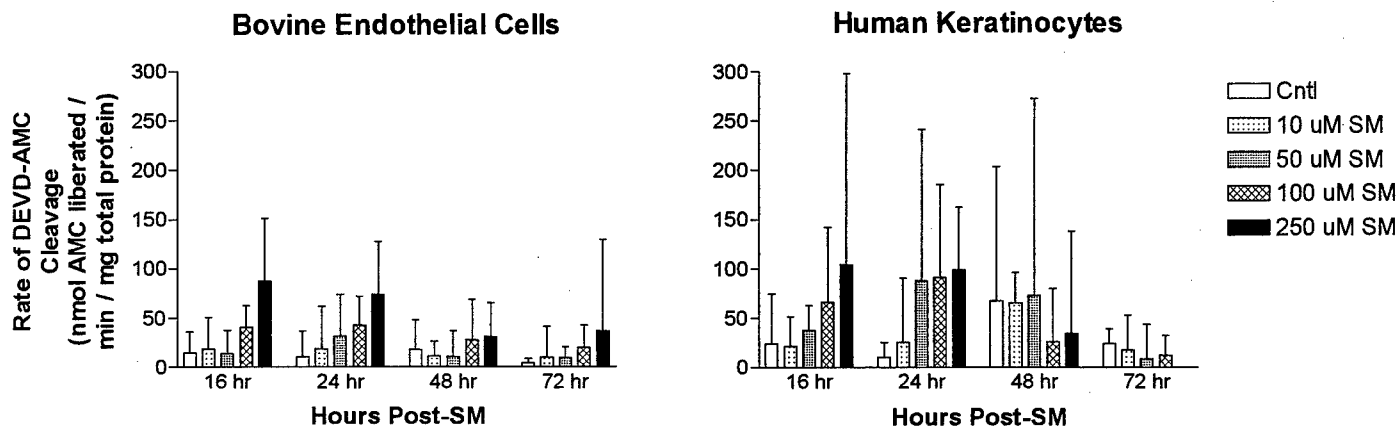
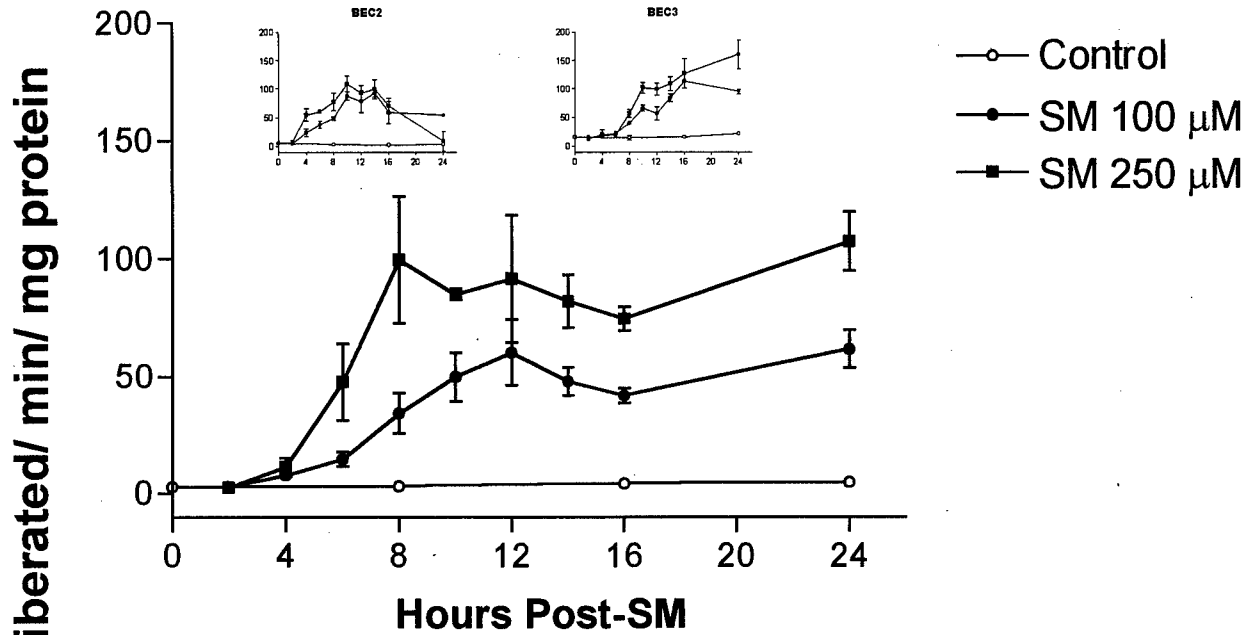


Figure 5A

Endothelial Cells



Keratinocytes

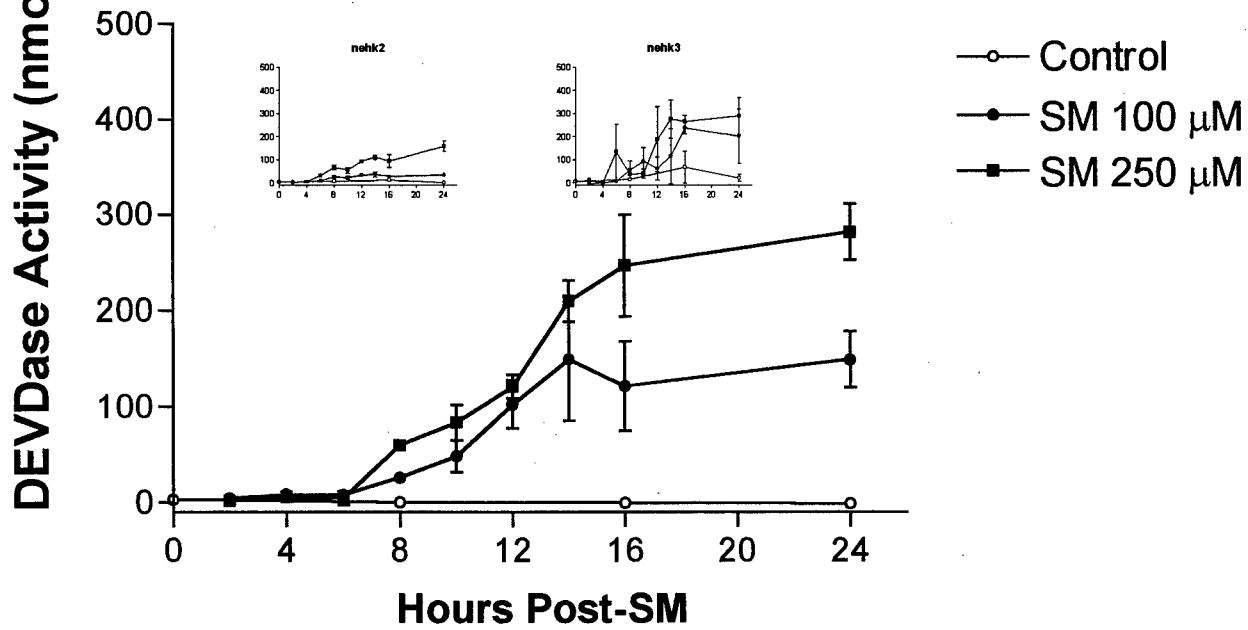


Figure 5B

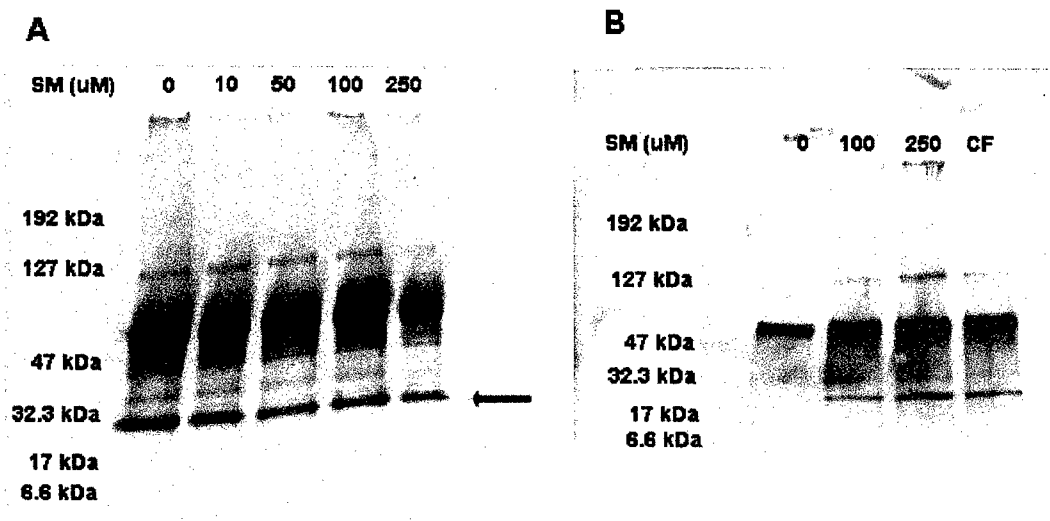


Figure 6

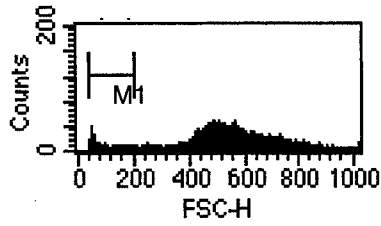
Bovine Endothelial Cells

Untreated

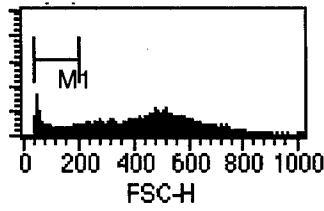
100 μ M SM

250 μ M SM

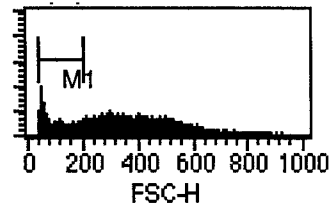
16 hr
Post-SM



Marker	% Total	Mean
All	100.00	536.73
M1	6.47	112.91

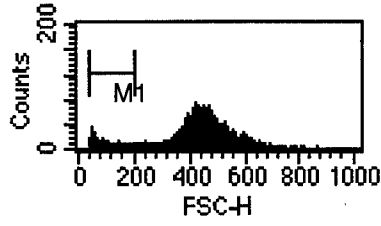


Marker	% Total	Mean
All	100.00	427.06
M1	13.68	119.44

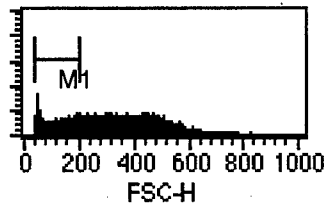


Marker	% Total	Mean
All	100.00	351.90
M1	20.28	120.72

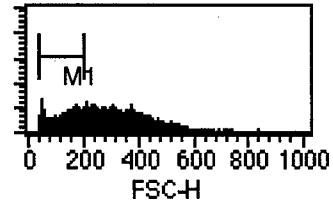
40 hr
Post-SM



Marker	% Total	Mean
All	100.00	428.79
M1	7.51	107.99



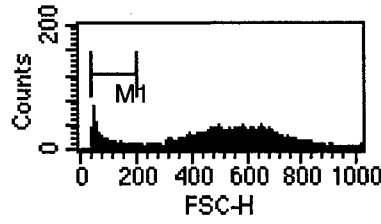
Marker	% Total	Mean
All	100.00	321.60
M1	24.88	131.80



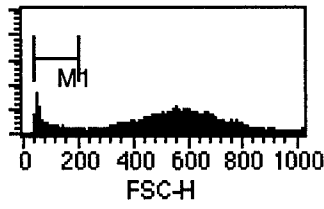
Marker	% Total	Mean
All	100.00	280.39
M1	31.29	136.85

Human Keratinocytes

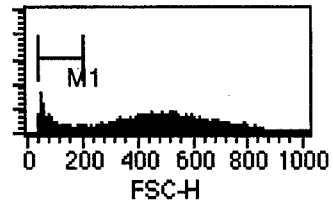
16 hr
Post-SM



Marker	% Total	Mean
All	100.00	513.52
M1	10.83	103.45

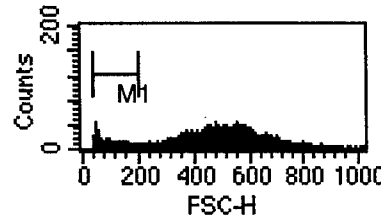


Marker	% Total	Mean
All	100.00	520.88
M1	9.62	102.16

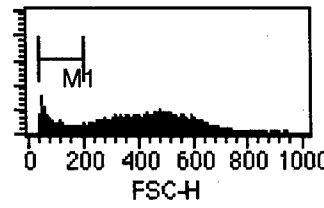


Marker	% Total	Mean
All	100.00	447.83
M1	15.51	103.76

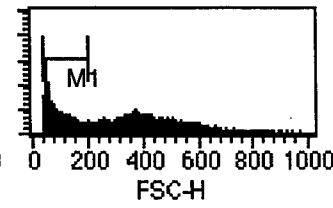
40 hr
Post-SM



Marker	% Total	Mean
All	100.00	467.02
M1	10.43	106.37



Marker	% Total	Mean
All	100.00	390.64
M1	17.28	108.76



Marker	% Total	Mean
All	100.00	316.78
M1	32.02	106.75

Figure 7

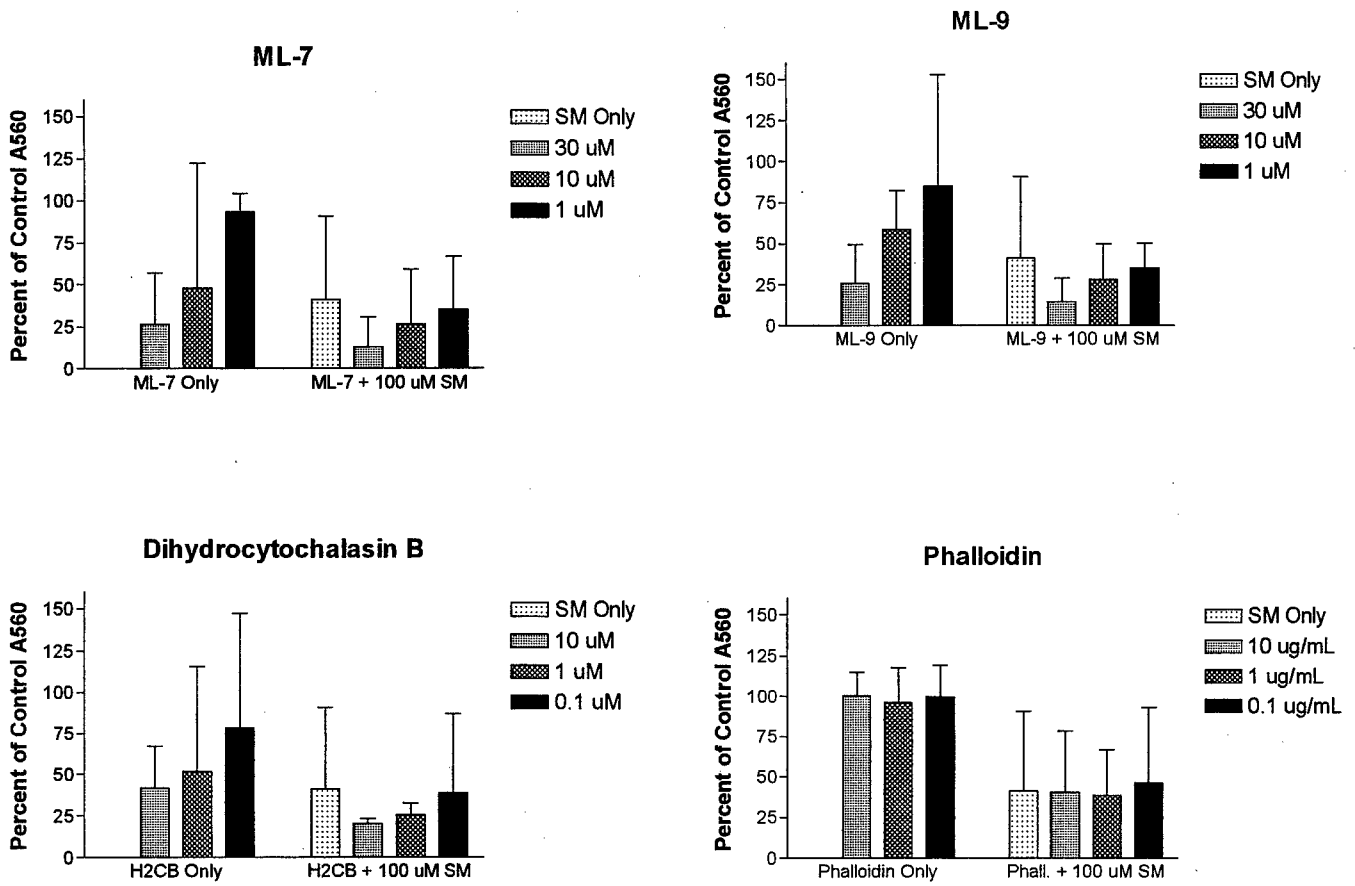


Figure 8.

Please see attached glossies.

Fig.9A-J

84

FIGURE 9A



FIGURE 9B

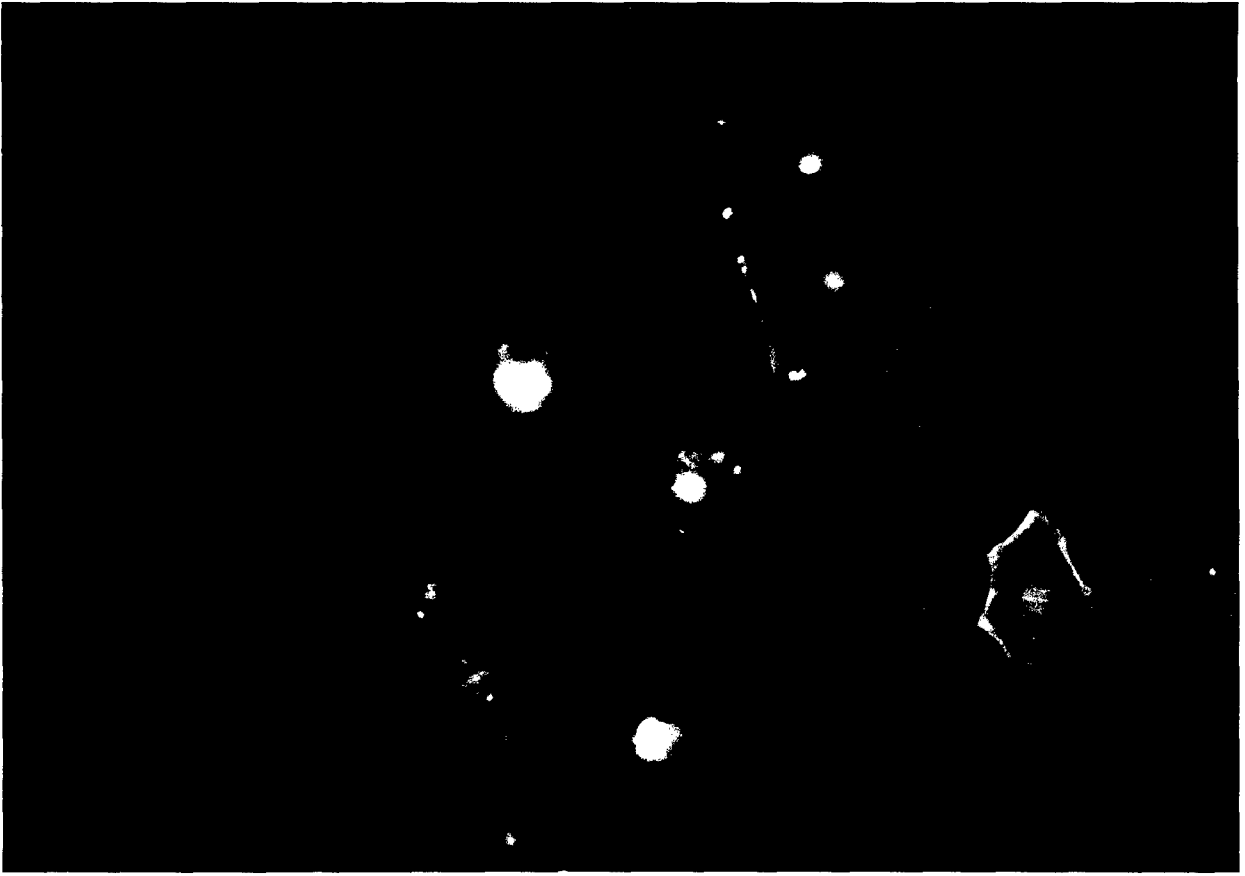


FIGURE 9C



FIGURE 9D

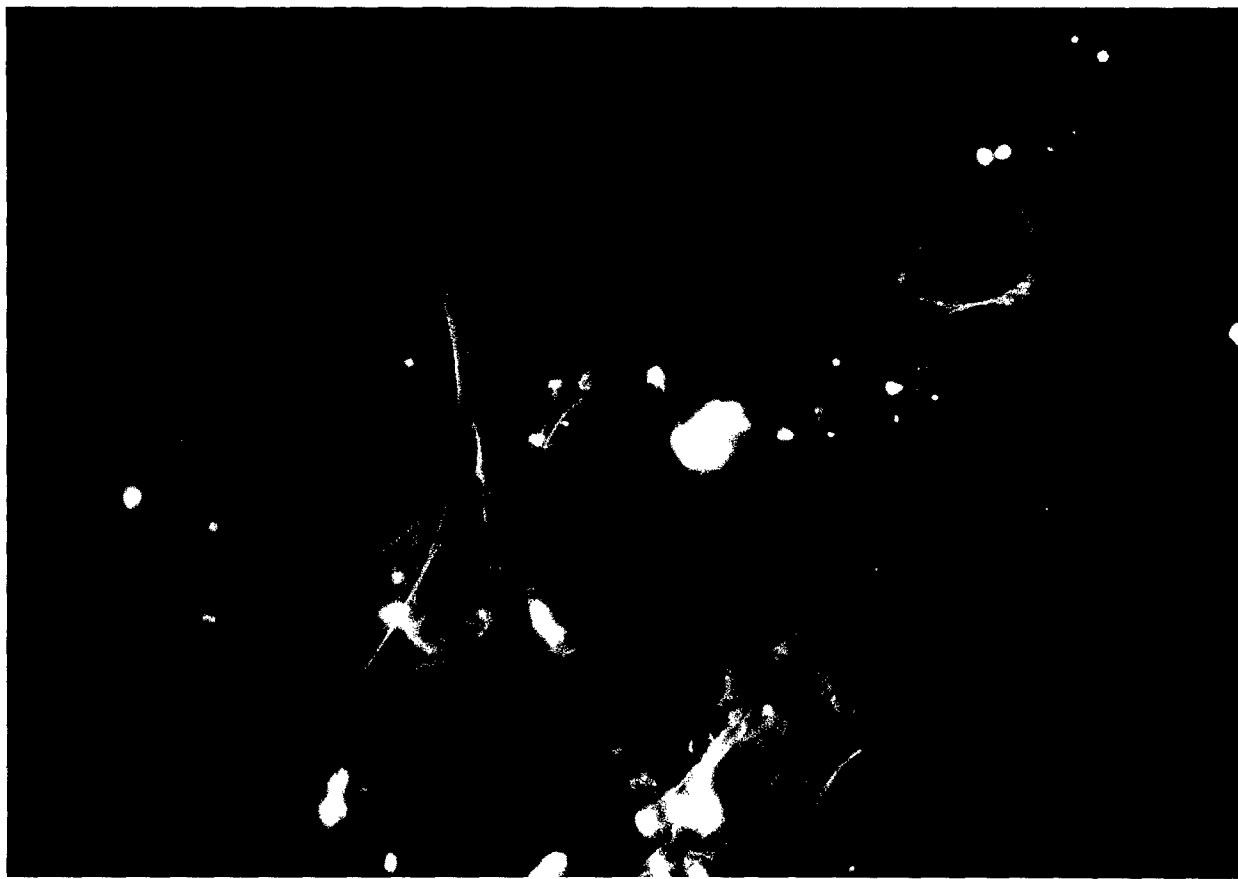


FIGURE 9E



FIGURE 9F

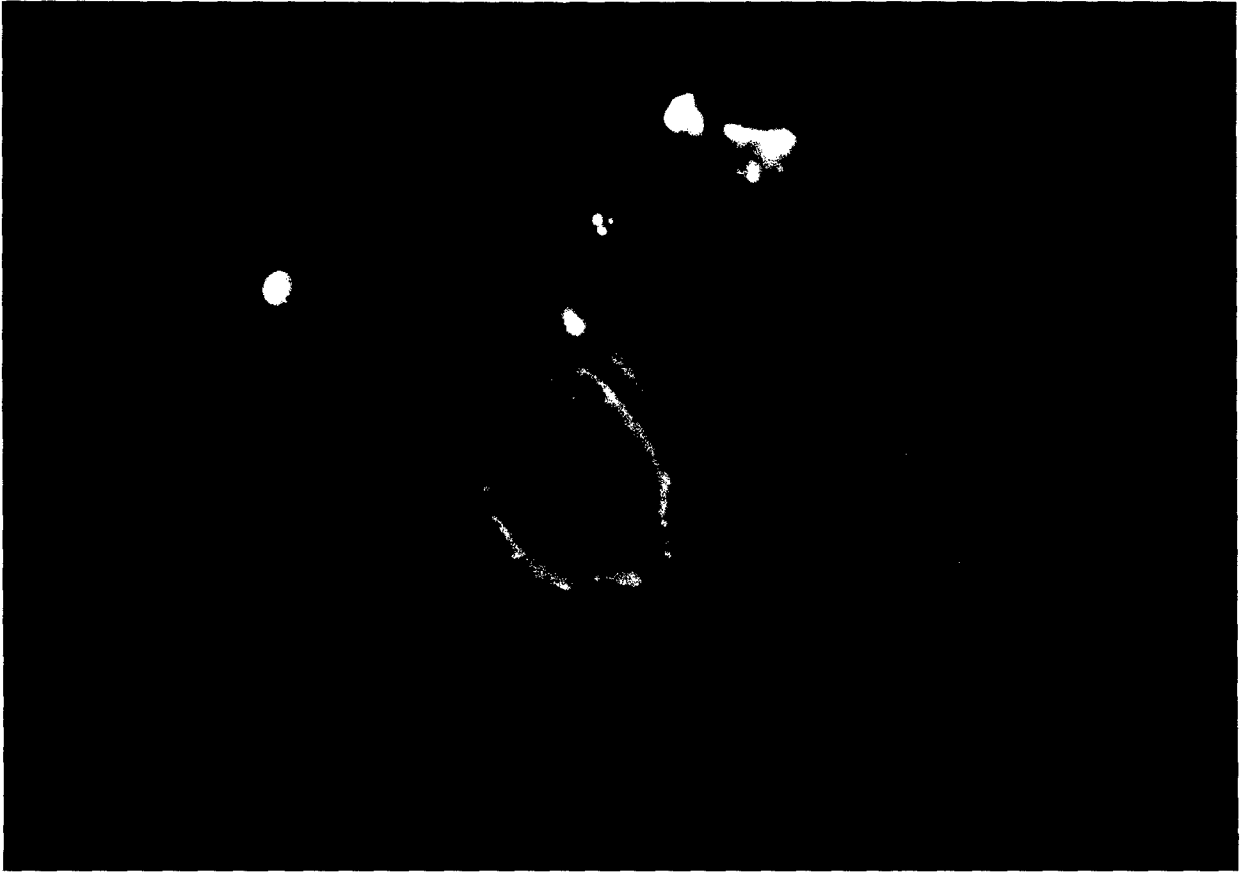


FIGURE 9G

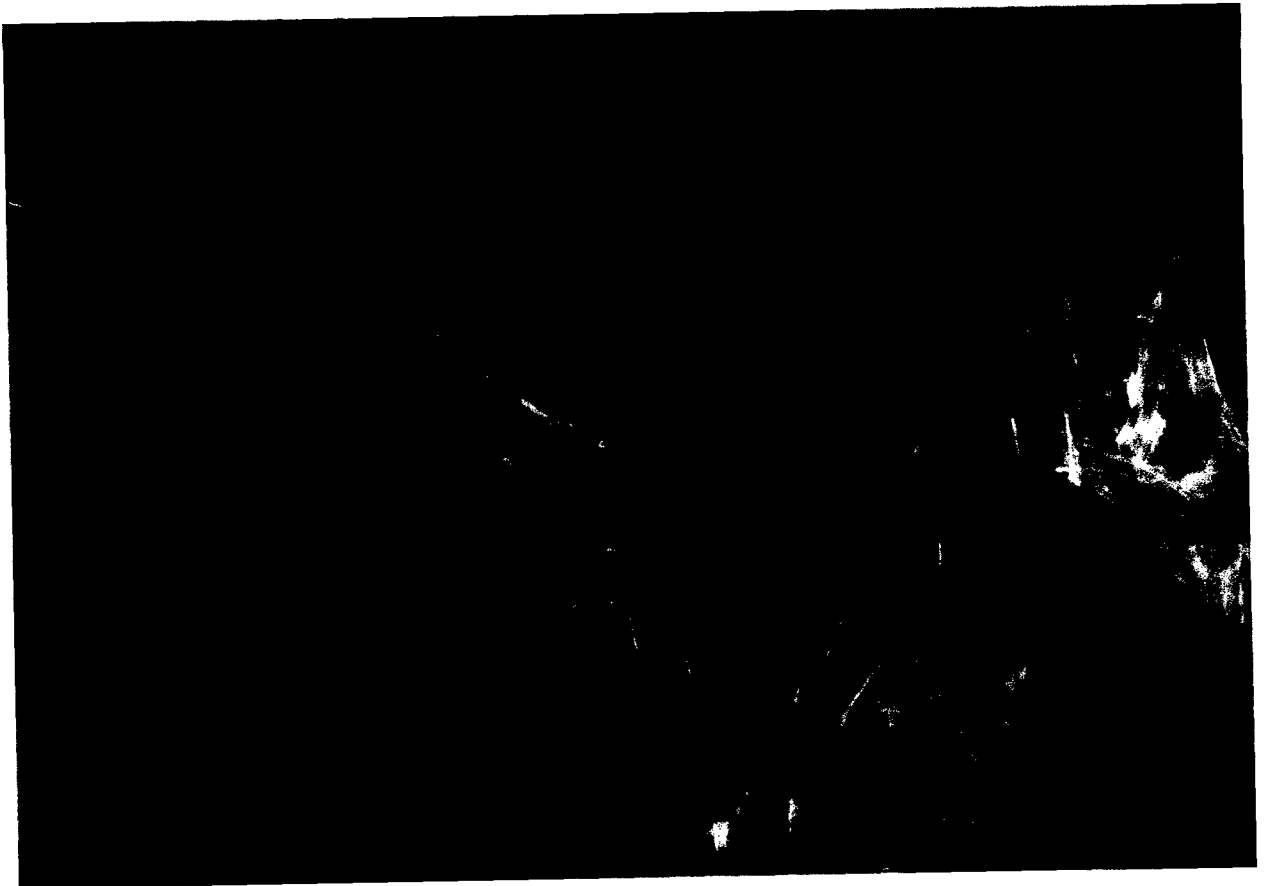


FIGURE 9H

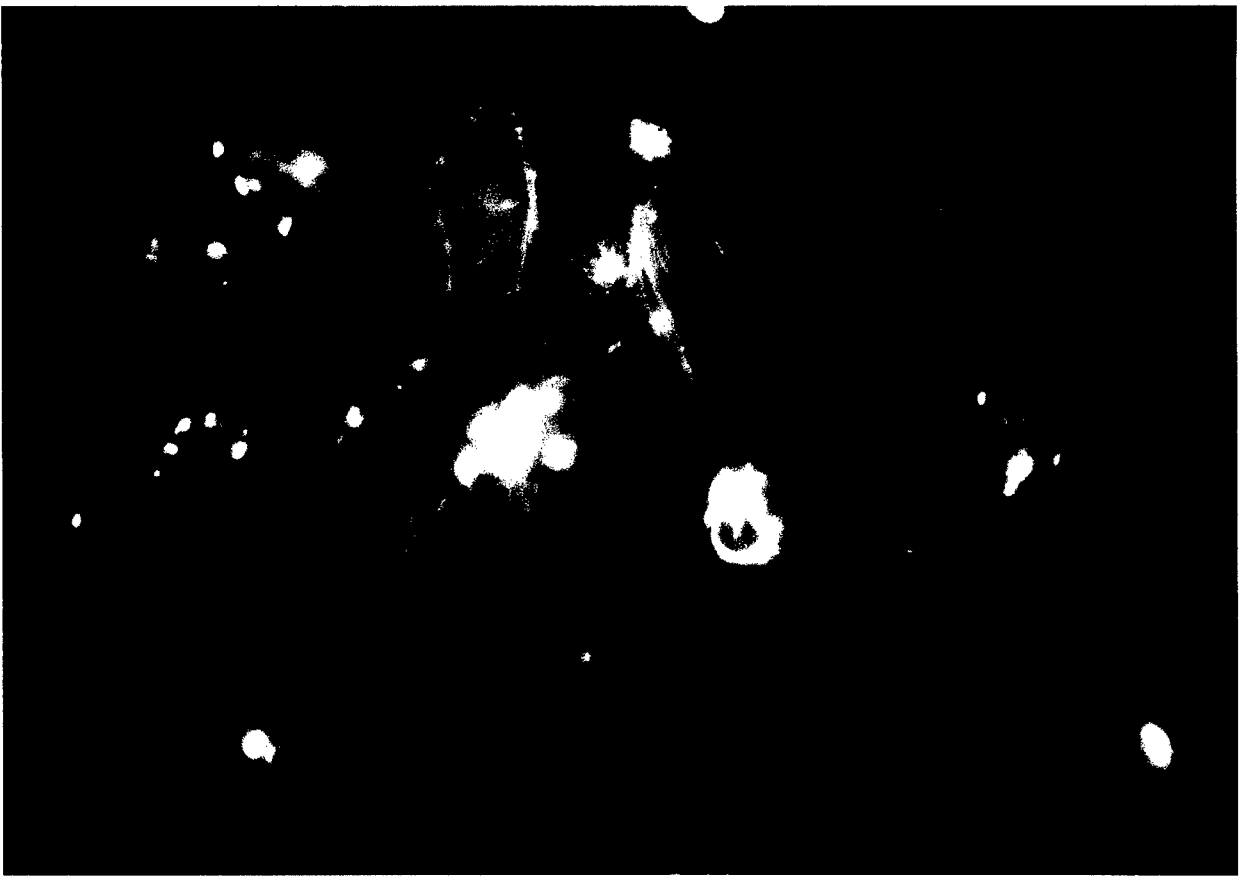


FIGURE 9I

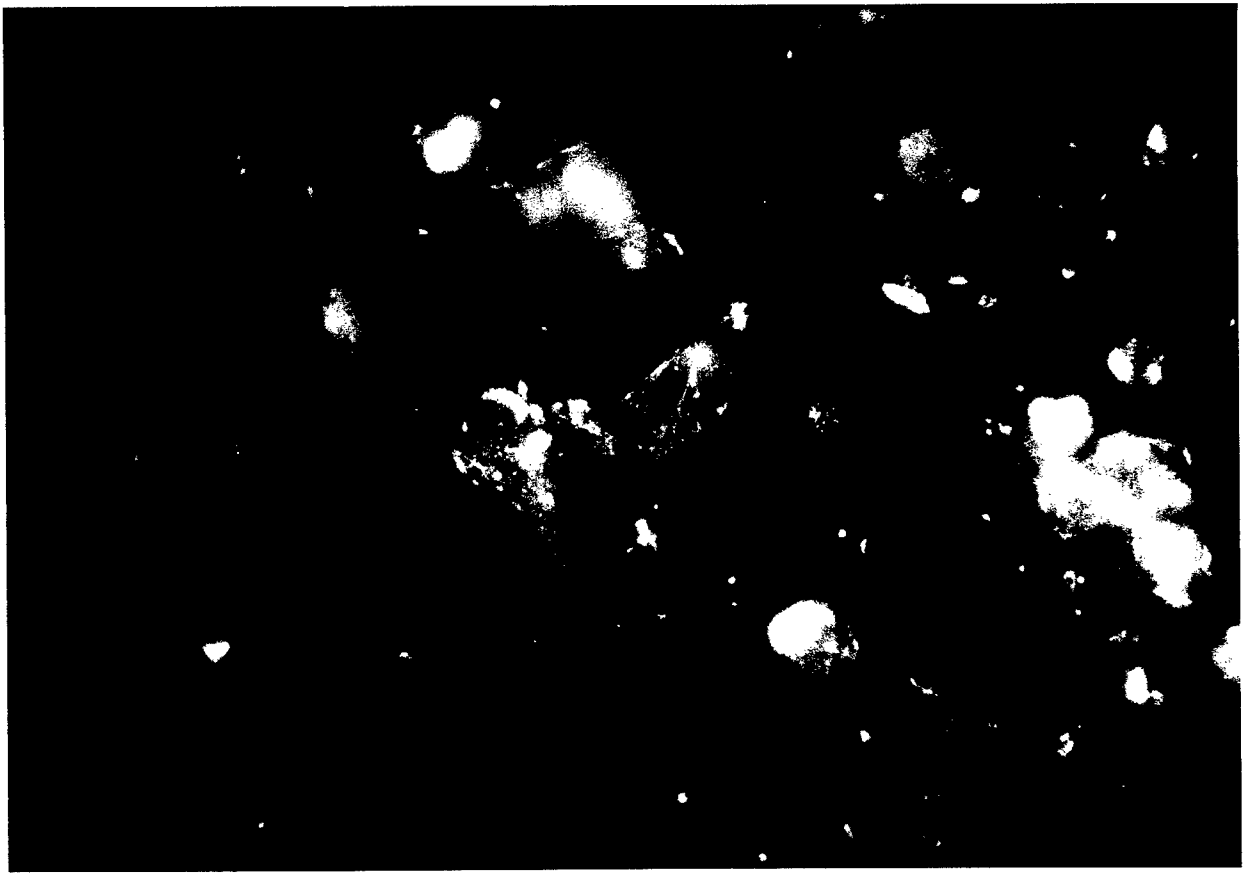
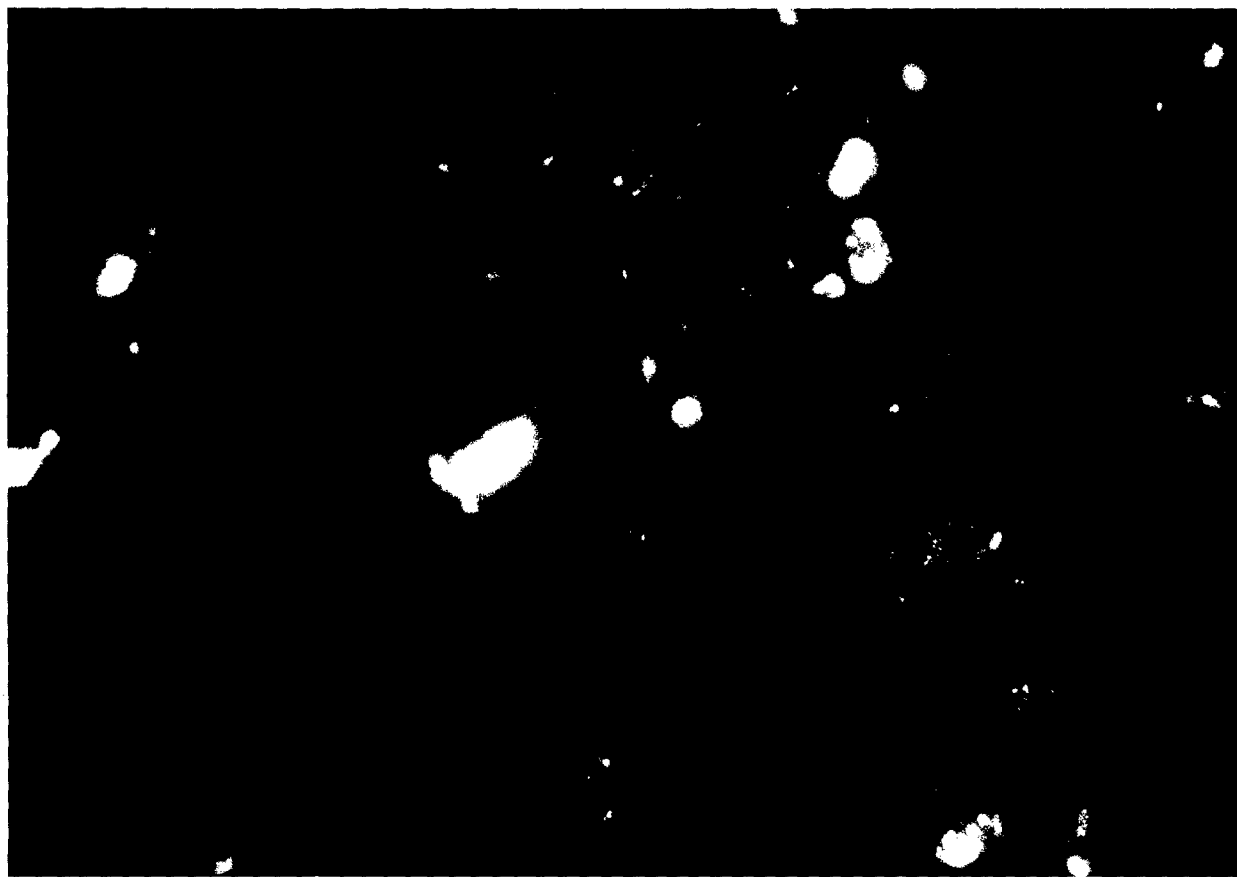


FIGURE 9J



BOVINE ENDOTHELIAL CELLS

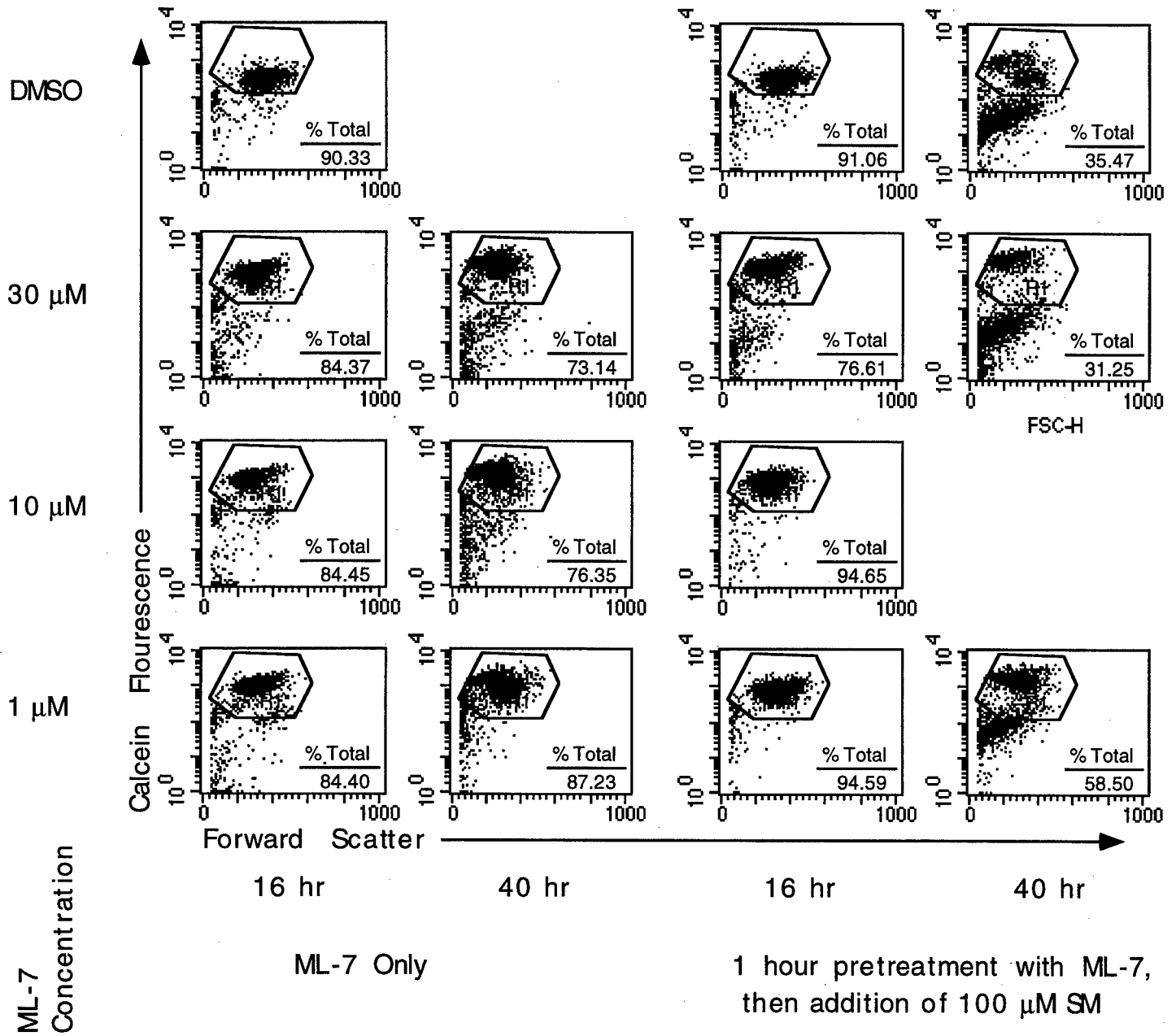


Figure 10A

BOVINE ENDOTHELIAL CELLS

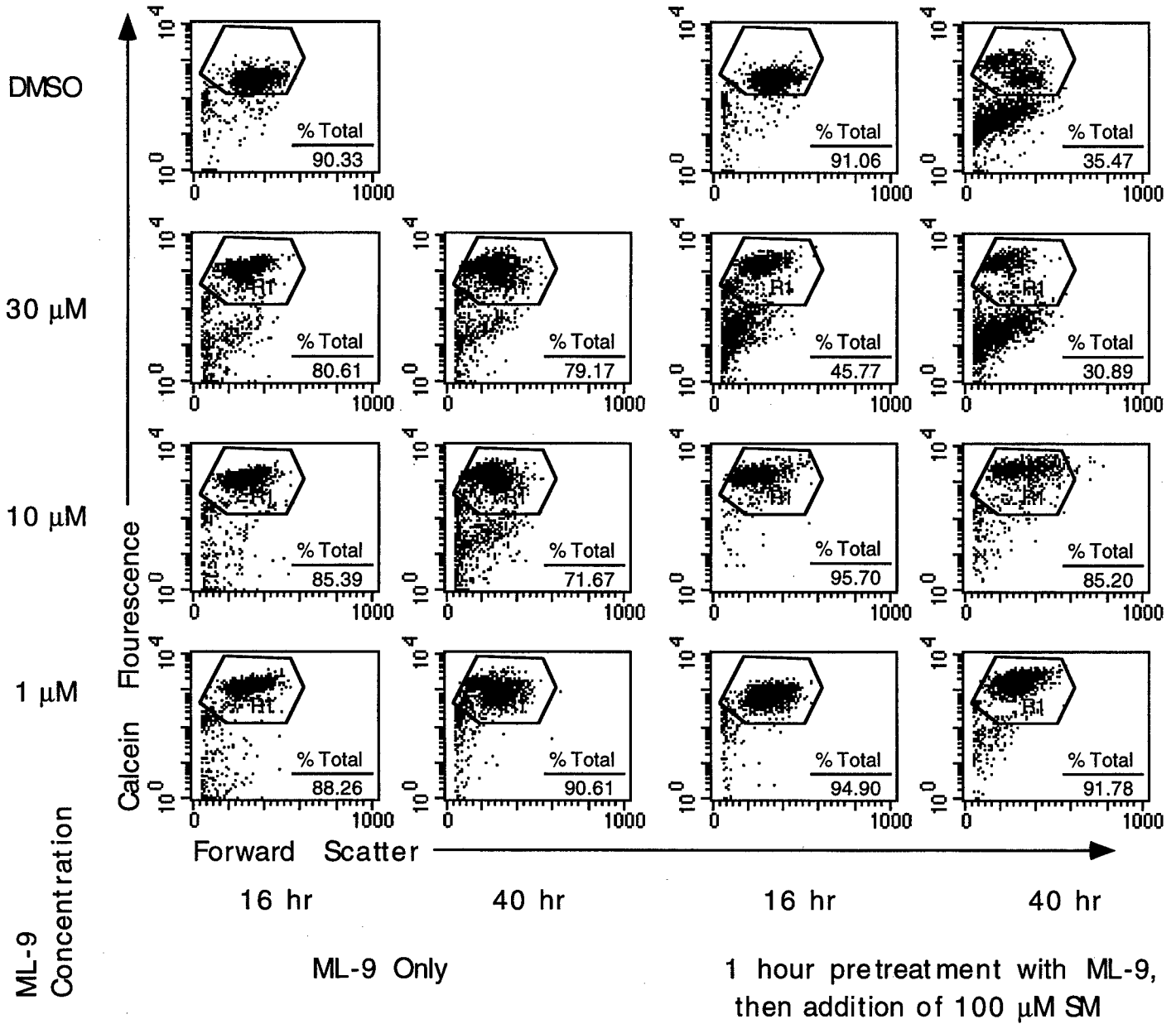


Figure 10B

BOVINE ENDOTHELIAL CELLS

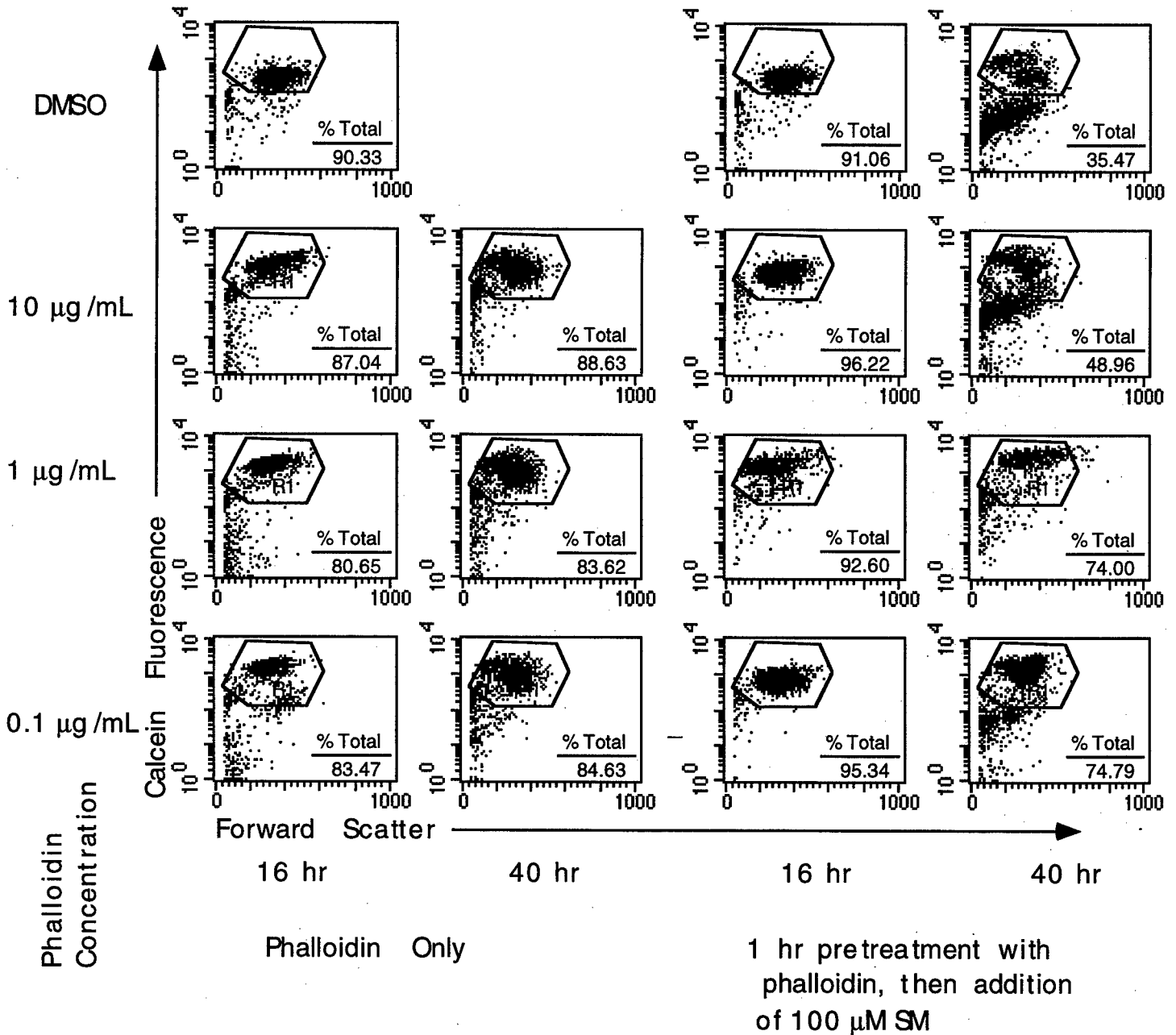


Figure 10C

BOVINE ENDOTHELIAL CELLS

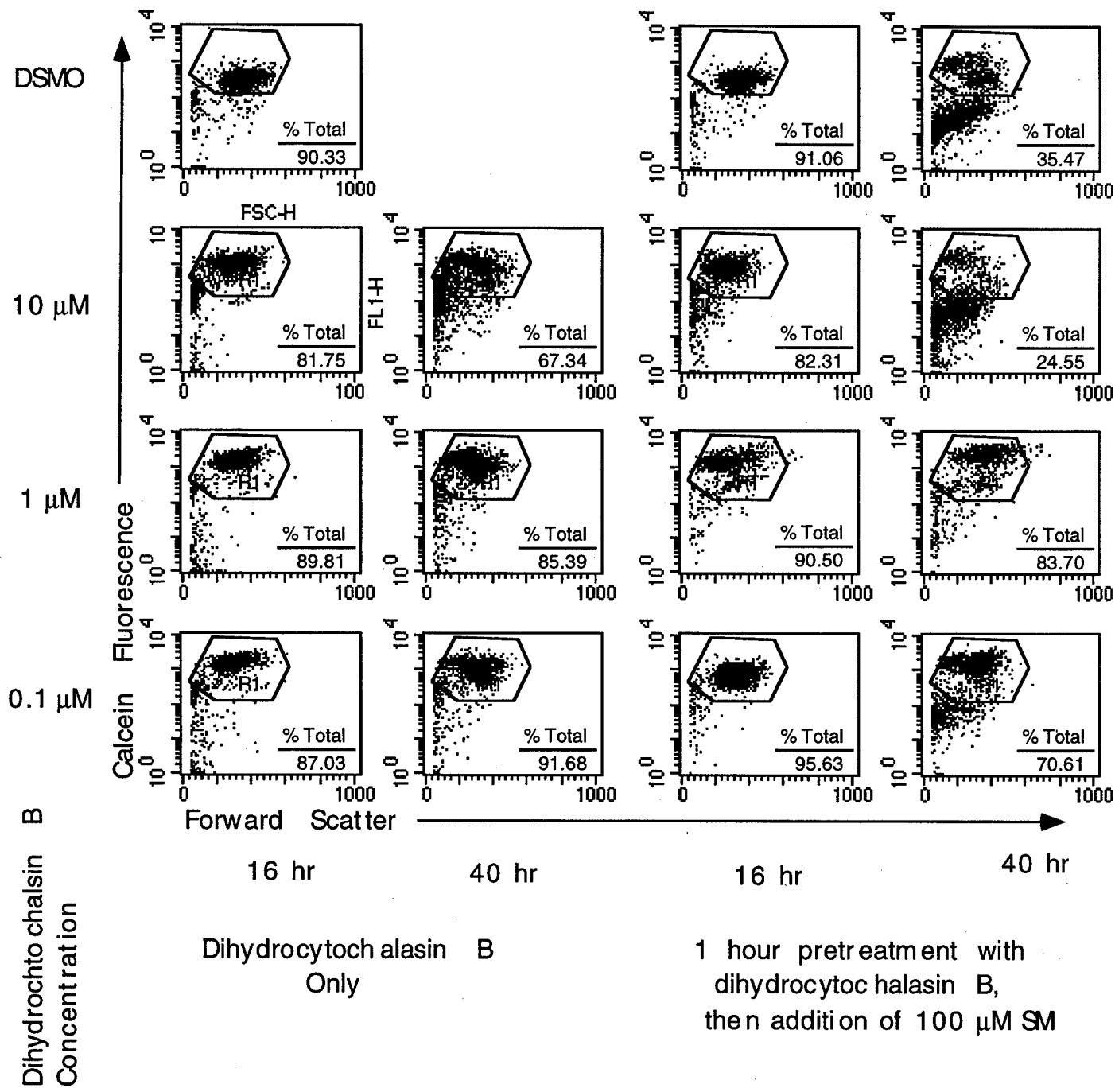


Figure 10D

HUMAN KERATINOCYTES

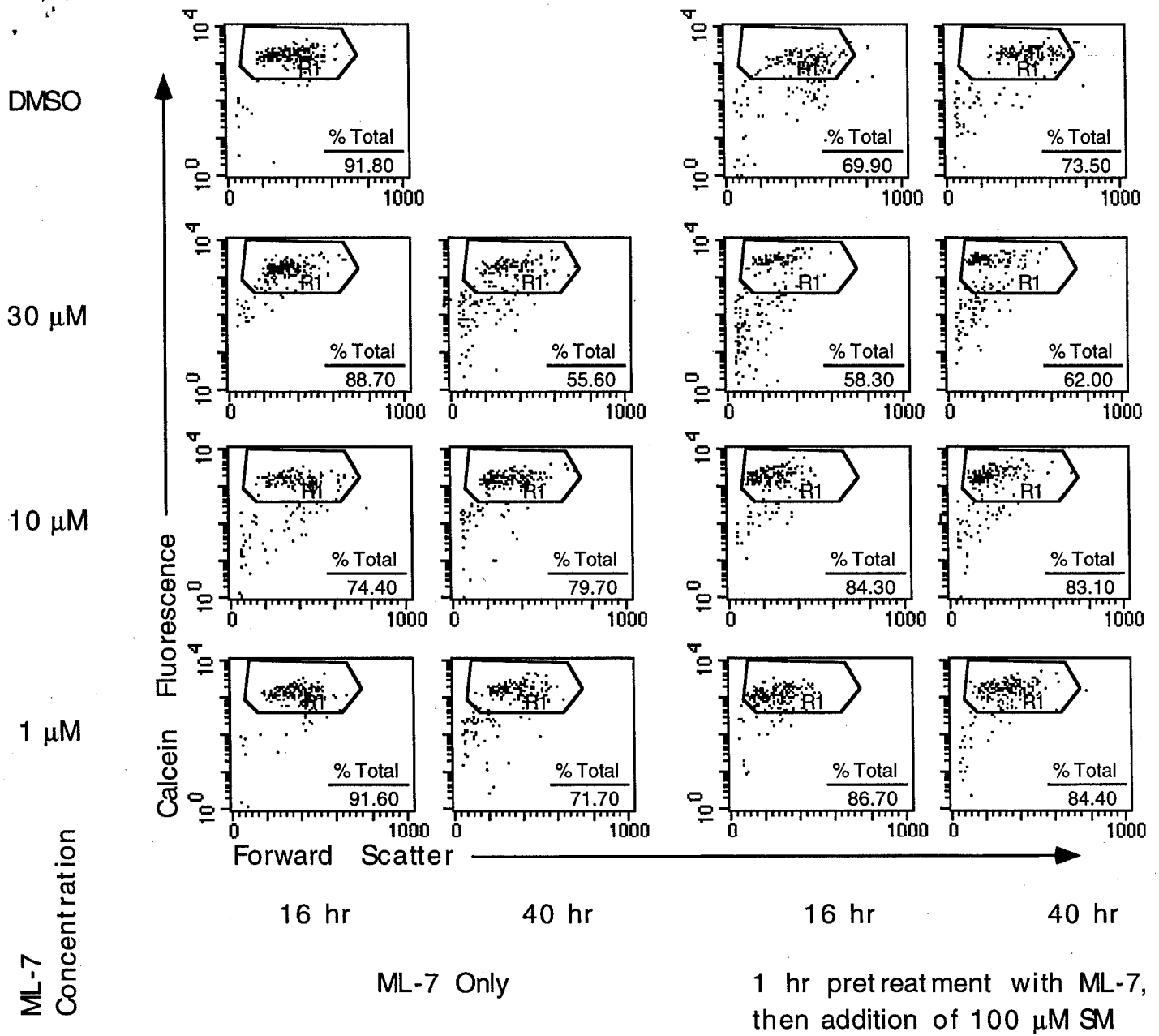


Figure 10A

HUMAN KERATINOCYTES

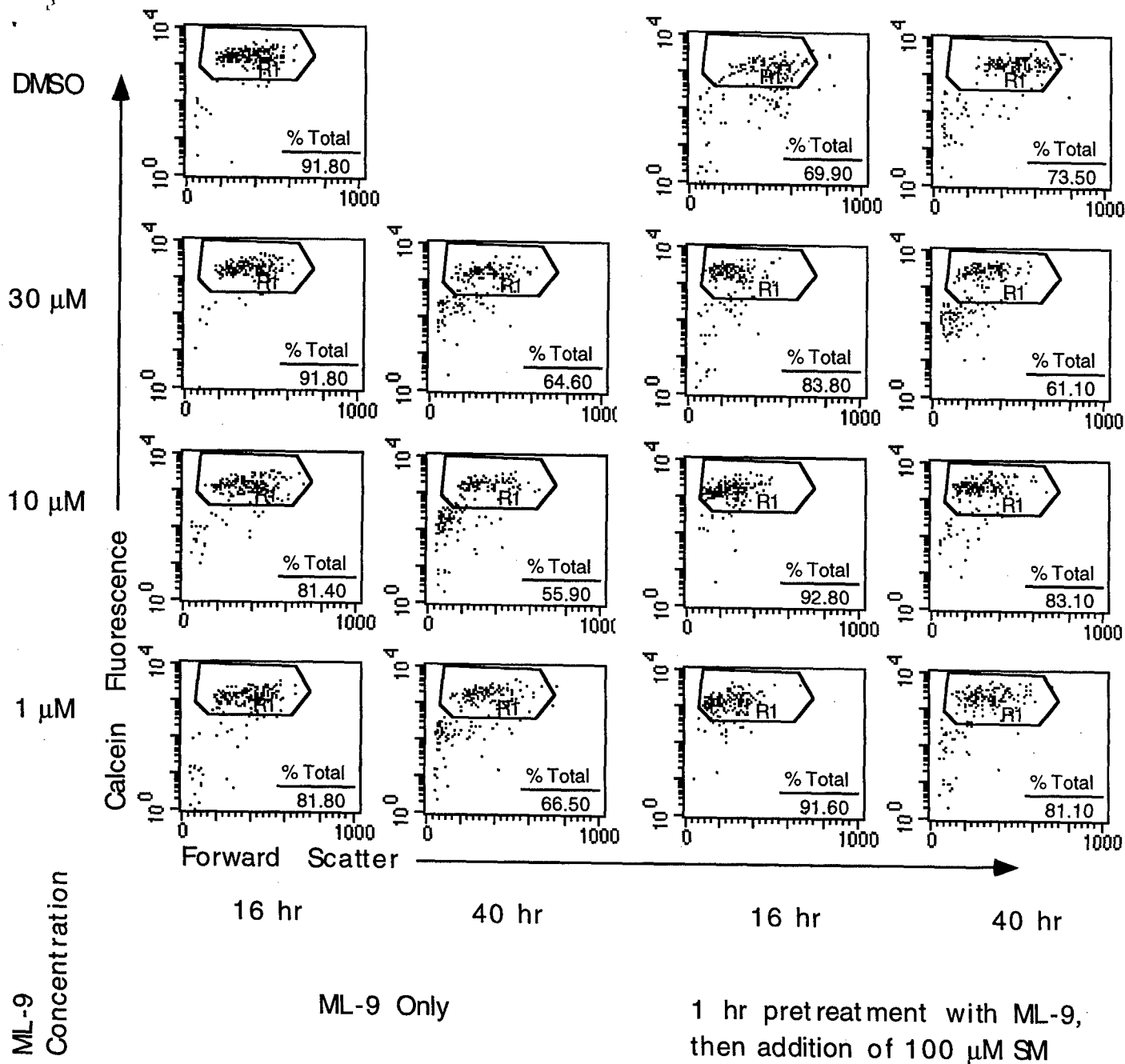


Figure 10B

HUMAN KERATINOCYTES

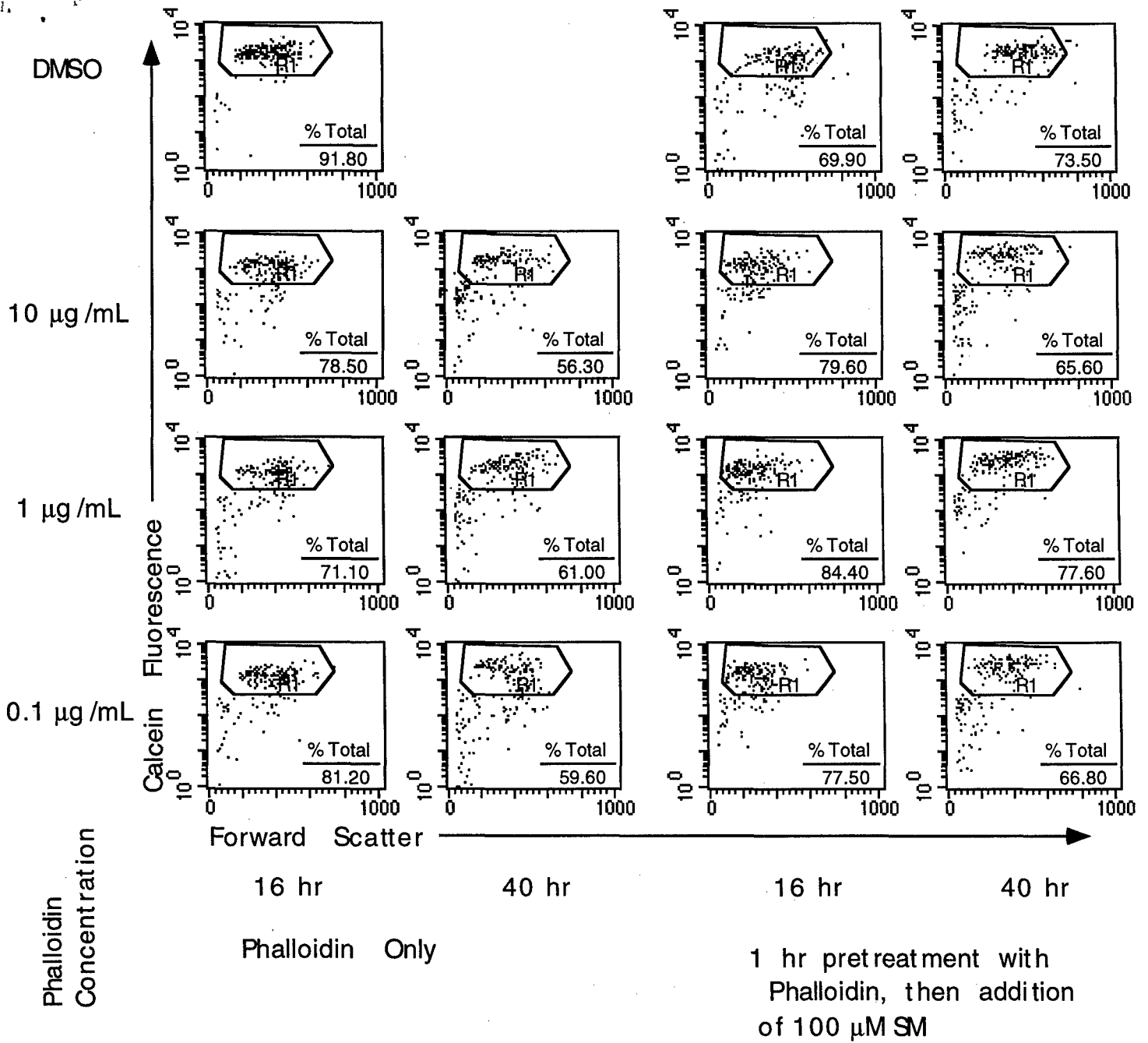


Figure 10C

HUMAN KERATINOCYTES

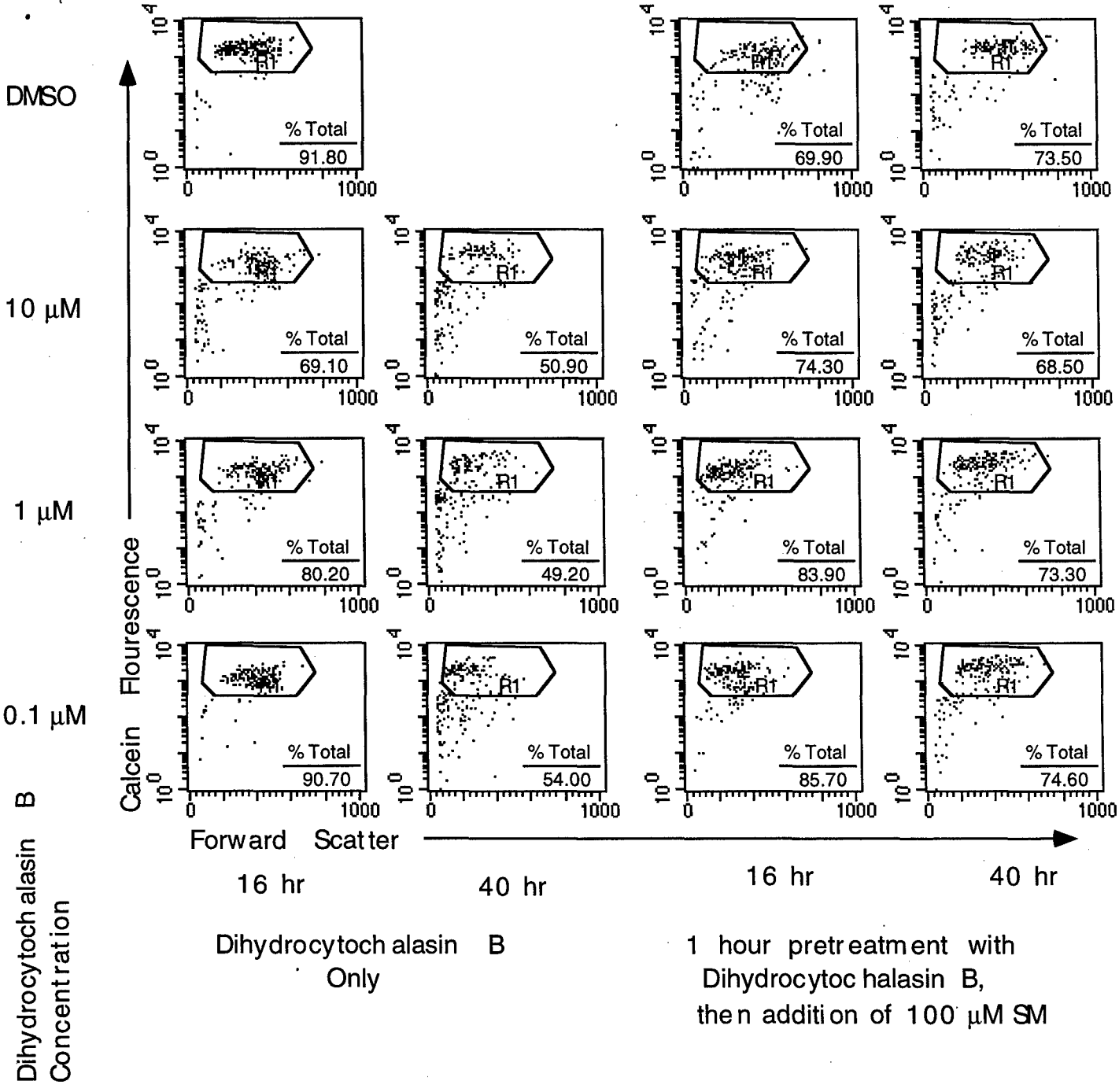


Figure 10D

BOVINE ENDOTHELIAL CELLS

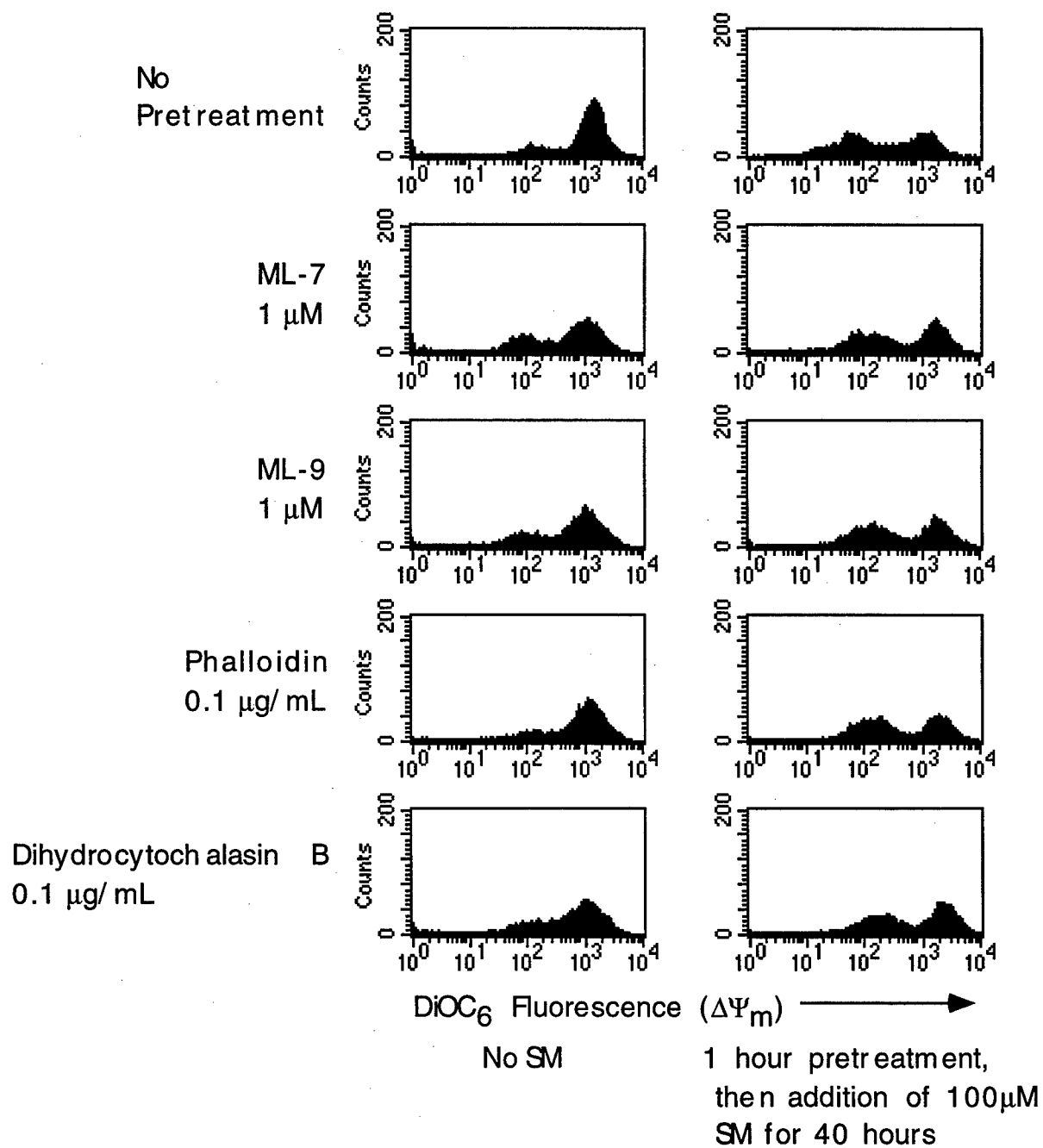


Figure 11

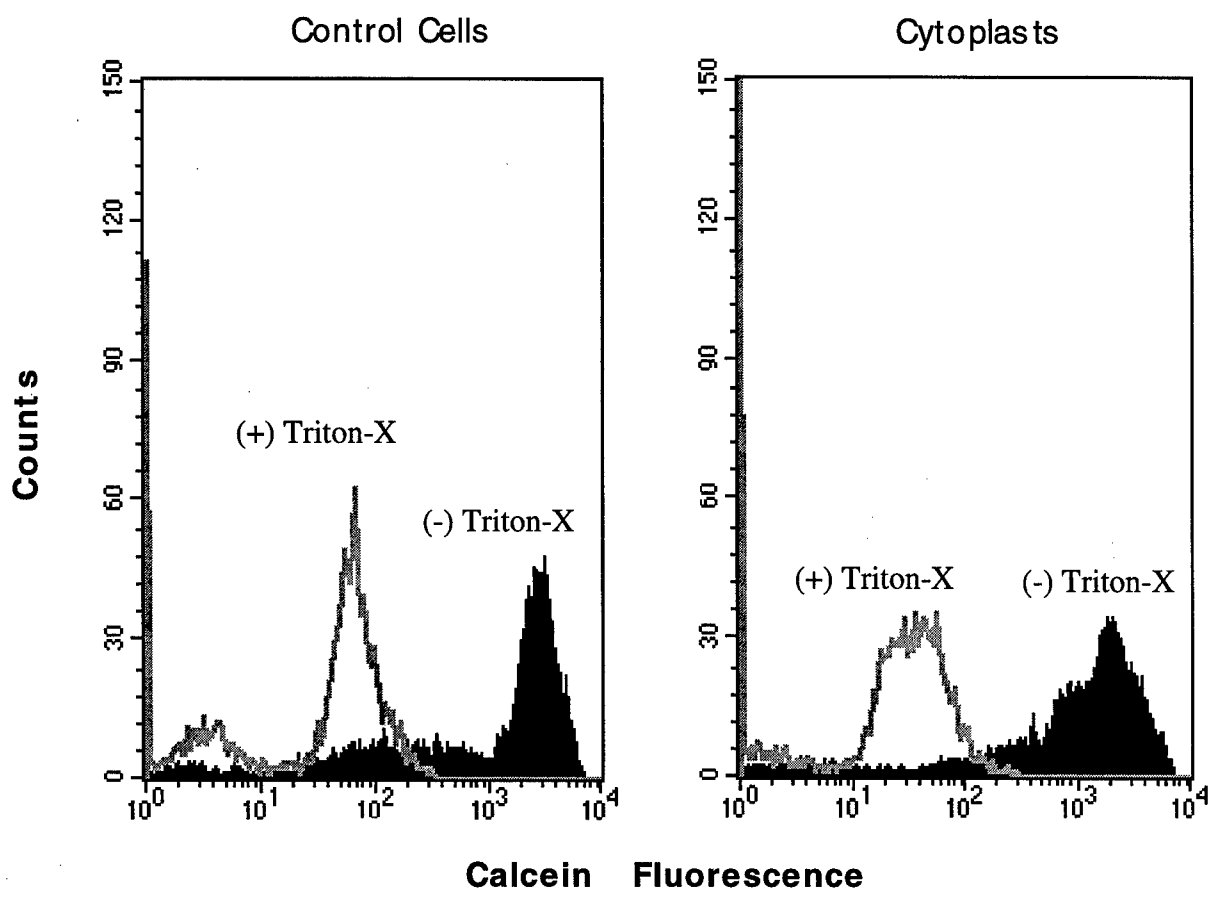


Figure 12

Please see attached glossies.

Fig.13A-F

FIGURE 13A



FIGURE 13B

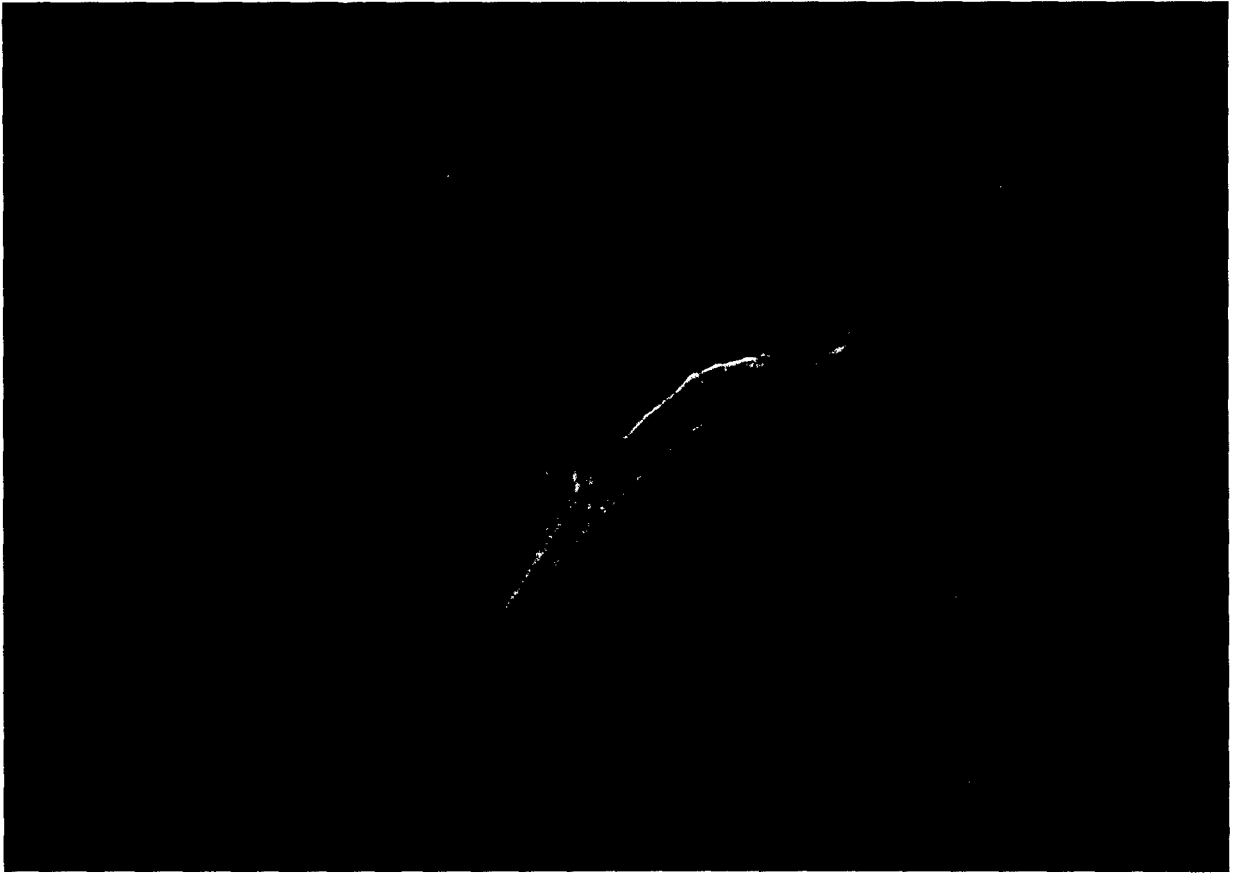


FIGURE 13C

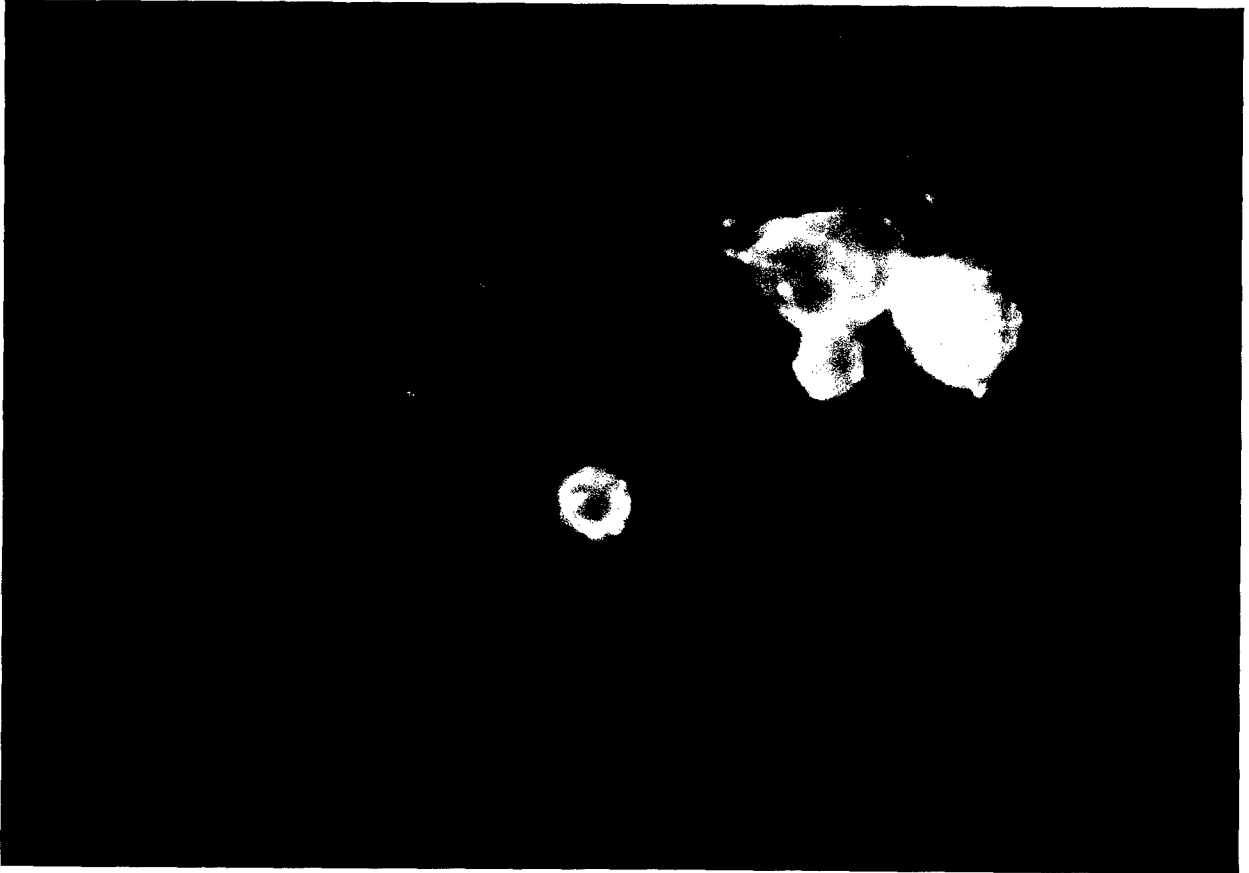


FIGURE 13D



FIGURE 13E

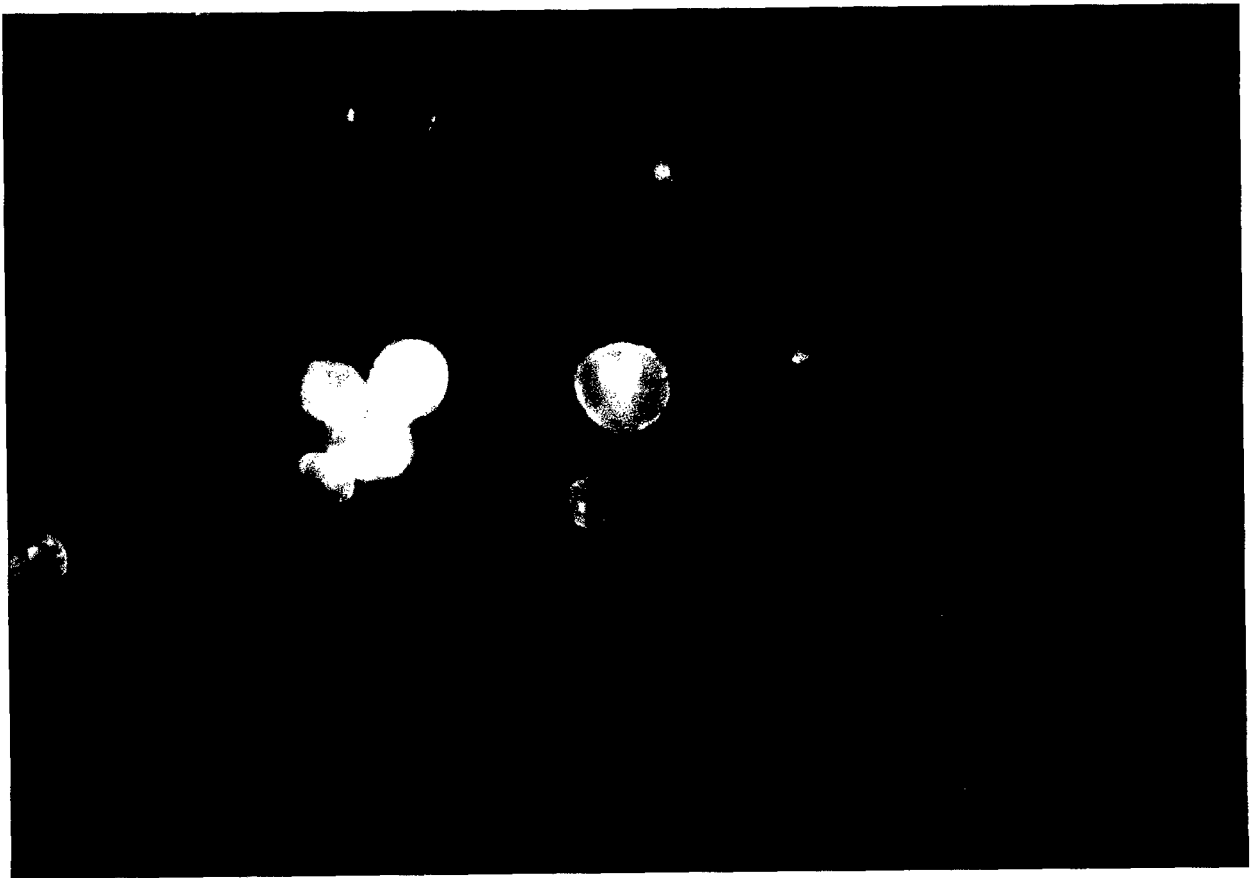
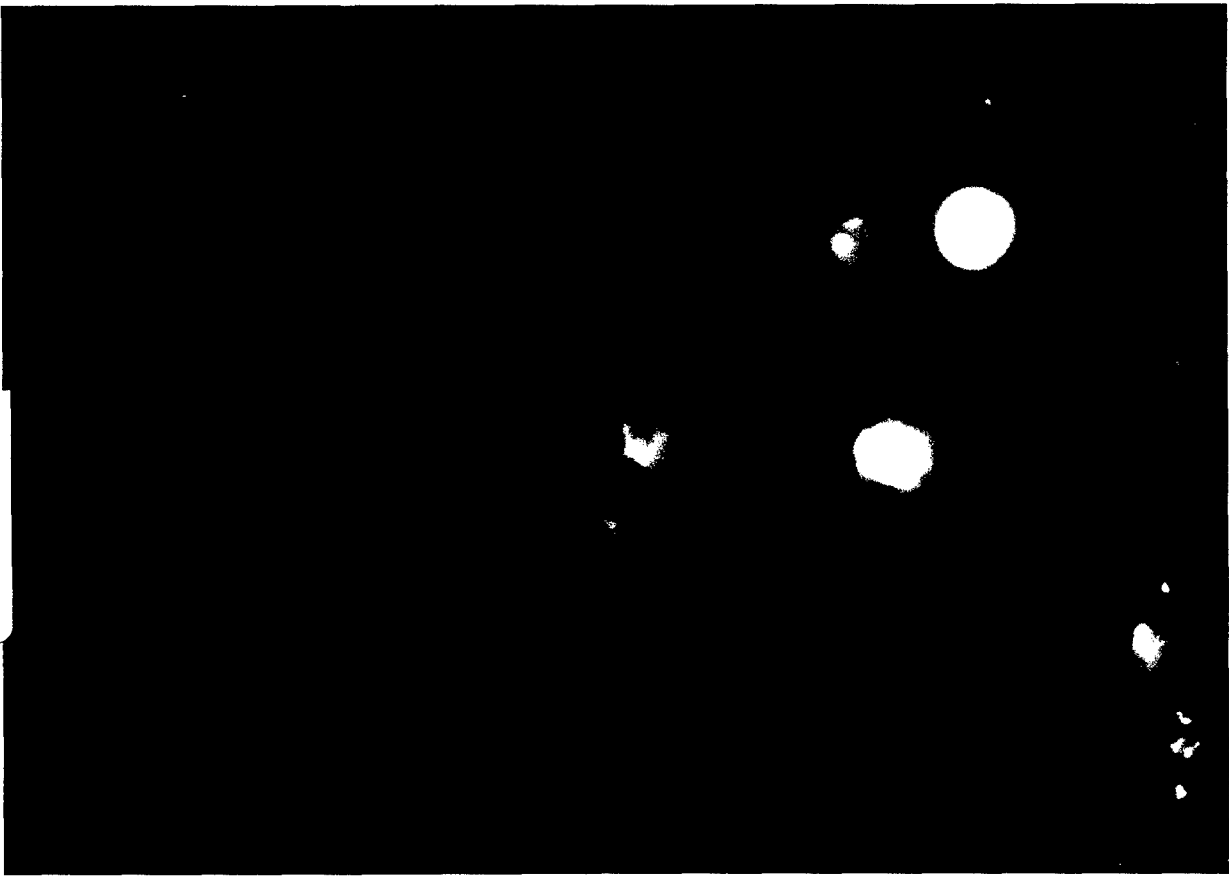


FIGURE 13F



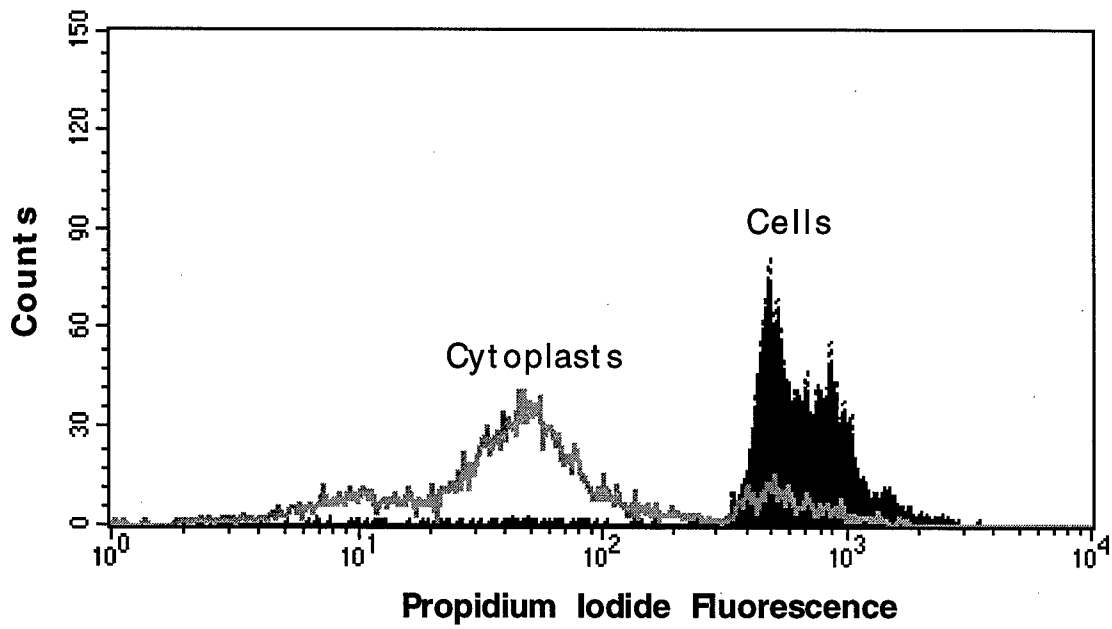
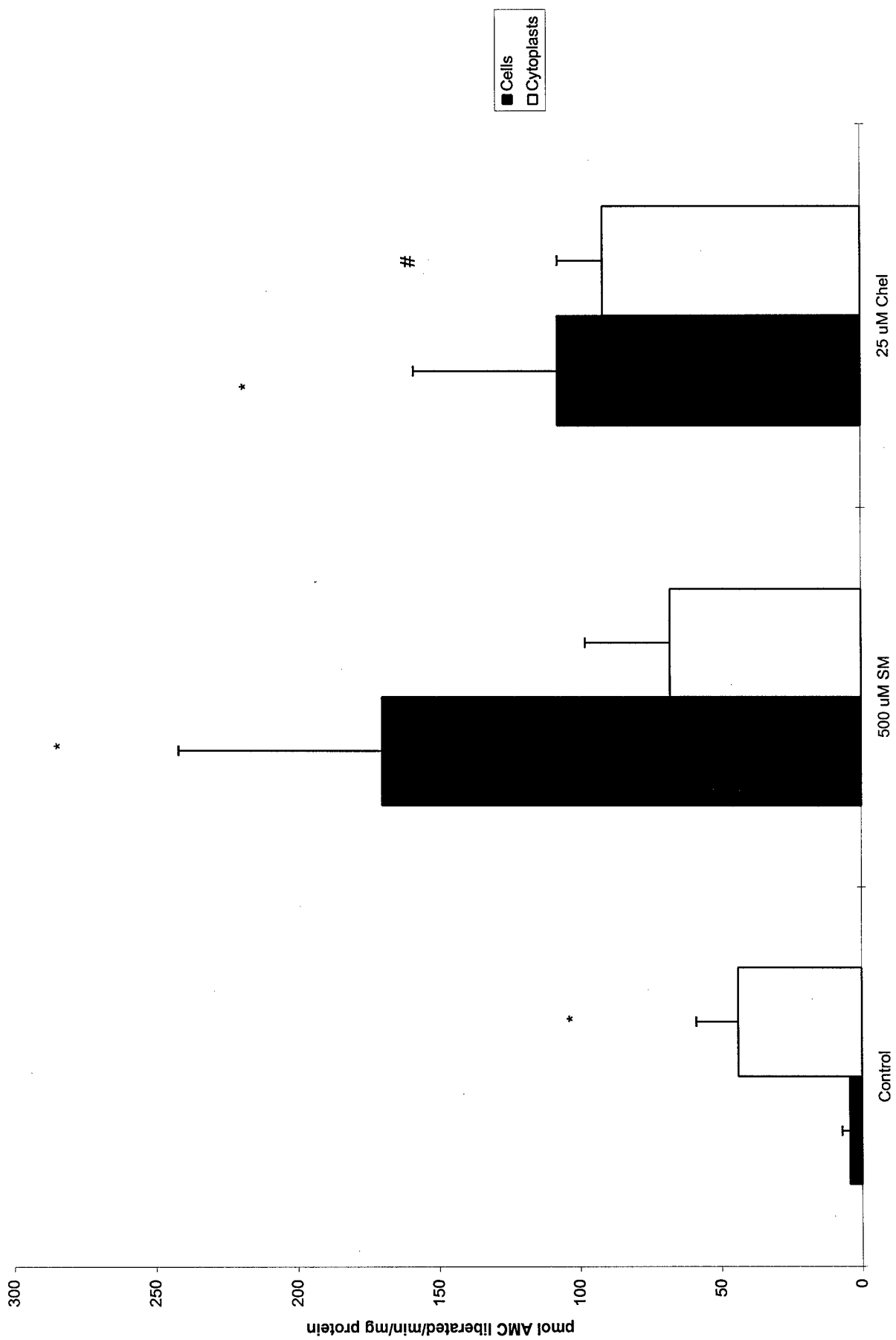


Figure 14



107

Figure 15

Propidium iodide

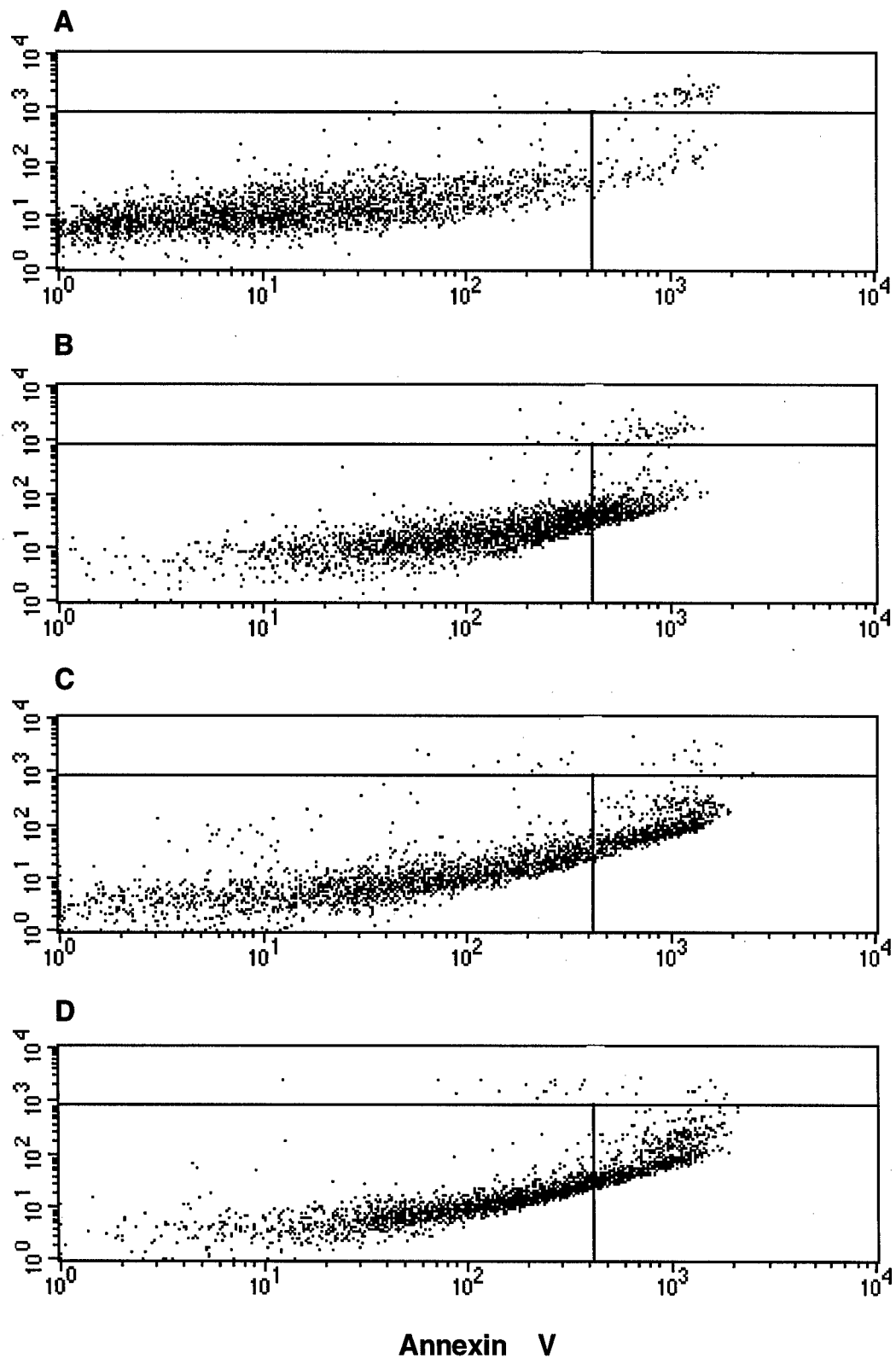


Figure 16

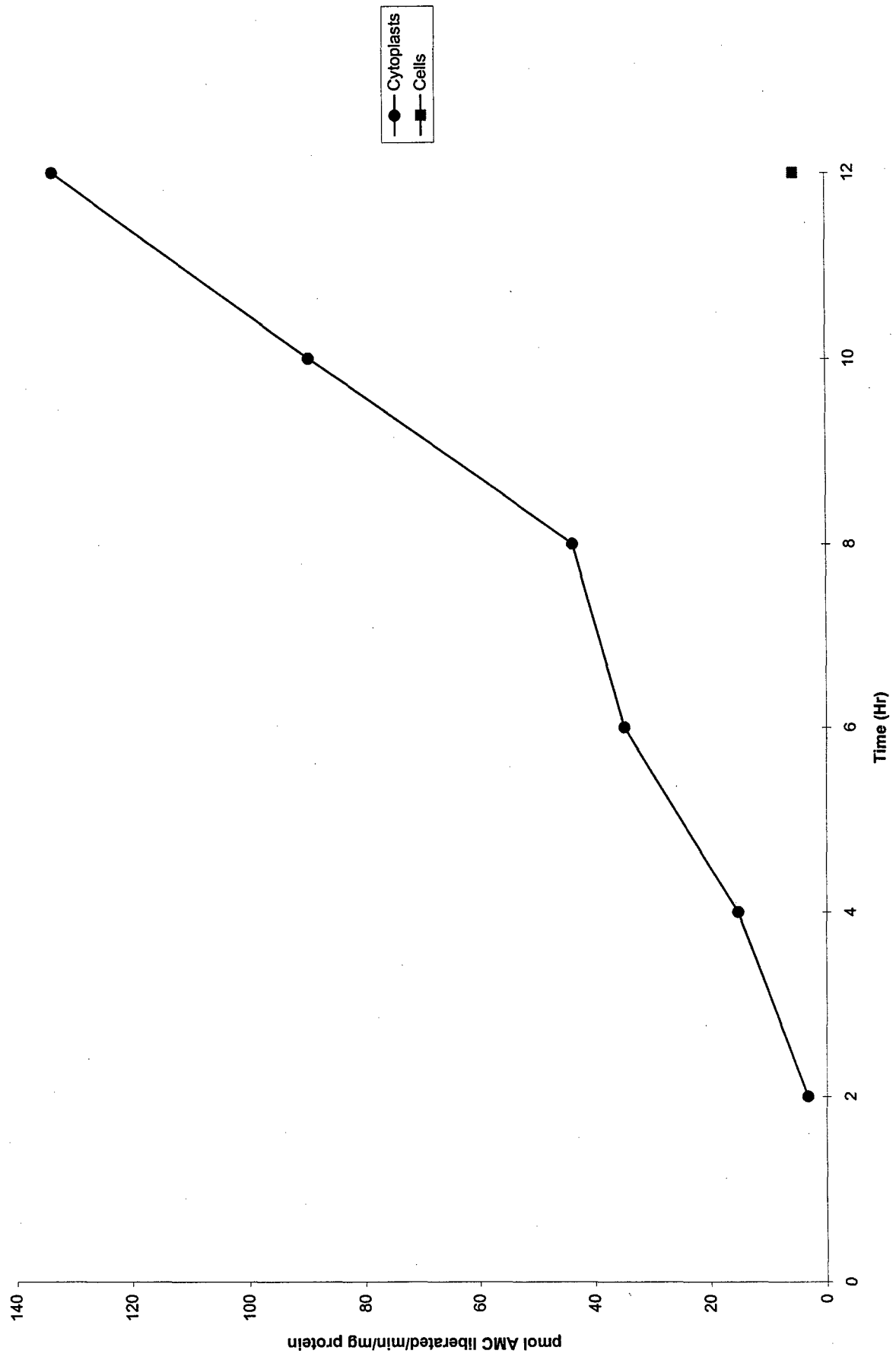


Figure 17

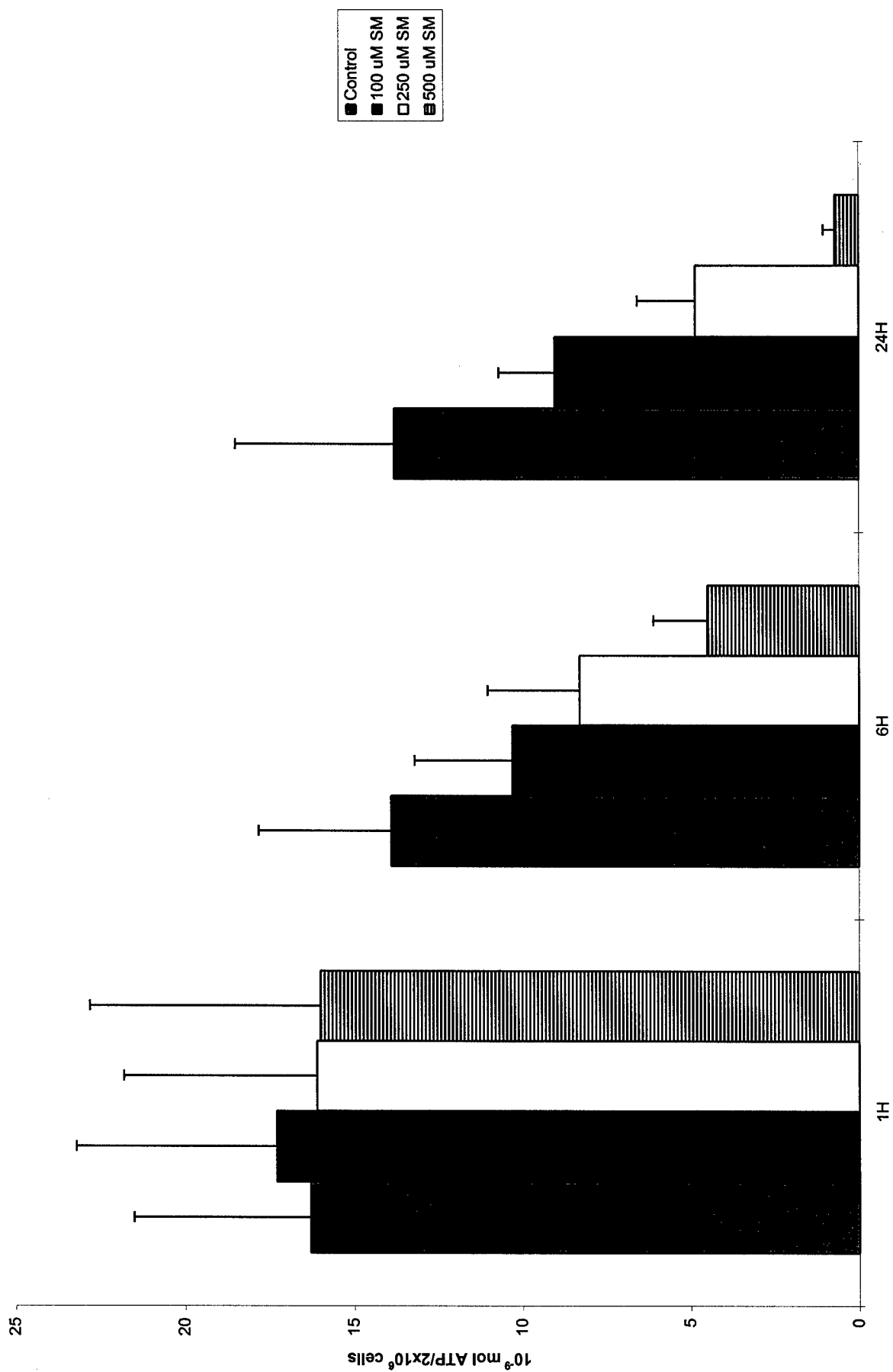


Figure 18A

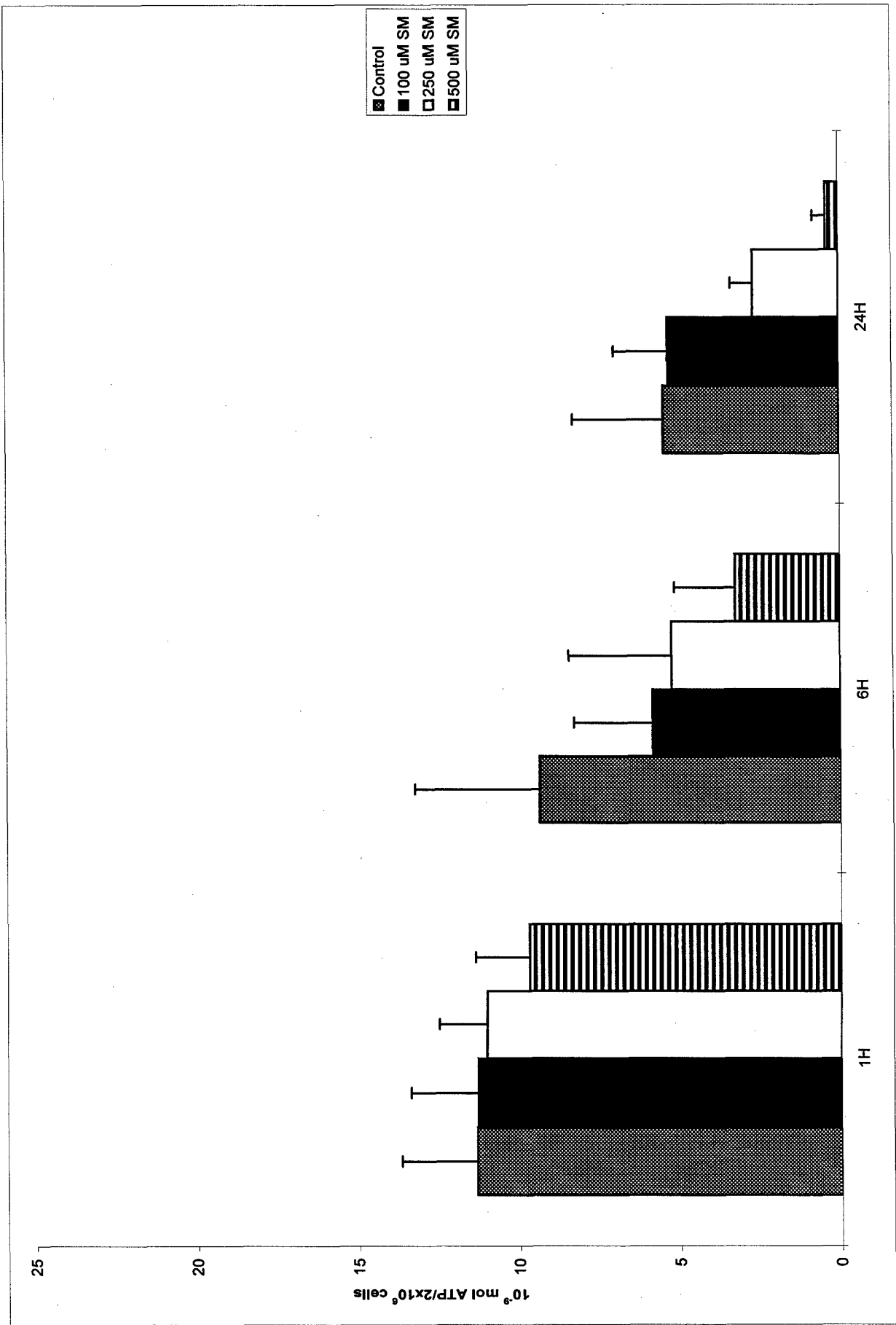


Figure 18B

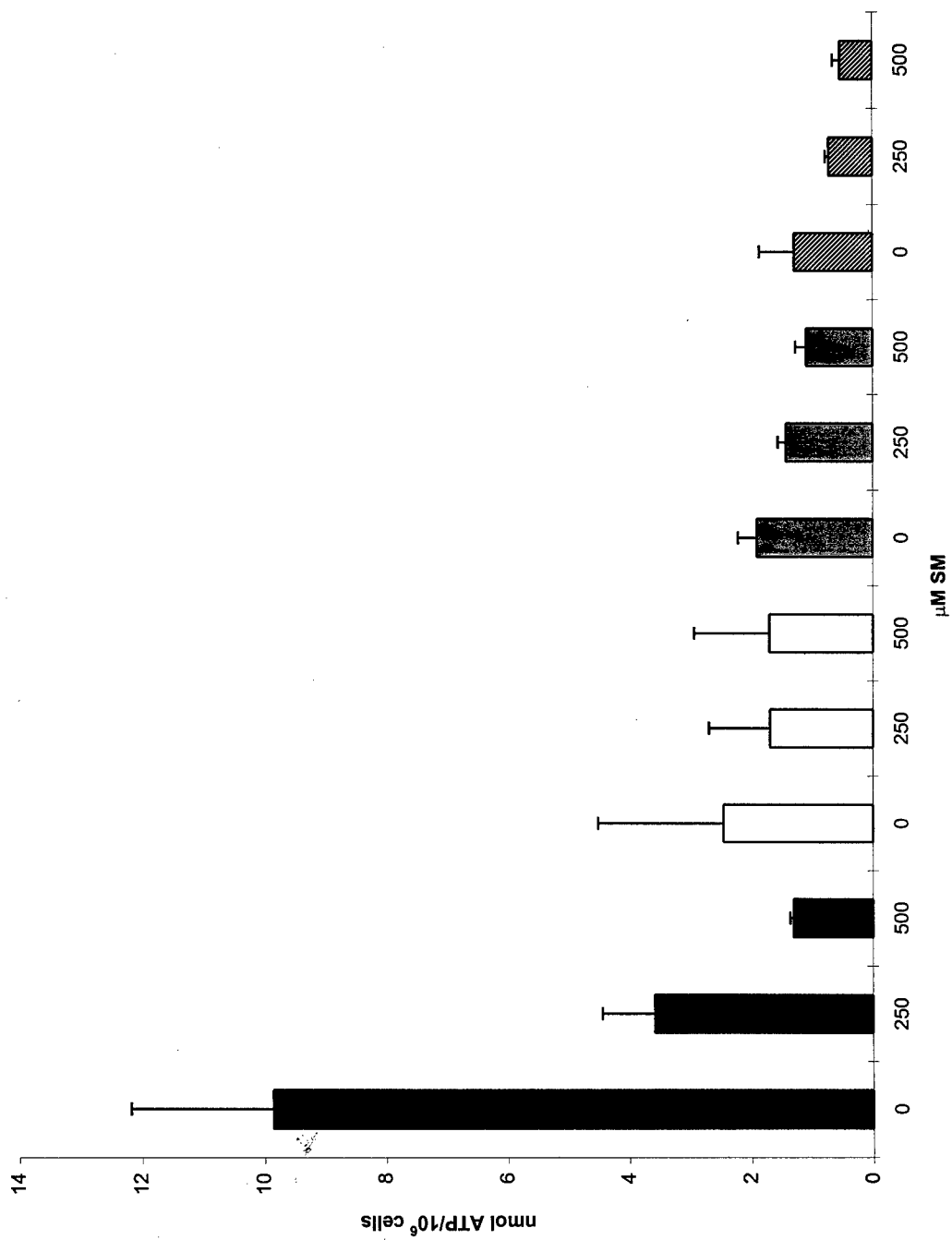


Figure 19

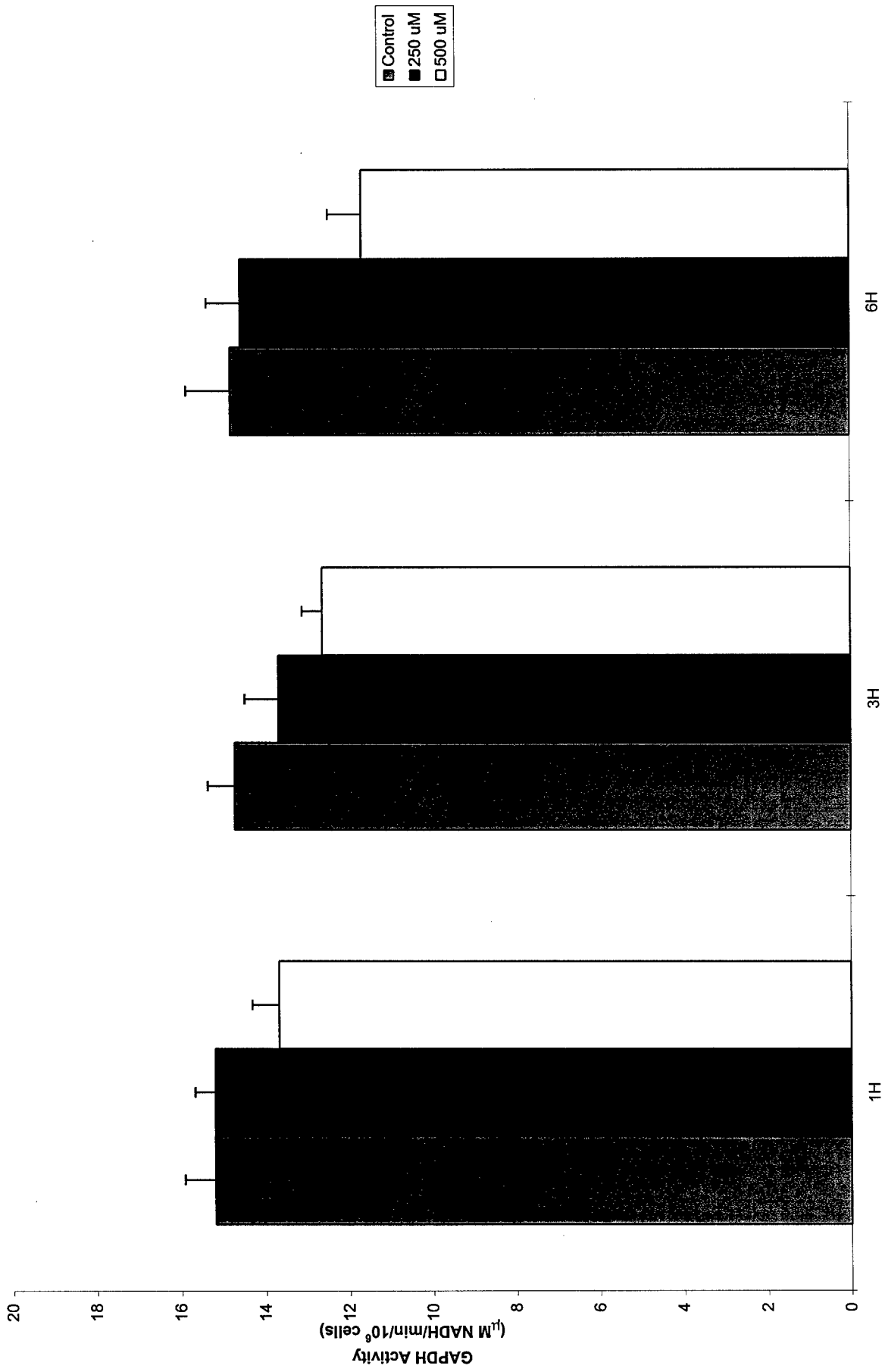


Figure 20A

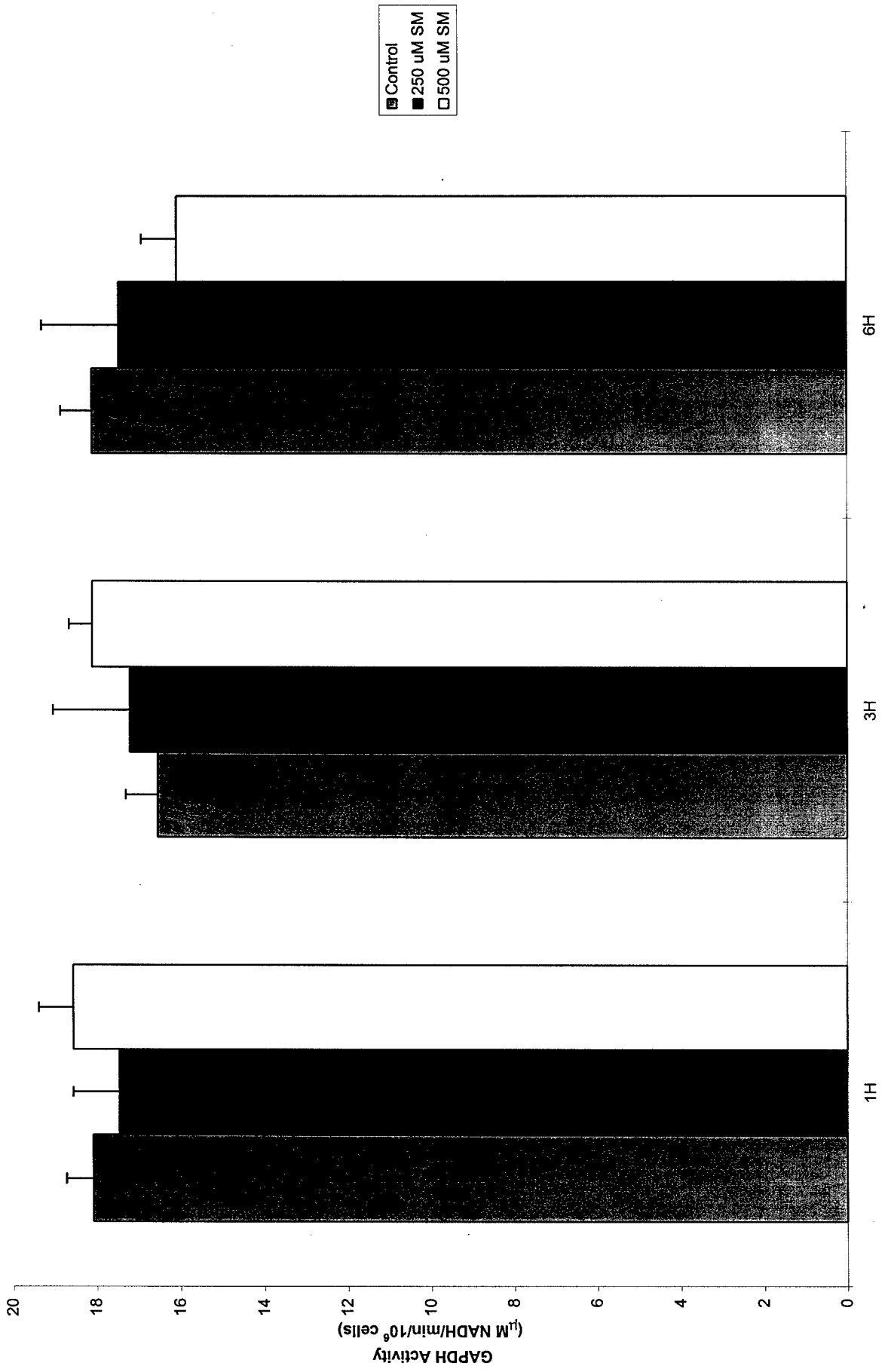


Figure 20B

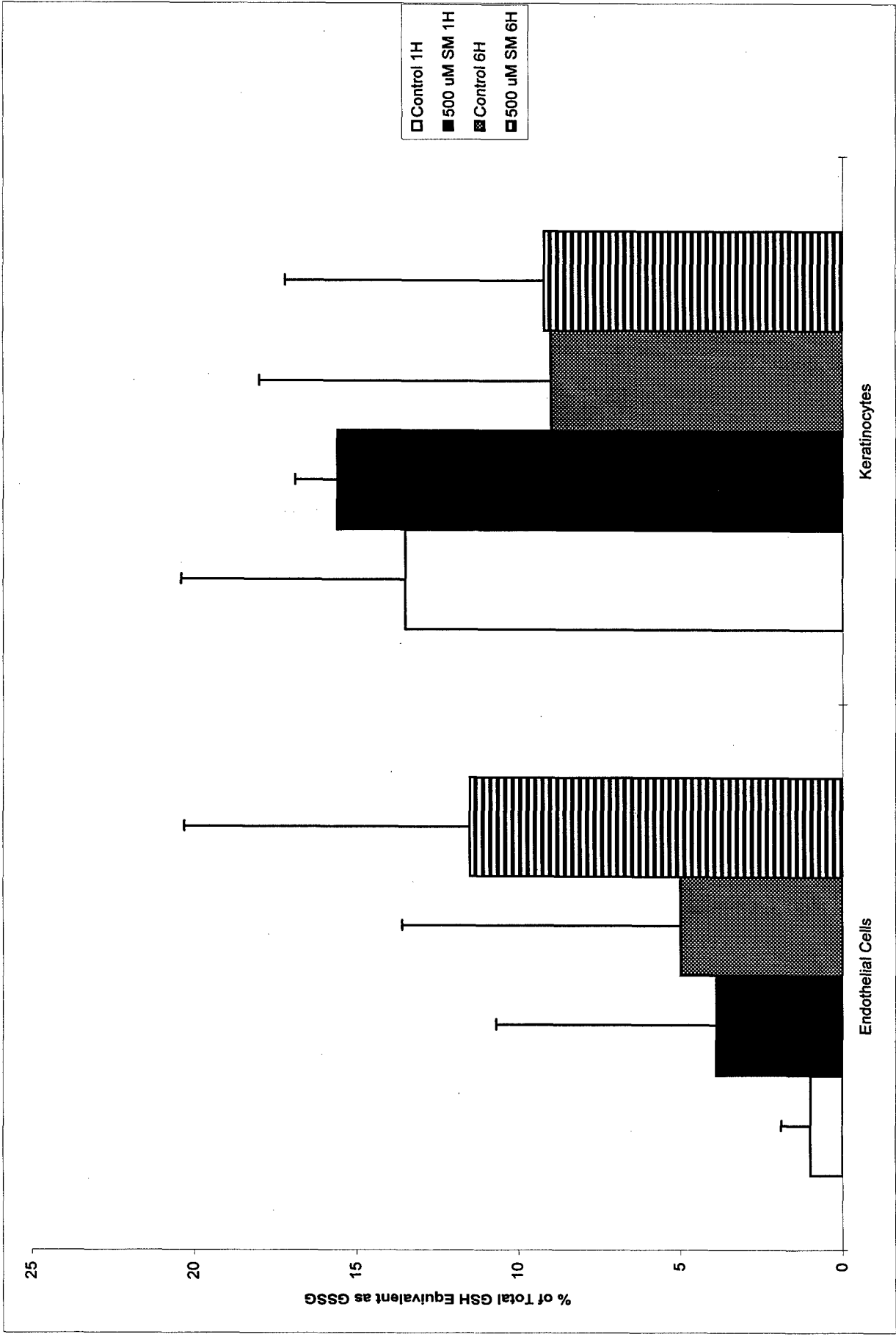


Figure 21

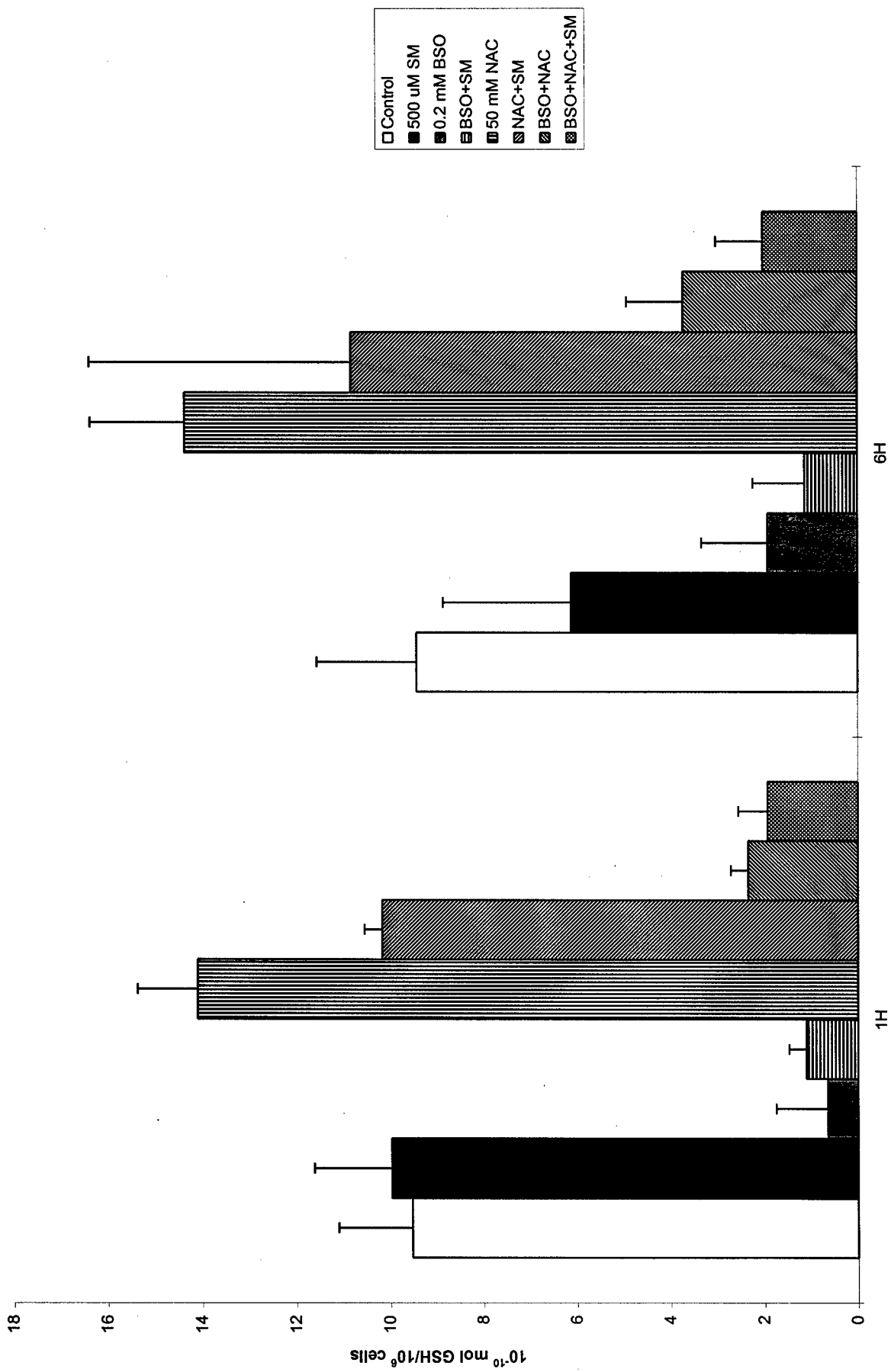


Figure 22A

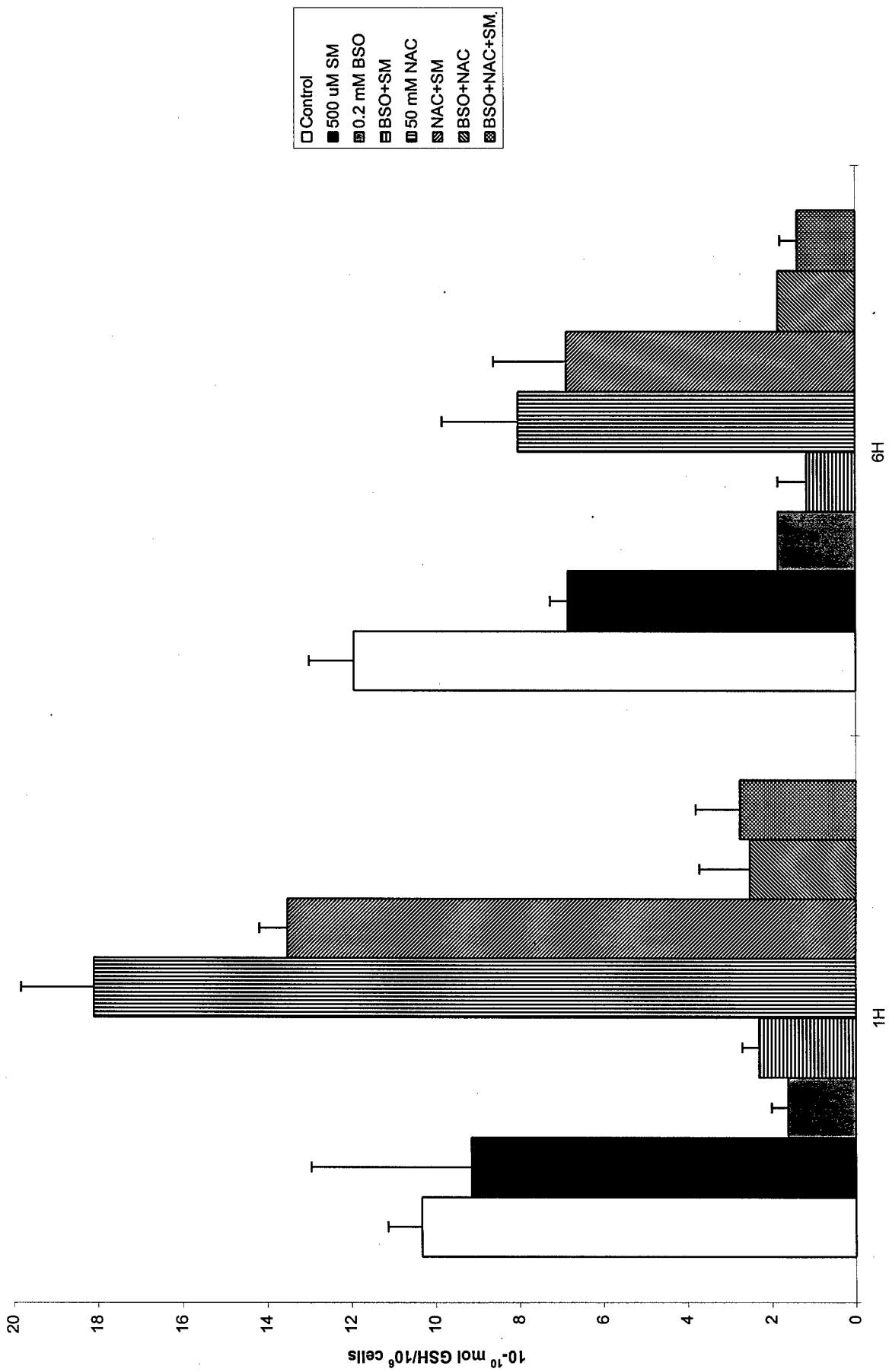


Figure 22B

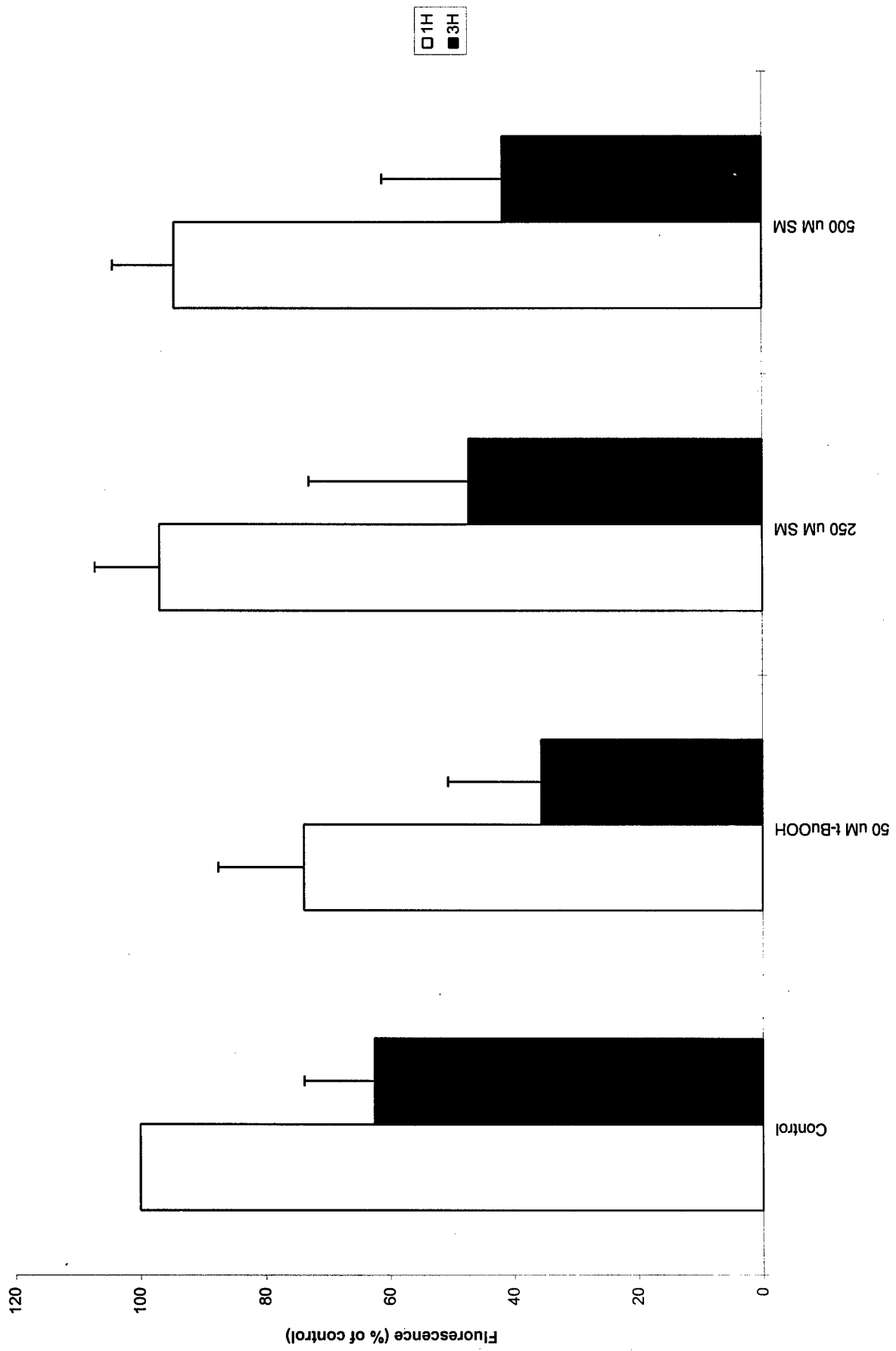


Figure 23A

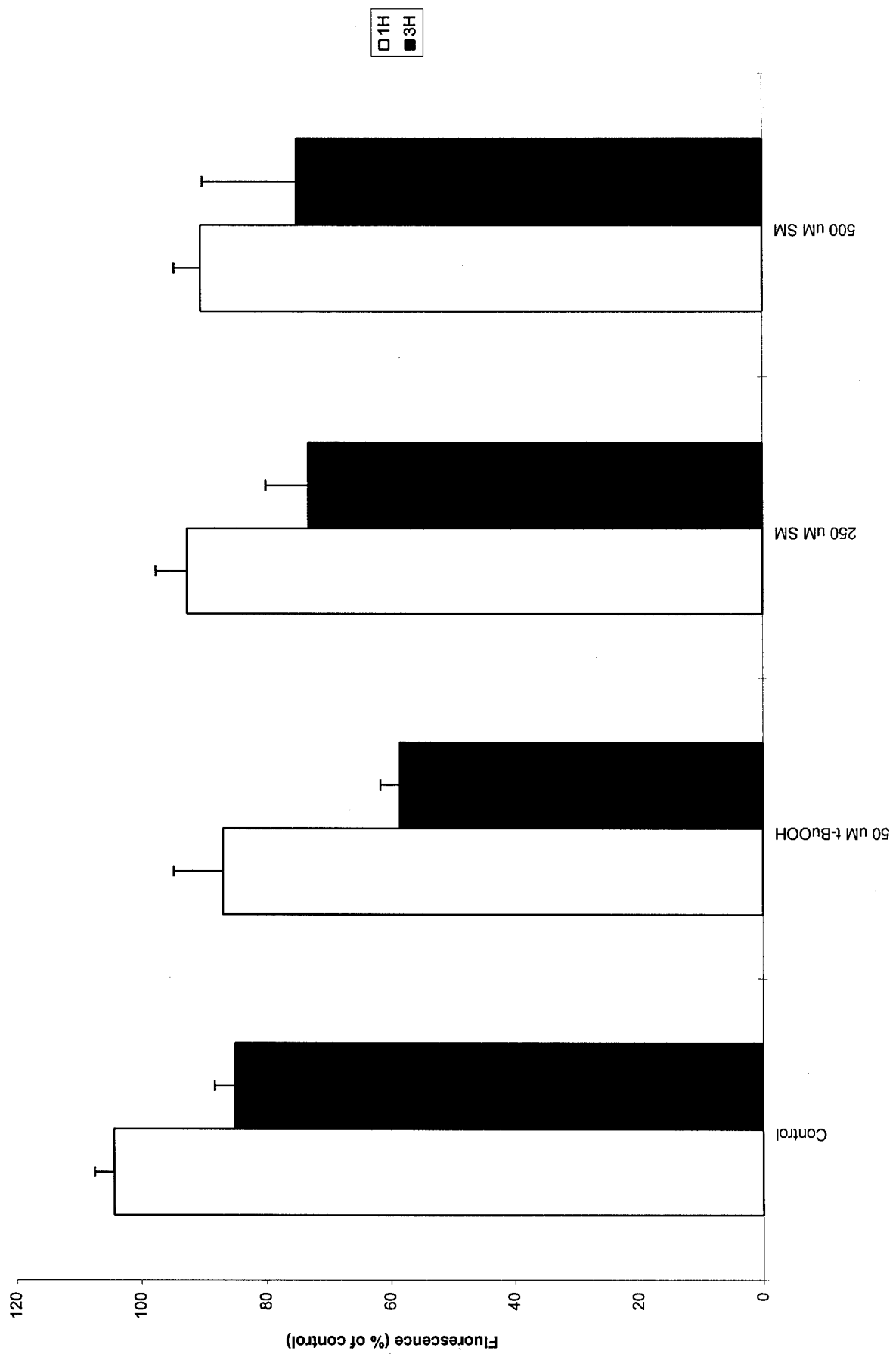
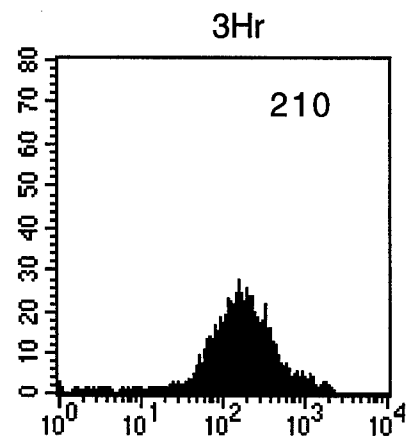
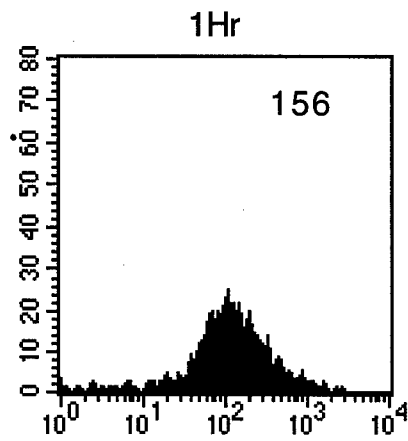
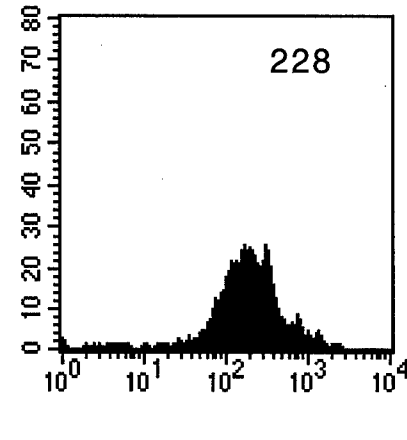
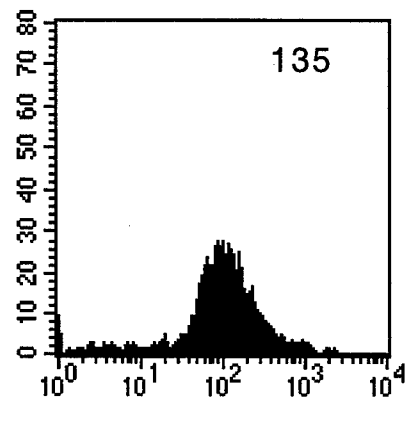


Figure 23B

i

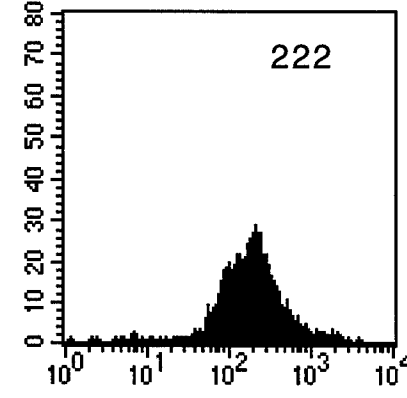
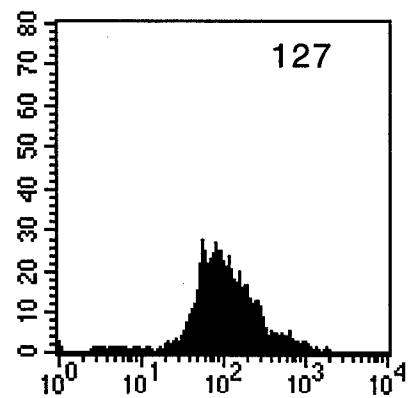


ii

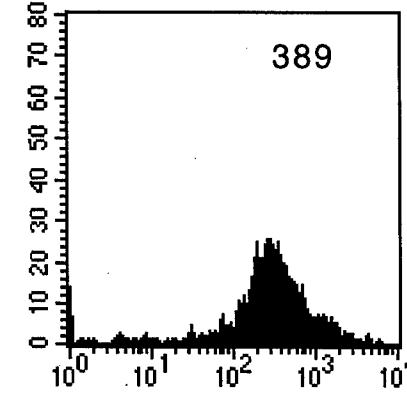
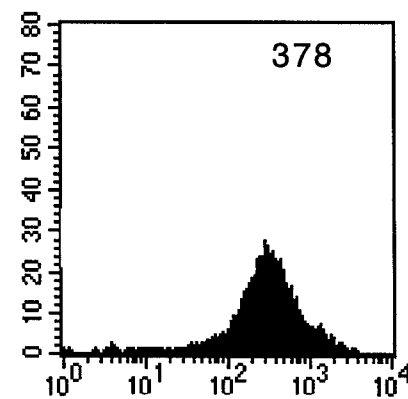


iii

Cell Counts



iv



Rhodamine Fluorescence

Figure 24A

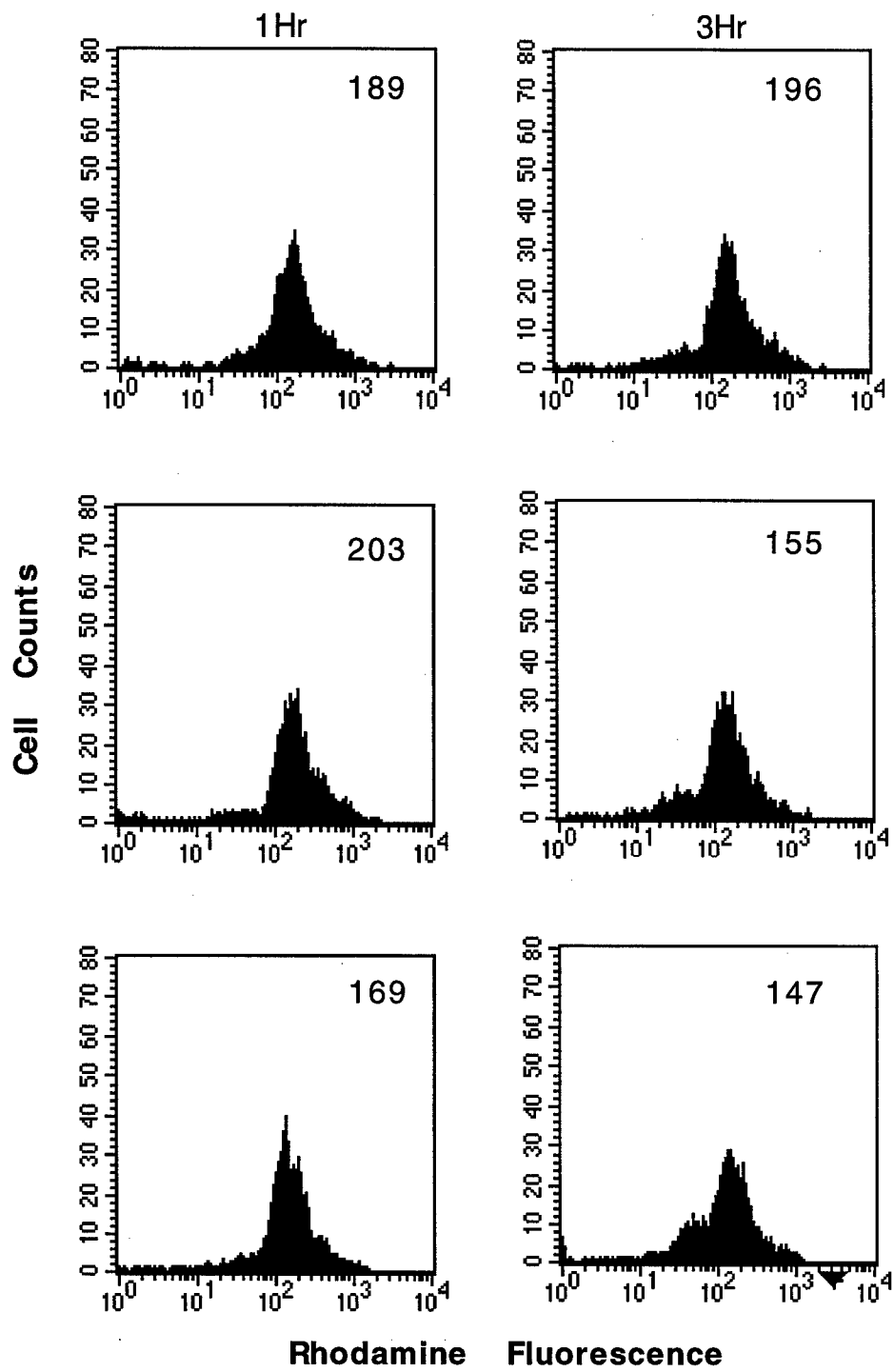


Figure 24B

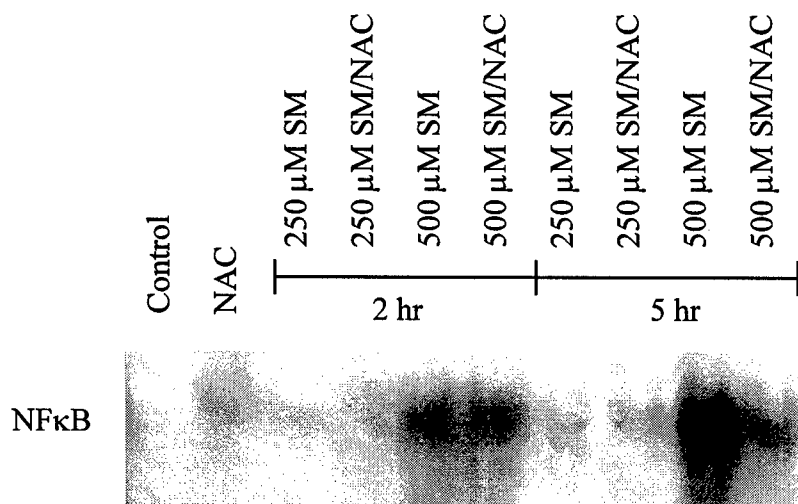
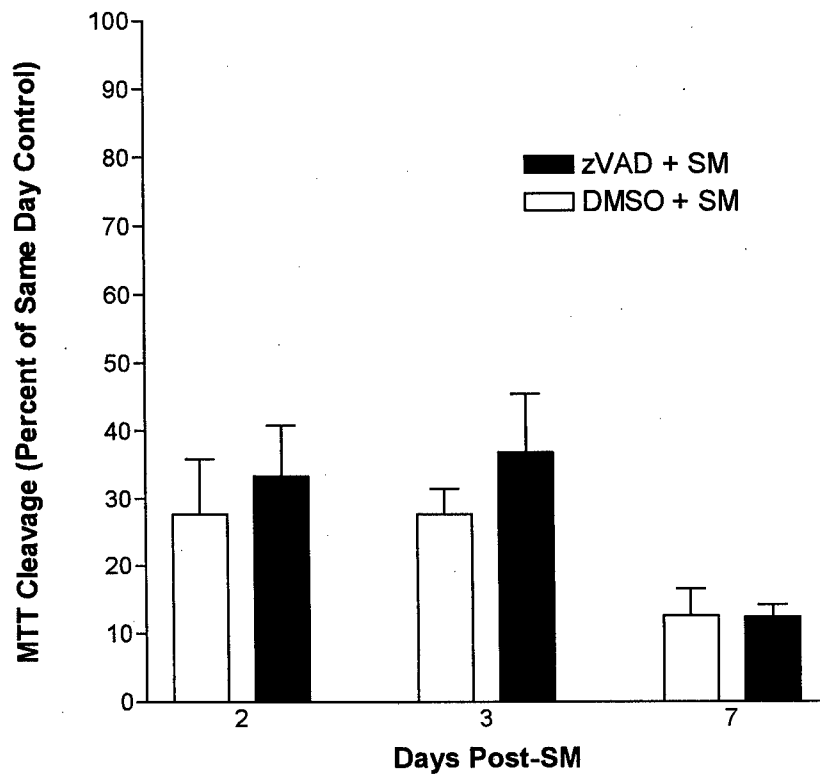


Figure 25



123

Figure 26

Please see attached glossies.

Fig.27A-F

124

FIGURE 27C

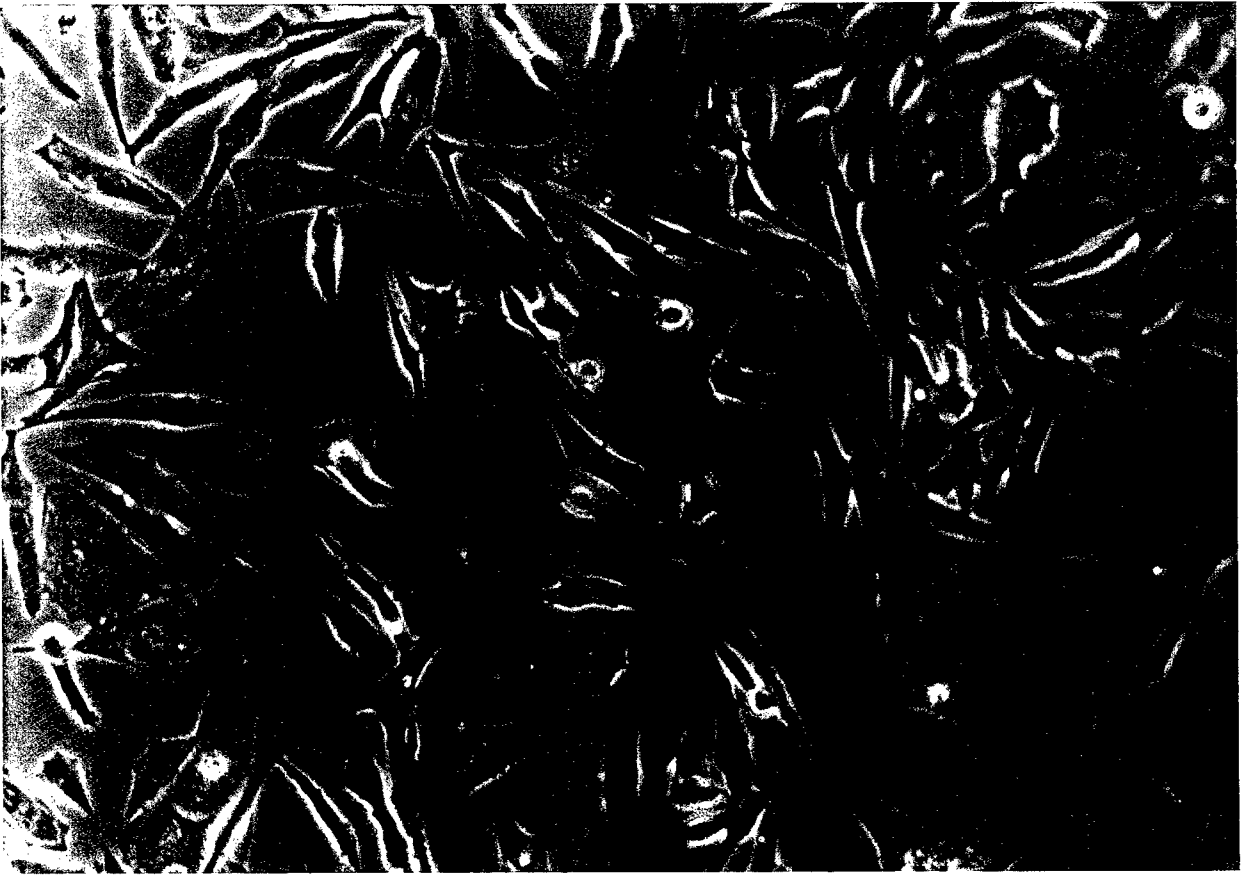


FIGURE 27D

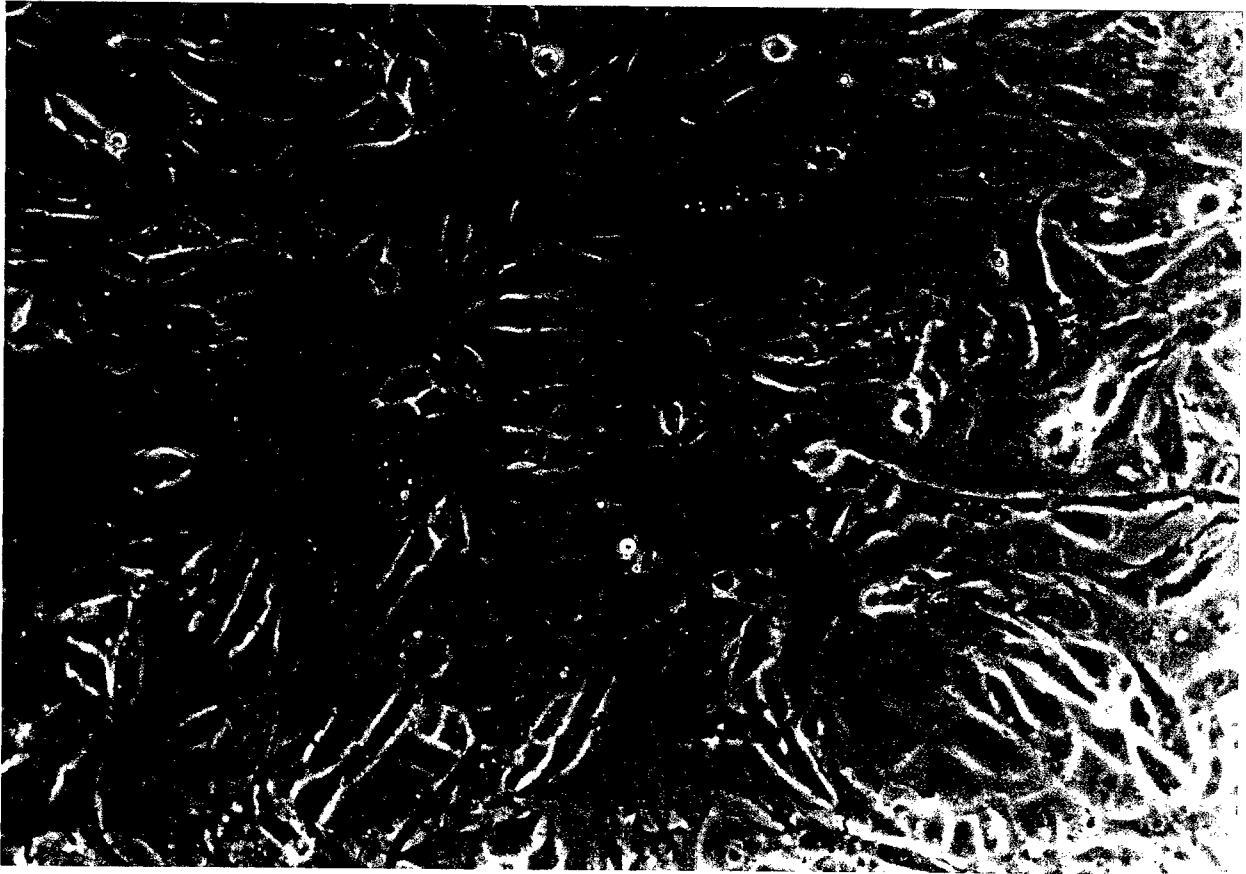


FIGURE 27A

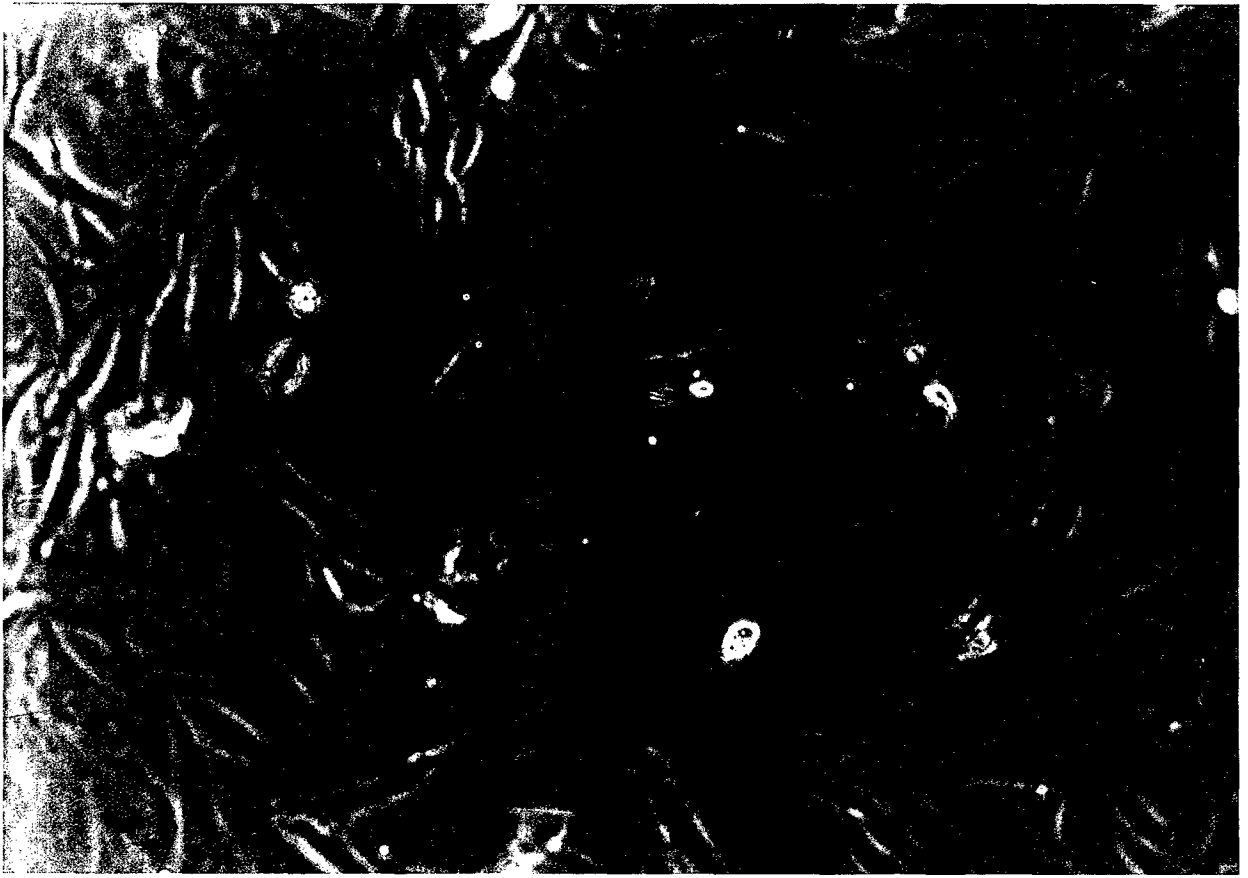


FIGURE 27B

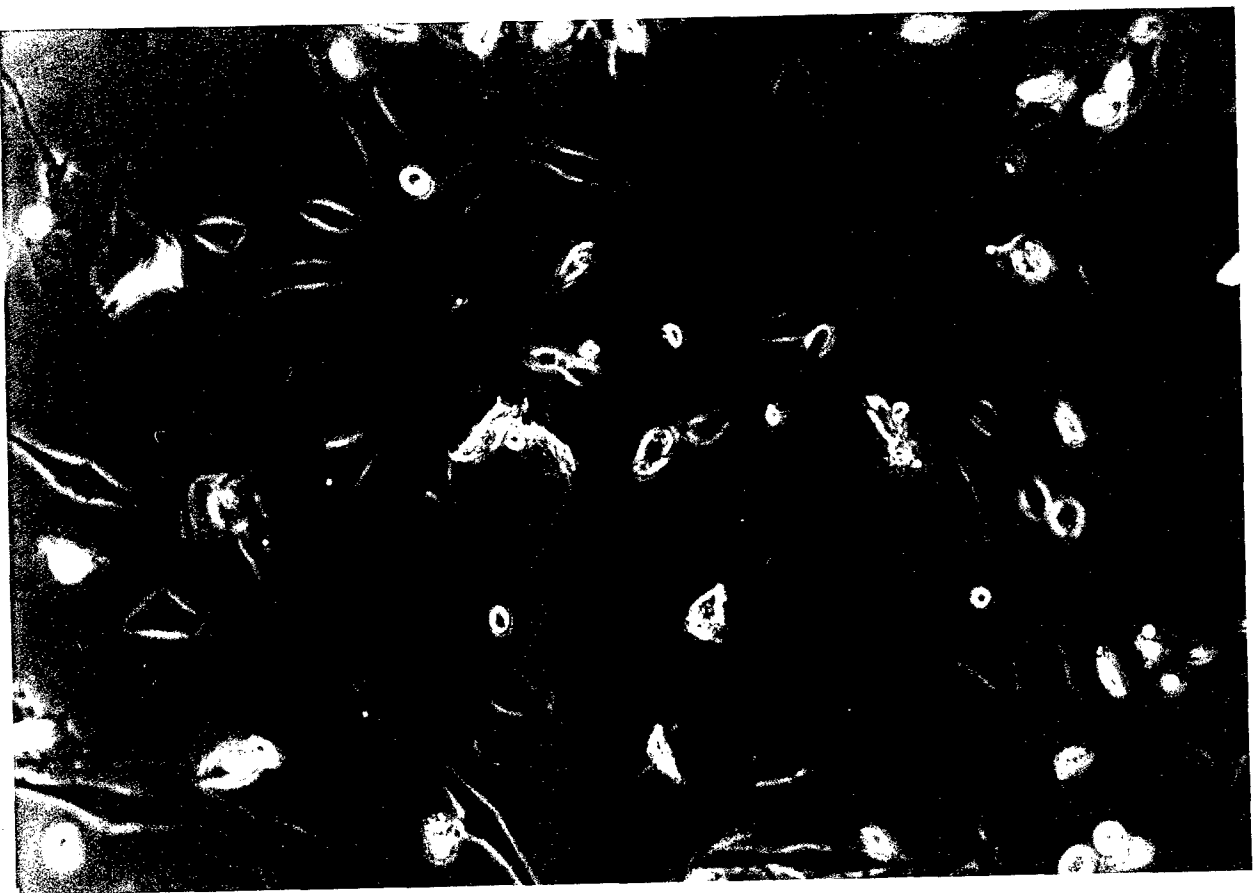


FIGURE 27E

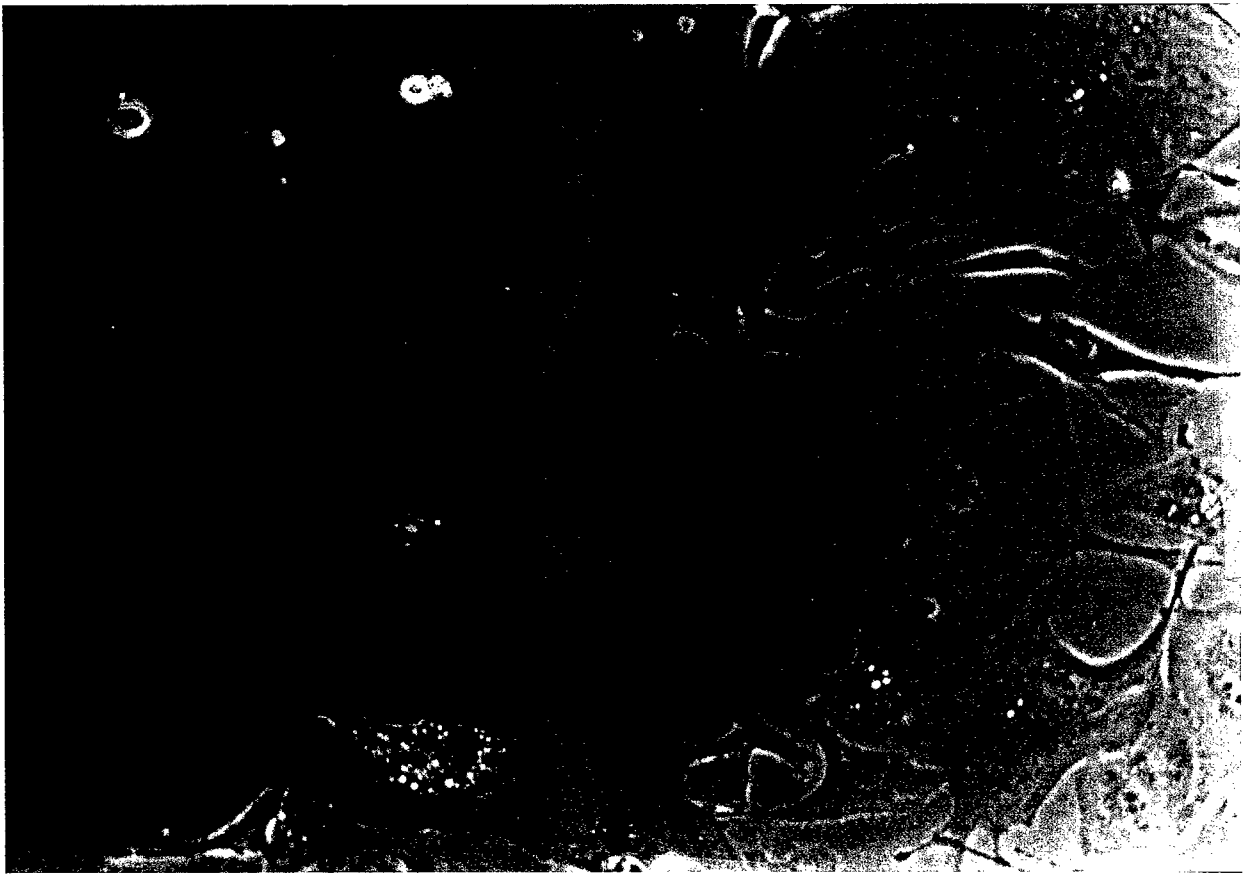
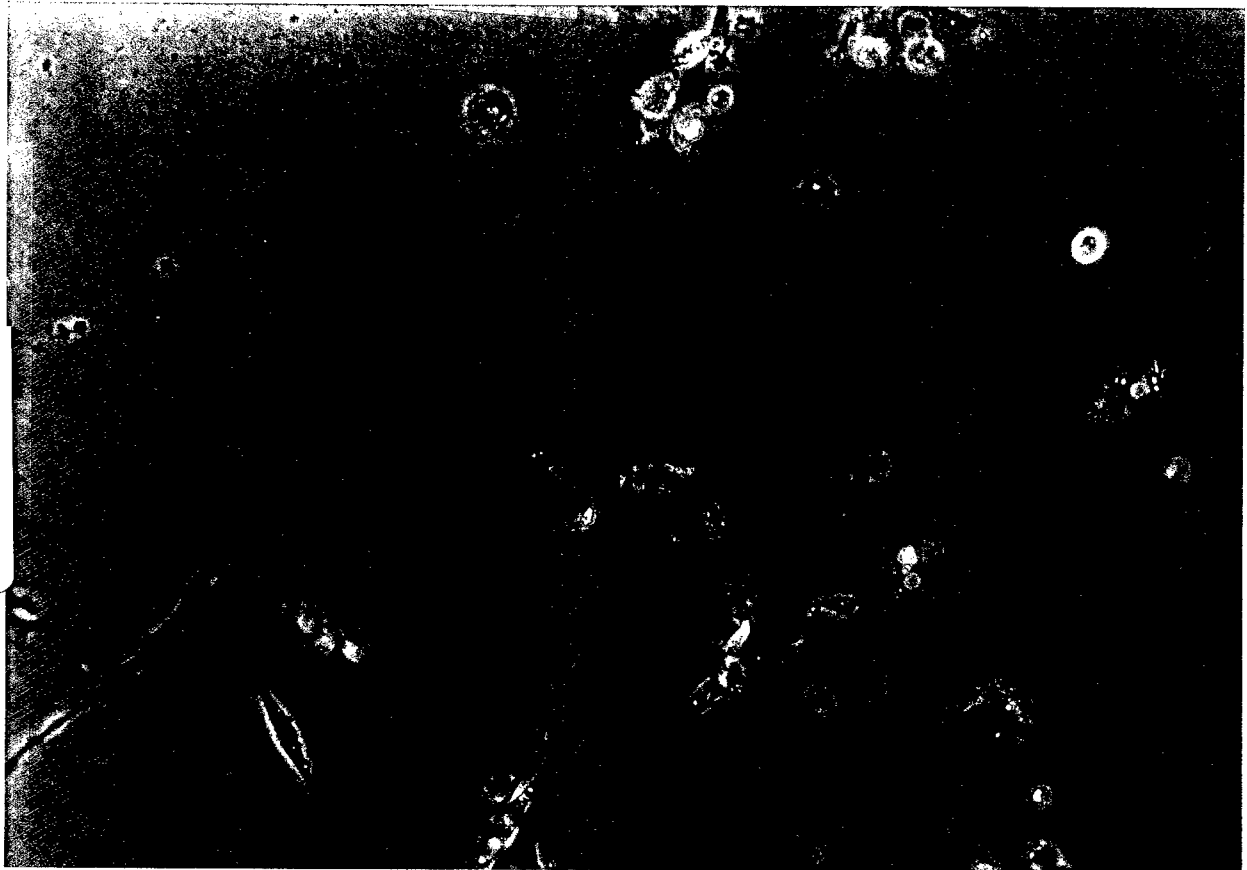


FIGURE 27F



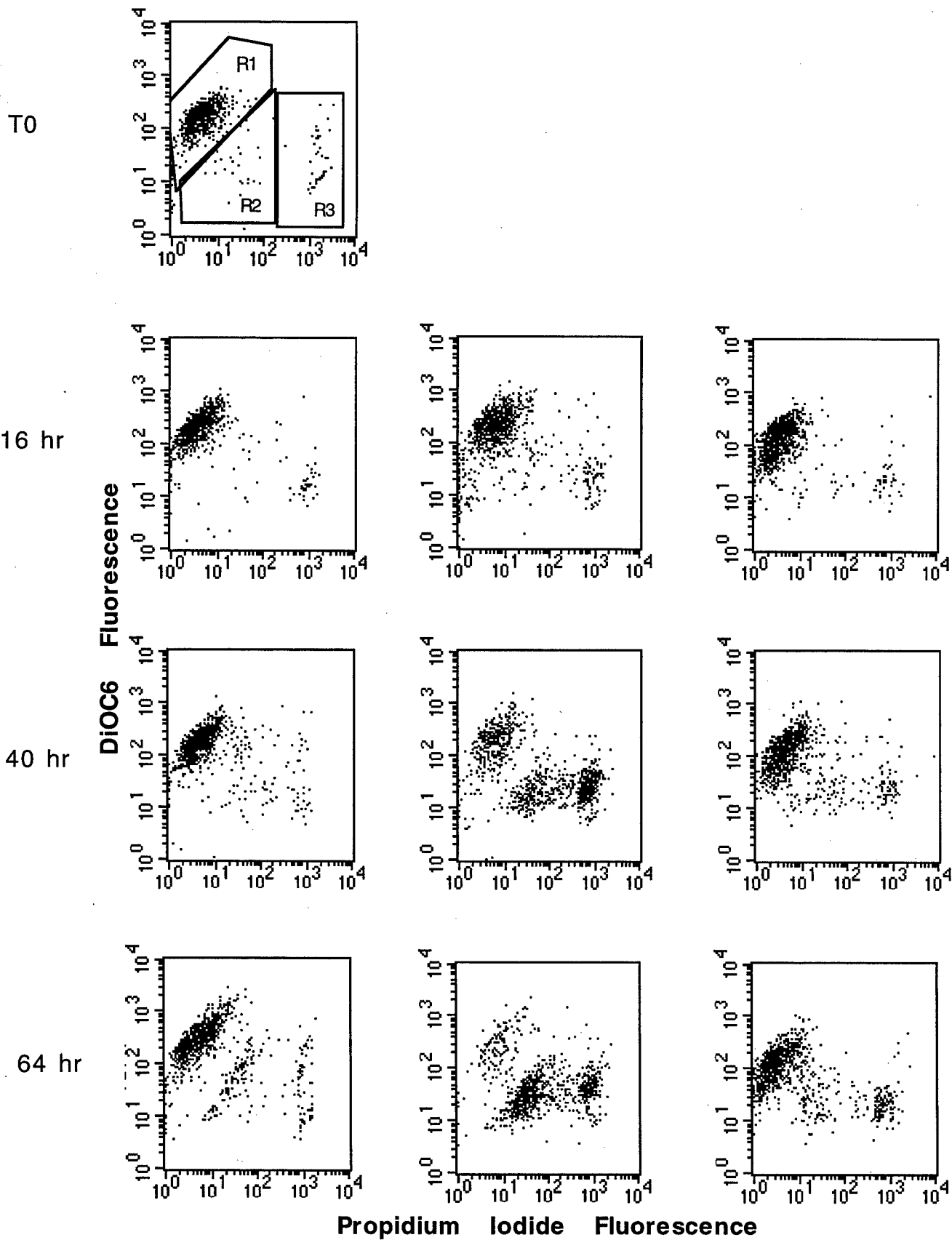


Fig. 28A DMSO Control

SM

zVAD+SM

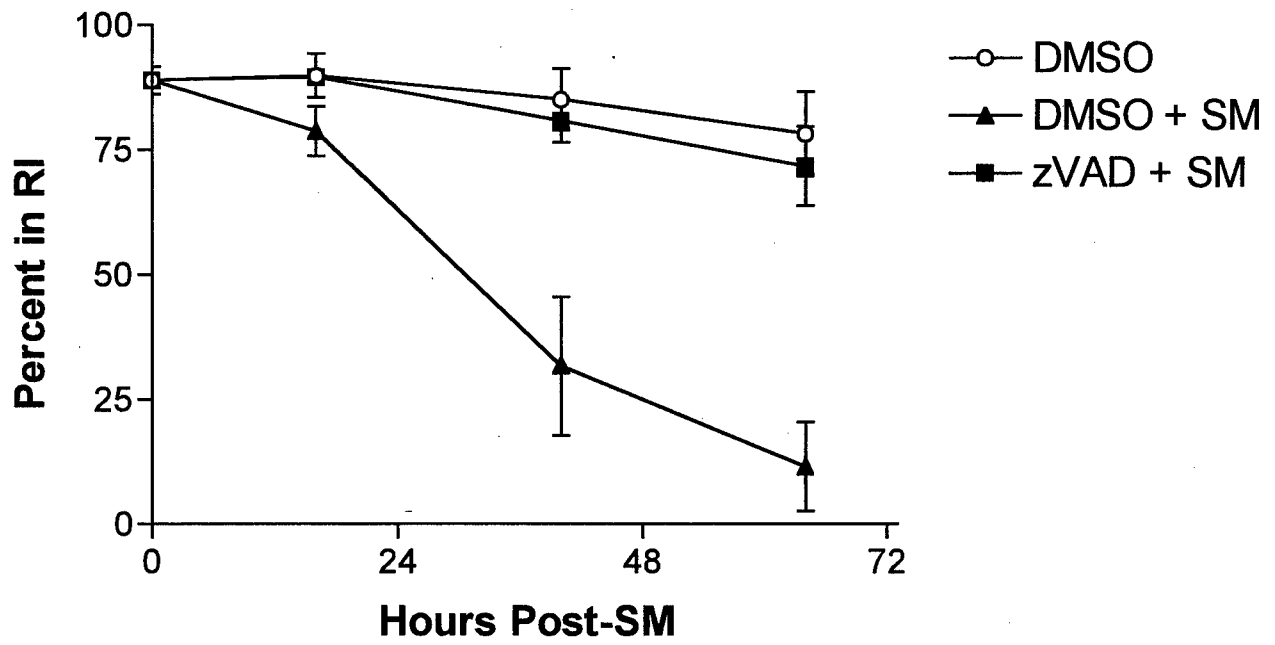


Figure 28B

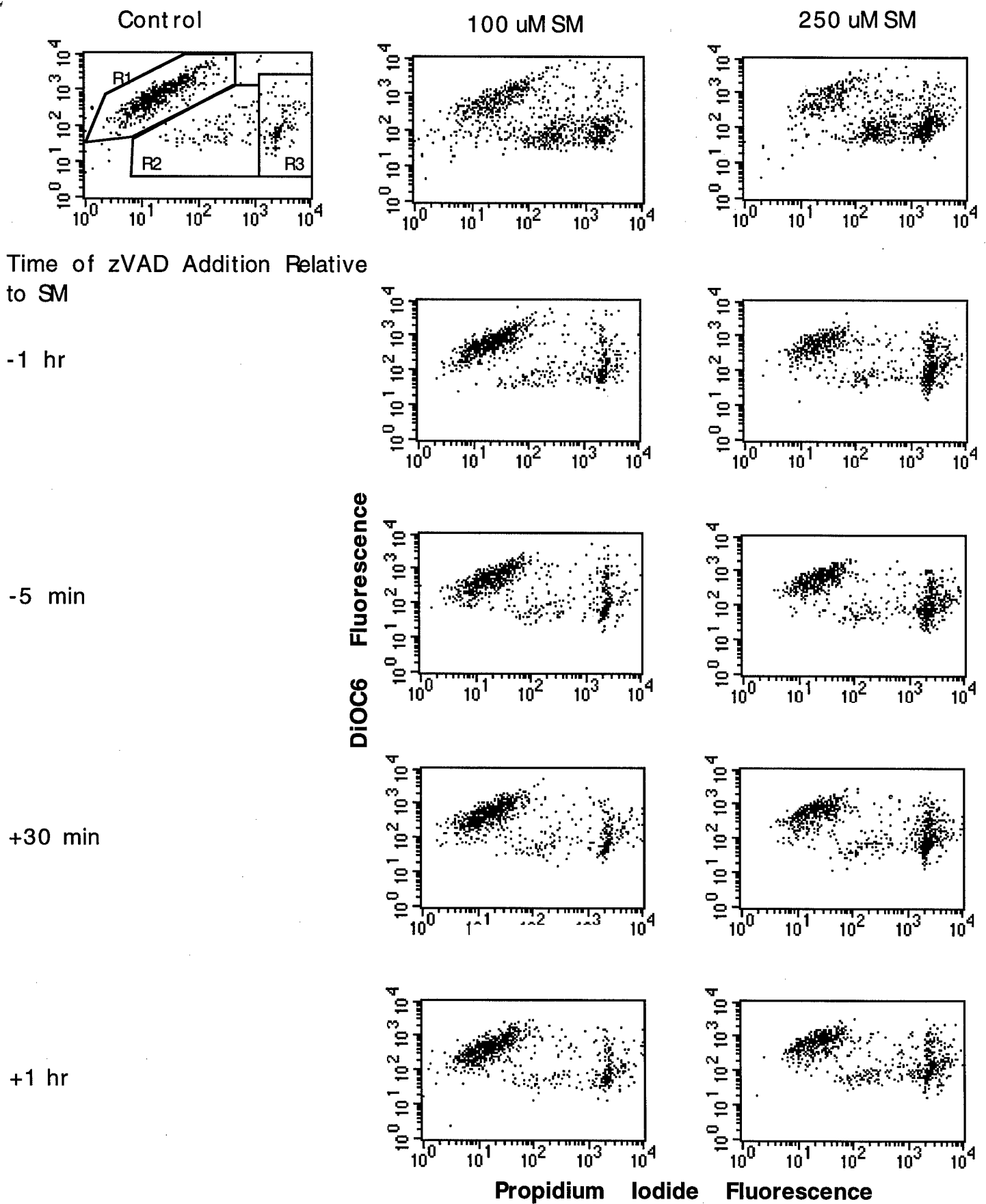


Figure 29



DEPARTMENT OF THE ARMY
US ARMY MEDICAL RESEARCH AND MATERIEL COMMAND
504 SCOTT STREET
FORT DETRICK, MARYLAND 21702-5012

REPLY TO
ATTENTION OF:

MCMR-RMI-S (70-1y)

20 Dec 02

MEMORANDUM FOR Administrator, Defense Technical Information
Center (DTIC-OCA), 8725 John J. Kingman Road, Fort Belvoir,
VA 22060-6218

SUBJECT: Request Change in Distribution Statement

1. The U.S. Army Medical Research and Materiel Command has reexamined the need for the limitation assigned to technical reports written for Grant DAMD17-00-1-0015 and Military Interdepartmental Purchase Request 5MCVEM6785. Request the limited distribution statement for Accession Numbers listed below be changed to "approved for public release; distribution unlimited." These reports should be released to the National Technical Information Service.

ADB282137
ADB283906

2. Point of contact for this request is Ms. Judy Pawlus at DSN 343-7322 or by e-mail at judy.pawlus@det.amedd.army.mil.

FOR THE COMMANDER:


PHYLLIS M. RINEHART
Deputy Chief of Staff for
Information Management